

REVIEW ARTICLE

Compton scattering and electron momentum determination

To cite this article: M J Cooper 1985 *Rep. Prog. Phys.* **48** 415

View the [article online](#) for updates and enhancements.

Related content

- [Directional Compton profiles and the electron density distribution in iron](#)
A J Rollason, R S Holt and M J Cooper
- [Compton scattering studies of the valence electron density distribution in GaAs](#)
D N Timms, M J Cooper, R S Holt et al.
- [The Experimental Determination of Electron Momentum Densities](#)
Brian G Williams

Recent citations

- [Temperature and Chemical Reaction Distribution of a Laminar Diffusion Flame Measured by X-ray Compton Scattering](#)
Hiroshi Sakurai et al
- [Hydrogen-bond network distortion of water in the soft confinement of Nafion membrane](#)
M. Plazanet et al
- [Sensitivity of the Fermi surface to the treatment of exchange and correlation](#)
E. I. Harris-Lee et al



IOP | ebooks™

Bringing together innovative digital publishing with leading authors from the global scientific community.

Start exploring the collection—download the first chapter of every title for free.

Compton scattering and electron momentum determination

Malcolm J Cooper

Department of Physics, University of Warwick, Coventry CV4 7AL, UK

Abstract

When radiation is Compton-scattered the emerging beam is Doppler-broadened because of the motion of the target electrons. An analysis of this broadened lineshape—the Compton profile—provides detailed information about the electron momentum distribution in the scatterer. The technique is particularly sensitive to the behaviour of the slower moving outer electrons involved in bonding in condensed matter and can be used to test their quantum-mechanical description.

The review begins with a brief survey of the historical development of the subject to within a decade of the present. The behaviour of quantum systems, from a momentum viewpoint, is explained and the conditions under which the scattering experiment can be interpreted directly in terms of electron momentum density are discussed. The experimental techniques with γ rays, x-rays and electron beams are compared. Finally, recent results on insulators and conductors are surveyed and the extent to which they challenge conventional assumptions of band theory is critically reviewed.

This review was received in September 1984.

Contents

	Page
1. Introduction	417
1.1. The Compton effect	417
1.2. Relationship between electron momenta and line broadening	419
1.3. The early development of Compton scattering	421
1.4. Modern momentum density studies	423
2. Electron momentum density	426
2.1. Wavefunctions in momentum space	428
2.2. Momentum and kinetic energy in bonding	430
2.3. Relationships between observables and density functions—the reciprocal form factor	433
3. Theory of Compton scattering	438
3.1. Scattering in the Born approximation	438
3.2. Relativistic effects	442
4. Experimental methods	445
4.1. Crystal spectrometers	446
4.2. γ -ray spectrometers	449
4.3. Data analysis	453
4.4. Electron spectroscopy	455
5. Recent studies	456
5.1. General considerations	456
5.2. Ionic solids	458
5.3. Semiconductors	462
5.4. Light metals—beryllium	464
5.5. Transition metals	467
5.6. Alloys and compounds	472
6. Summary	474
Acknowledgments	476
References	477

1. Introduction

The description of charge density in terms of the electron momentum distribution and its study by Compton scattering techniques was reviewed in 1977 when a comprehensive text (*Compton Scattering* edited by B G Williams) and a popular article (Cooper 1977) appeared. This review is intended to bridge the gap between those publications and, of course, to report on the activity in the intervening years.

The past decade has seen a considerable improvement in the quality of the data. Increased experimental activity has been paralleled by advances in the theoretical treatment; the topic has moved on from a period of exploration to one of exploitation. The subject has come of age and the results are as valuable, or more valuable, than those gleaned from the more traditional charge density studies, but always with the added benefit of a novel viewpoint.

1.1. The Compton effect

Most physicists recollect the Compton effect from their student days as an early vindication of quantum ideas. Many would associate the scattering process with the realm of high-energy physics but few would link the phenomenon to study of electron density distributions. Ten or fifteen years ago such ignorance would have been excusable, if not exactly laudable; there was precious little contemporary work of note, certainly nothing in the recent past. An inordinately long time had elapsed between the pioneering experimental work of DuMond in the 1930s, which was characterised by ingenuity and invention, and the resurgence of more pedestrian but persistent investigations in the mid-1960s. It is instructive and illuminating to introduce the subject by following this curious development.

The Compton effect, the inelastic scattering of a photon by an electron, is enshrined in a formula for the increase in wavelength which is so familiar that no derivation is necessary:

$$\Delta\lambda = \frac{h}{mc} (1 - \cos \varphi) \quad (1.1)$$

where φ is the angle of scattering. Figure 1 shows the interaction schematically and introduces the terminology to be adopted for the energies and momenta of the photons and electrons. Recasting equation (1.1) in terms of initial (ω_1) and final (ω_2) photon energies yields the equivalent, if less elegant, expression:

$$\omega_2 = \omega_1 \left[1 + \frac{\omega_1}{mc^2} (1 - \cos \varphi) \right]^{-1}. \quad (1.2)$$

This equation is plotted in figure 2(a) for a few angles of scattering. The curves emphasise the fact that the scattering process is a major energy loss mechanism for high-energy photons.

Whereas Einstein's much earlier (1905) quantum explanation of the photoelectric effect had, for the most part, been studiously disregarded, Compton's derivation of equation (1.1) (1923a) and his subsequent experimental verification of it (1923b)

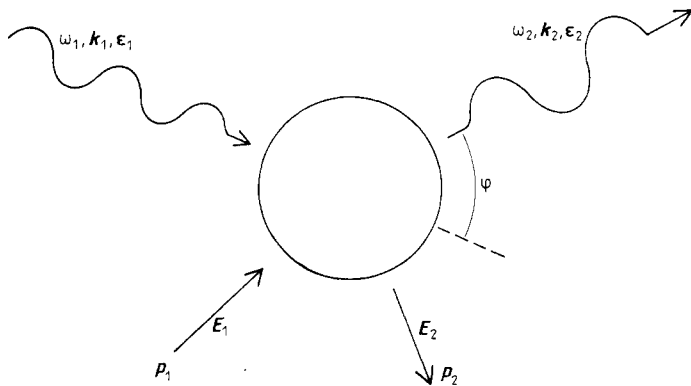


Figure 1. Schematic diagram of the Compton scattering interaction between an incoming photon and a moving electron. The nomenclature of the text follows that of this figure with subscript 1 referring to the incoming and subscript 2 the outgoing particles, \mathbf{k}_1 , \mathbf{k}_2 are the photon wavevectors and the scattering vector $\mathbf{k}_1 - \mathbf{k}_2$ is denoted by \mathbf{K} .

The photons have energies $\hbar\omega_1$ and $\hbar\omega_2$ or simply ω_1 and ω_2 when atomic units ($e = \hbar = m = 1$; $c = 137$) are adopted.

The unit polarisation vectors are ϵ_1 and ϵ_2 . The electron momenta and energy are \mathbf{p}_1 , E_1 and \mathbf{p}_2 , E_2 where $E^2 = c^2(M^2c^2 + |\mathbf{p}|^2)$.

The scattering angle is φ ($= 2\theta$ in the nomenclature of Bragg diffraction).

triggered off a general acceptance of quantum ideas. For Compton, in common with most physicists grounded in classical electrodynamics, it was a grudging acceptance. This turbulent period in the evolution of physics is fully described in Stuewer's (1975) aptly-titled book *The Compton Effect—Turning Point in Physics*. An abridged description of the discovery of the effect and its subsequent exploitation is given in chapter 1 of Williams (1977).

Whatever its importance as a verification of quantum principles and relativistic kinematics, the Compton shift formula (equation (1.1) or (1.2)) is devoid of information about the target; consequently the scattering process appears to be an unlikely probe of the target matter. Klein and Nishina's subsequent quantum electrodynamic derivation of the scattering cross section in 1929, whilst explaining the puzzling asymmetry between forward and back scattering, contains no parameter specific to the scatterer:

$$\left(\frac{d\sigma}{d\Omega} \right)_{K-N} = \frac{1}{2} \left(\frac{e^2}{mc^2} \right)^2 \left(\frac{\omega_2}{\omega_1} \right)^2 \left(\frac{\omega_2 + \omega_1}{\omega_1} - \sin^2 \varphi \right). \quad (1.3)$$

This particular formulation refers to unpolarised photons scattered from free electrons with no net spin (Jauch and Rohrlich 1976). The cross section is plotted as a function of angle for a few energies in figure 2(b).

Equations (1.1)–(1.3) relate to an idealised scatterer, namely a free stationary electron. The interest arises with the realisation that target atoms necessarily contain bound electrons; bound electrons cannot be stationary. Jauncey (1925) was the first to link the motion of the target electrons to a Doppler broadening of the Compton scattered beam: Compton himself did not, at that time, accept this idea. Unfortunately Jauncey chose to base his calculations on the Bohr-Sommerfeld orbital model and, not surprisingly, his predicted lineshapes were somewhat curious. DuMond had more success when he used the novel Fermi-Dirac distribution function to predict the lineshape; indeed his results on beryllium (DuMond 1929) possibly constitute the

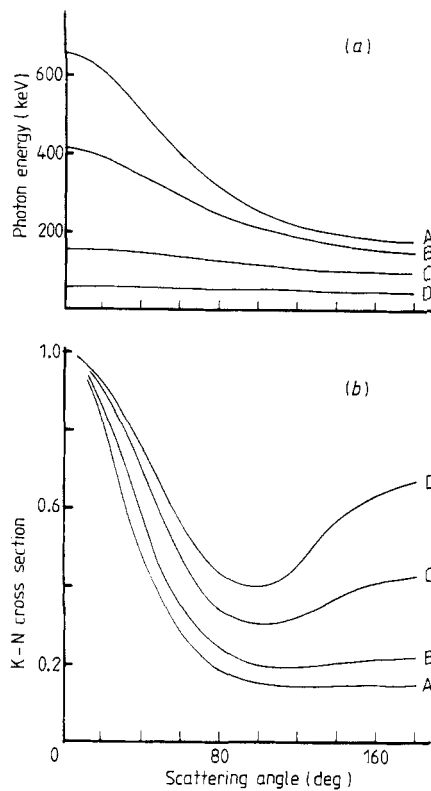


Figure 2. (a) The degradation in photon energy upon Compton scattering through the angular range 0–180° for a selection of initial energies: A, 662 keV, ^{137}Cs ; B, 412 keV, ^{198}Au ; C, 159 keV, $^{123}\text{Te}^m$; D, 60 keV, ^{241}Am . The curves are determined from equation (1.2) of the text. Note that at high incident energies back-scattering is an effective energy loss mechanism. In the limit as $\omega_1 \rightarrow \infty$, ω_2 drops to $\frac{1}{2}mc^2$. (b) The Klein-Nishina cross section in units of $(e^2/mc^2)^2$ (see text: equation (1.3)) as a function of scattering angle for the same incident energies as in (a) above. Note that at low energies the cross section loses its forward/backward asymmetry and approaches the classical Thomson expression.

earliest direct evidence for the validity of Fermi-Dirac as opposed to Maxwell-Boltzmann statistics for the electron gas.

1.2. Relationship between electron momenta and line broadening

The interpretation of the Compton lineshape, usually referred to as the Compton profile, is wittingly or unwittingly based upon an impulse approximation. DuMond and Jauncey pretended that they were seeing scattering from free but moving electrons. If their assumption is to be appropriate to electrons bound in atoms, molecules, etc, the collision between photon and electron must be impulsive. The other electrons are mere spectators when the interaction is extremely brief; they cannot relax to take account of the hole left by the recoiling electron until it has completely escaped from the system. In other words, the potential seen by the target electron is the same immediately before and immediately after the interaction: the potential energy term will therefore cancel in the conservation of energy equation. In this sense the collision occurs between a photon and an individual electron which appears to be moving but unbound. DuMond (1933) likened the Doppler-broadening process to the reflection

of light from a moving mirror (the electron) with the addition of a wavelength shift fixed by the scattering angle.

If an impulse approximation is to be valid the energy transfer to the recoil electron must greatly exceed its binding energy, a condition which is not difficult to attain for conduction electrons, even with x-rays. Using the nomenclature of figure 1 and assuming the cancellation of potential energy terms, the conservation equation can be written:

$$\begin{aligned}\omega_1 - \omega_2 &= \frac{1}{2}m[\mathbf{p} + \hbar(\mathbf{k}_1 - \mathbf{k}_2)]^2 - \mathbf{p}^2/2m \\ &= \frac{\hbar^2|\mathbf{K}|^2}{2m} + \frac{\hbar\mathbf{K}\cdot\mathbf{p}}{m}\end{aligned}\quad (1.4)$$

where $\mathbf{K} = \mathbf{k}_1 - \mathbf{k}_2$ is the scattering vector and is conventionally chosen as the z axis of a Cartesian coordinate system. In addition to the Compton shift of equations (1.1) or (1.2) equation (1.4) now contains a second term which is linearly dependent upon one component, p_z , of the electron's ground-state momentum. Thus for target electrons possessing a probability density distribution $n(\mathbf{p})$ the Compton profile, $J(p_z)$, is simply the projection of $n(\mathbf{p})$ along the scattering vector:

$$J(p_z) = \int_{p_x} \int_{p_y} n(p_x, p_y, p_z) dp_x dp_y. \quad (1.5)$$

In an isotropic system the expression is commonly rewritten in terms of the radial momentum distribution $I(p) = 4\pi p^2 n(p)$ and a scalar momentum variable, q , as

$$J(q) = \frac{1}{2} \int_{|q|}^{\infty} \frac{1}{p} I(p) dp. \quad (1.6)$$

Since $n(\mathbf{p})$ and $I(p)$ are probability distributions the Compton profile is subject to the useful normalisation rule

$$\int_{-\infty}^{+\infty} J(p_z) dp_z = \int_{-\infty}^{+\infty} J(q) dq = Z$$

the number of electrons.

In equation (1.4) it can be seen that the energy shift and the electron momentum causing it are related by a scaling factor which at low energies ($\omega_1 \ll mc^2$) takes the linear form

$$\omega_1 - \omega_2 = \Delta\omega = \frac{2\omega_1}{mc} \sin(\varphi/2)p_z. \quad (1.7)$$

These energy shifts are quite measurable because electron velocities are surprisingly high. For example, an electron at the Fermi surface of aluminium has a velocity $\sim 2 \times 10^6 \text{ m s}^{-1}$ and hence $\Delta\omega/\omega_1 \sim \frac{1}{50}$, which is easily resolved. The core electrons have higher speeds and therefore produce even greater Doppler shifts but the attraction of the experiment is that the momentum distribution $n(\mathbf{p})$ and hence the Compton profile $J(p_z)$ is dominated by the behaviour of the slower moving outer electrons which are precisely those of most chemical and physical interest. The interpretation of lineshapes will be discussed in § 2 but figure 3 illustrates the general point with a typical γ -ray Compton spectrum of aluminium. The ten core electrons contribute the broad background but the central peak is governed by the three conduction electrons. Considerable practical problems stem from the general weakness of the scattered radiation and this is exacerbated in the x-ray region by very high photoelectric absorption.

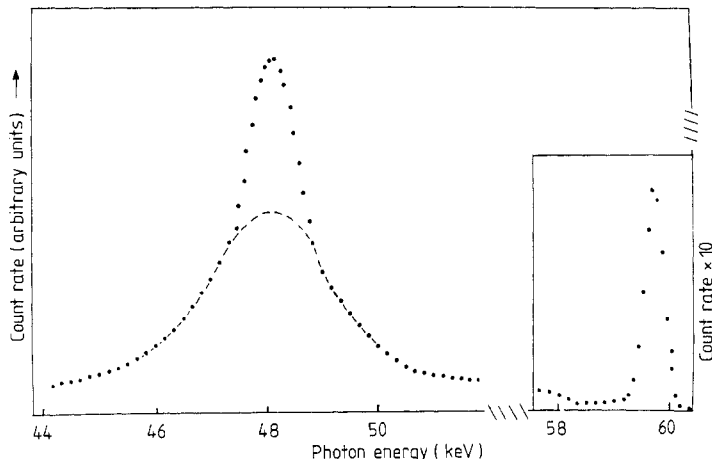


Figure 3. The spectrum of ^{241}Am γ radiation ($\omega_1 = 59.54$ keV) scattered at 171° from an aluminium sample. The count rate under the Compton peak is typically between $10\text{--}10^2$ CPS depending upon experimental conditions. The broken curve delineates the core (10 electrons) and conduction (3 electrons) contributions. The latter is an inverted parabola with a cut-off corresponding to the maximum electron momentum of 0.926 au. The experimental resolution smearing this spectrum is ~ 350 eV FWHM. Note the elastic scattering is very weak ($\sim 1\%$ of the Compton flux) and is shown on a $\times 10$ scale for clarity.

The semi-classical analysis above, which identifies the line broadening as a Doppler effect, emerges largely unscathed from a rigorous treatment, as will be established in § 3.

Although the term ‘Compton scattering’ is traditionally associated with photon-electron collisions there is no reason why similar kinematic arguments, within the same impulse approximation, should not be applied to electron-electron scattering. This process is governed by the Rutherford cross section which peaks strongly in the forward direction and drops off rapidly with increasing beam energy. However, for the scattering of low-energy electrons ($\omega_1 < 50$ keV) through small angles ($\varphi < 10^\circ$) the scattering cross section is much larger than for photons; the approximations hold and the analogous non-relativistic equations for the Compton shift and line broadening become

$$\Delta\omega = \omega_1 \sin^2 \varphi \quad (1.8)$$

$$\omega_1 - \omega_2 = \Delta\omega + p_z \left(\frac{2\Delta\omega}{mc^2} \right)^{1/2} .$$

Electron Compton scattering has played an important role in the historical development of this subject (see Bonham and Wellenstein 1977) and recently the ability to detect both scattered and recoil electrons had led to the possibility of a measurement of complete momentum distributions, shell by shell, rather than the projection implied by equation (1.5). However, not only are the experiments highly complex but also the conditions required for interpretable single scattering are highly restrictive; only gas scatterers can be used (see §4.4).

1.3. The early development of Compton scattering

Despite the fact that both the energy shift (equation (1.2)) and the Doppler broadening (equation (1.7)) increase with increasing source energy, early experiments (1930–40) were not carried out with high-energy γ rays but with low-energy ($E_\gamma < 20$ keV) x-rays.

There were several practical reasons for this: radioisotopes typically produce photon fluxes four orders of magnitude lower than x-ray tubes, the available γ -ray sources were polychromatic, and in any event there was no detector with the necessary resolution capable of performing a spectral analysis of high-energy radiation.

On the other hand, x-ray generators, tubes and crystal spectrometers had been extensively developed during the rapid expansion in x-ray studies which occurred during the 1920s and 1930s. Crystal spectrometers, focusing and non-focusing, provided high-resolution energy dispersion ($E/\Delta E \sim 10^4$) although methods of detection—film or ionisation chamber—were relatively inefficient. Long exposures were consequently the norm; in one Herculean experiment DuMond and Kirkpatrick (1937) took 2000 h to record the Compton profile of helium!

The experimental work of this period comes almost entirely from DuMond and his co-workers at the California Institute of Technology in Pasadena. Some of it is summarised in DuMond's own review (1933) which also describes the ingenious multicrystal focusing spectrograph designed to overcome the conflicting requirements of a precise angle of scattering and a large sample volume. Figure 4 is a schematic representation of the instrument and indicates the sophistication of their experimental approach. 50 calcite analysing crystals had to be individually aligned in order to attain the focusing condition. Later, faced by the weakness of the scattered radiation, Ross and Kirkpatrick (1934) invented an x-ray tube with an annular anode as a means of maximising the flux at a well-defined scattering angle; this geometry has been adopted in some recent γ -ray studies for the same reason. Eventually they standardised on the conventional fine focus x-ray tube and the curved crystal spectrometer normally associated with DuMond's name (DuMond and Kirkpatrick 1937). DuMond's results for hydrogen and helium were in good agreement with calculations based upon Hylleraas wavefunctions (Hicks 1937). For metals such as beryllium Kirkpatrick *et al* (1936) improved upon DuMond's 1929 result in confirming the free-electron behaviour of the metal.

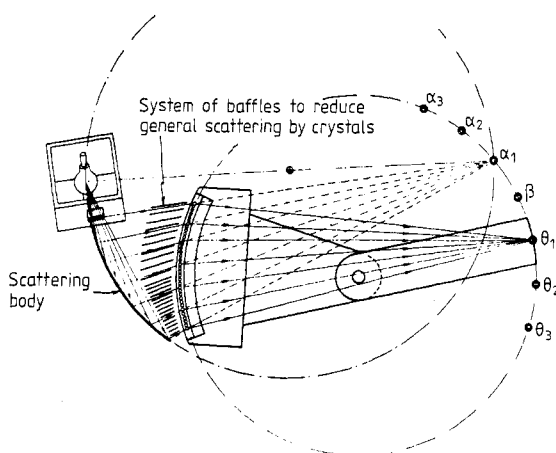


Figure 4. Schematic diagram of the multicrystal spectrograph designed and built for x-ray Compton studies by DuMond and Kirkpatrick (1930). The point source and extended scatterer lie on the circumference of the left-hand circle such that an unique angle of scattering can be maintained with a large-area scatterer. The 50 calcite analysing crystals lie on the circumference of the right-hand circle and x-rays of a given wavelength are all focused to a well-defined point on the circumference of that circle.

Electron Compton scattering measurements on helium by Hughes and Mann (1938) agreed with the DuMond and Kirkpatrick result and this was taken as a vindication of the former technique. Further electron scattering measurements by Hughes and Enns (1941) on light hydrocarbon gases attracted the attention of Coulson and Duncanson who in a series of papers (Coulson 1941a, b, Coulson and Duncanson 1941, 1942, Duncanson and Coulson 1941) showed how momentum density, and hence Compton profiles, could be calculated from LCAO wavefunctions for electrons in C—H, C—C, C=C and C≡C bonds. They showed that each bond had a characteristic anisotropic momentum distribution complementary to the familiar position space bond density distribution. Assuming transferability, an idea first applied to Compton profiles by Hicks (1940), the bonded density of a large molecule can be synthesised from fragments calculated for the more tractable small molecules. All that was required was to test these calculations against the profiles measured by Hughes and Enns. Unfortunately the agreement was poor. The experimental profiles were too broad and, with hindsight, that was probably due to multiple scattering. At the time exchange between scattered and recoil electrons was cited as a likely culprit. The upshot was that whereas the theoretical studies of Coulson's school continued undeterred, electron Compton scattering stopped and was not revived for 30 years.

A similar hiatus occurred in the x-ray work. Despite the successes DuMond's group turned their attention elsewhere. Another experimentalist did, however, bequeath an inexplicable result which eventually led to a renaissance of this work. Kappeler (1936) measured Compton profiles of gaseous neon, nitrogen, oxygen and solid lithium, carbon and sodium fluoride. He dispensed with the spectrometer and used the K-edge discontinuity of an absorber and a variable scattering angle to record successive integrated Compton intensities and reconstruct the profile by differences. In five out of the six investigations his results were in satisfactory agreement with theory, but in the case of lithium his profile was a bewildering 250% wider than the free-electron prediction! Strangely the measurement was not repeated by DuMond; in fact lithium remained unmeasured until 1965 when two independent measurements (Cooper *et al* 1965a, b) confirmed that Kappeler's result was indeed in error.

That aberrant result did serve a useful purpose; it goaded Coulson's collaborators, Donovan and March, to develop models for momentum density beyond the free-electron approximation. Both Thomas-Fermi (Coulson and March 1950, March 1954) and Wigner-Seitz (Donovan and March 1956) methods were tried and the effect of electron-electron correlations was estimated by Kilby (1963). In the end, although each refinement produced some small increase in the linewidth (the virial theorem provides a link between the total energy and the profile variance, see § 2.2 below) the enormous gap between experiment and theory remained unbridged until the experimental result was overthrown. Nevertheless Kappeler's 'red herring' had served a purpose: it is doubtful whether theoretical interest would have been sustained without it, or experimental work begun again. The disjointed nature of the historical development of momentum density studies, as illustrated by publication rates, is summarised in histogram form in figure 5.

1.4. Modern momentum density studies

1.4.1. Revival of experimental work. Whilst the re-measurement of lithium signalled the renaissance of experimental work the data that emerged were little better than those from the previous era. Although x-ray generators had improved stability, tubes

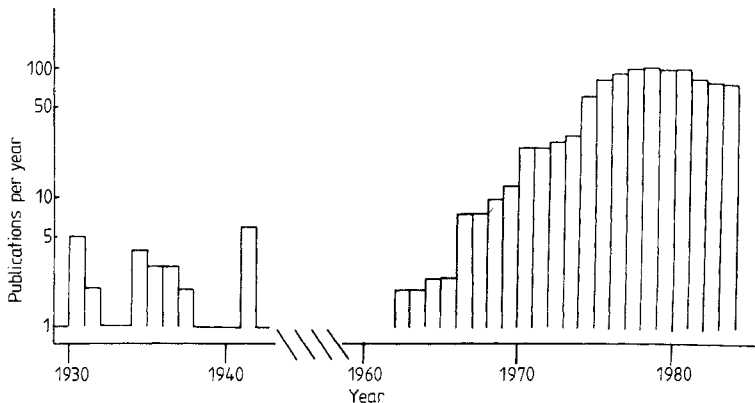


Figure 5. Histogram of annual publications in the area of Compton scattering studies of electron momentum density. A logarithmic display has been used to offset the general exponential expansion in scientific research. This emphasises the activity of DuMond's group in the decade from 1929 and Coulson's group in the early 1940s. The levelling off in the last few years probably reflects the cessation of experimental activity in North America. (Sources: Physics Abstracts, and Current Awareness profiles in Charge, Spin and Momentum Density, published by Indiana University.)

had higher power ratings and efficient scintillation counters were used, the choice of non-focusing x-ray spectrometer was still a prescription for tedious, low-resolution, experiments. There were two major drawbacks to the x-ray method. Firstly, characteristic x-ray emissions are limited to a maximum energy ~ 25 keV (Mo $K\alpha$, 17.6 keV; Ag $K\alpha$, 22.2 keV) by the commercial availability of anode material and generator voltage; therefore the range of elements which could be studied was severely restricted by photoelectric absorption of the incident and scattered beams. In practice, aluminium was the heaviest element seriously studied. Secondly, with non-focusing optics, there was insufficient intensity for monochromatisation so that the Compton spectrum was necessarily compounded of $K\alpha_1$ and $K\alpha_2$ lines and superimposed upon a bremsstrahlung background.

A third drawback is theoretical. The energy transferred to the recoil electron in an x-ray experiment is 1 or 2 keV at most and therefore the impulse approximation may be invalid. Then the measured spectrum will not be simply related to the Compton profile integral of equation (1.5). The seriousness of the failure of the approximation was calculated by Platzman and Tzoar (1965), Eisenberger and Platzman (1970) and Mendelsohn and Biggs (1973). Experimental studies charting the failure were made by Currat *et al* (1971b) and more recently by Weiss *et al* (1977). The validity of the impulse approximation is discussed in § 3.1; in general, the corrections are mercifully small. Although an awareness of the problem promoted a preference for higher energy γ -ray experiments it did not by itself spell the end of x-ray work.

It was recognised, at an early stage, that the Compton experiment afforded a unique opportunity to observe correlations in the electron gas. Whilst the earliest attempts were too crude (Cooper *et al* 1965a, b), Eisenberger *et al* (1972) succeeded in demonstrating the effect in sodium. Their results, reproduced in figure 6, show that the electrons are promoted to states above the Fermi surface as predicted by Daniel and Vosko (1960). Quantitative agreement only becomes good when core orthogonalisation and electron-ion interactions are included in the theory (Pandey and Lam 1973). Similar effects have been demonstrated in aluminium (Cooper *et al* 1974).

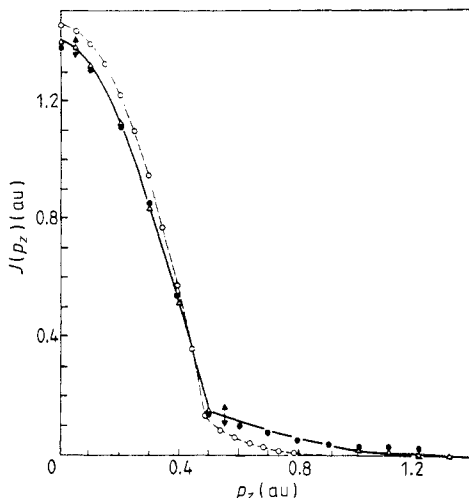


Figure 6. The x-ray Compton profile of sodium. The experimental results (Δ) and the prediction (\circ) of an interacting electron gas model are taken from the work of Eisenberger *et al* (1972). The second theoretical curve (\bullet) taken from Pandey and Lam (1973) includes core orthogonalisation and this clearly improves the agreement with experiment above the Fermi momentum.

The limitations on experimental work are less forbidding for simple organic molecules than crystalline solids. Binding energies are small, i.e. the impulse approximation will not be infringed, and photoelectron absorption will be low, i.e. intensities will not be prohibitively attenuated. Furthermore there is no shortage of systems to study or calculations with which to compare them. Eisenberger and Marra (1971) carried out a series of measurements on liquid hydrocarbons which were successfully analysed in terms of invariant bond profile contributions, supporting the idea of transferability. This approach was investigated theoretically by Epstein (1970) and Epstein and Lipscomb (1970) for hydrocarbons and boron hydrides. Their LMO calculations questioned the universality of bond transfer but the comprehensive work of first Epstein (1973) and then Smith and Whangbo (1974) did much to establish the advantages of interpreting chemical bonding from a momentum viewpoint (see also § 2.2). This area has been recently reviewed by Williams and Thomas (1983).

Unfortunately measurements on liquids and gases introduce an averaging over orientations which dilutes the information content of the experiment. However liquid samples, as opposed to single crystals, are easily available and that led to the choice of water for an international measurement project. The results (Williams 1976) of both x-ray and γ -ray studies showed that Compton profiles could then be reproduced, on an absolute basis to an accuracy of 2%. This reassuring result helped to boost confidence in the experimental method. The major problem that it highlighted was one of parasitic multiple scattering degrading the data. Experimentalists had tended to respond to the weakness of the scattering by increasing the volume of the scatterer. This produced an unconscionable amount of multiple scattering in samples with low absorption. The problem—up to 50% of the scattering could be double Compton scattering which has a characteristically broader spectrum than the single scattering—had been predicted by DuMond (1930) and then conveniently forgotten until Phillips and Chin (1973) studied its effect in beryllium. The matter was quickly tackled and a flurry of activity led to a satisfactory method of correction by Monte Carlo computer

simulation (see, for example, Felsteiner *et al* 1974) as an alternative to the use of ultra-thin samples or empirical extrapolation procedures.

1.4.2. Trends and innovations. The change which led to a wholescale improvement in the quality and quantity of Compton work was undoubtedly the replacement of low-energy x-ray spectrometers by high-energy ($E_\gamma > 50$ keV) γ -ray spectrometers. This was made possible by the technical development of energy-dispersive detectors based on doped, or later intrinsic, single-crystal germanium. At high energies the Compton spectrum energy spread is much broader than the resolution of the detector so that simultaneous detection and analysis of the radiation is possible. This contrasts sharply with the slow step-by-step mode of analysis of the flat crystal x-ray spectrometer; indeed, without this advantage radioisotopes, with a flux typically three orders of magnitude less than an x-ray tube, could not be used. A further benefit of the transition to higher energies is that of higher energy transfers to the target and hence greater security in the impulse approximation. The disadvantage is that the resolution is rather poor.

The method was established by Eisenberger and Reed (1972) with a series of measurements on gases and the first comparative review was published by Reed (1976). A brief glance at the γ -ray results presented in later sections of this review compared with the x-ray work reviewed earlier (Cooper 1971) clearly establishes the progress which has followed from this transition.

The past decade also saw the revival of electron Compton scattering experiments: Wellenstein and Bonham (1973) measured helium and this was quickly followed by other measurements. An understanding of multiple scattering and exchange effects, absent at the time of Hughes and Enns, led to a reliable interpretation of the data. In the same year (1973), the more ambitious electron coincidence experiment was carried out on argon by Weigold *et al* and these powerful but extremely complicated experiments continue (§ 4.4).

This introduction has surveyed the development of the subject to within one decade of the present. Only key references have been given because an exhaustive bibliography of the period exists in the monograph edited by Williams (1977) which also includes a comparative review of the related positron annihilation experiment.

For the remainder of this article the conventional system of atomic units (au) will be adopted, i.e. $e = m = \hbar = 1$, $c = 137$: the symbols will be included in equations where necessary to clarify the meaning. In this system the unit of energy is 27.21 eV (i.e. 2 Hartree), the unit of length is 5.29×10^{-11} m (i.e. the Bohr radius) and the unit of momentum is 1.99×10^{-24} kg m s⁻¹.

2. Electron momentum density

The density distribution is central to an understanding of the behaviour of electrons in quantum systems. It is the observable through which orbitals and bonds are visualised; together with the Fermi surface in metals it provides the insight necessary for the development of an intuitive understanding of physics and chemistry. The wavefunction may be the traditional working medium for quantum systems, but it remains one step from the reality of the density distribution. The modern density functional approach (Smith 1980) reflects the shift in emphasis from the former to the latter: the fundamental role of the density is based on the theorem of Hohenberg and

Kohn (1964) which states that the non-degenerate ground state of an electronic system is a unique functional of $\rho(r)$.

Traditionally the charge density distribution is studied through elastic scattering experiments performed within the Born approximation. The form factor, $f(\mathbf{k})$, is deduced from the scattering cross section:

$$f(\mathbf{k}) = \int \rho(\mathbf{r}) \exp(-i\mathbf{k} \cdot \mathbf{r}) d\mathbf{r} \quad (2.1)$$

where

$$|\mathbf{k}| = \frac{2\pi \sin \theta}{\lambda}$$

X-ray and electron diffraction studies of crystalline solids are described in numerous texts: see Becker (1980) for a comprehensive review of contemporary charge density determination and interpretation, or Weiss (1965) for a more concise text that also includes an introduction to momentum density measurements. It appears wholly natural to think and work in terms of position space densities, a switch to the momentum representation seems perverse and hardly justified by the mere fact that momentum densities are accessible to measurement through the Compton effect. Only in delocalised systems such as electrons in metals is there any hint that a description in terms of momentum, \mathbf{p} , or at least wavevector, \mathbf{k} , might be preferable. Yet by adopting the complementary viewpoint a real insight can be gleaned into the behaviour of electrons in isolated atoms and molecules as well as in condensed matter.

The essential point is that the peaks in $n(\mathbf{p})$, the momentum density, and hence in $J(p_z)$, the Compton profile, originate from the slowly moving outer electrons which are precisely those of physical and chemical interest. This was indicated in the spectrum of aluminium shown in figure 3 and is demonstrated more clearly in figure 7 where

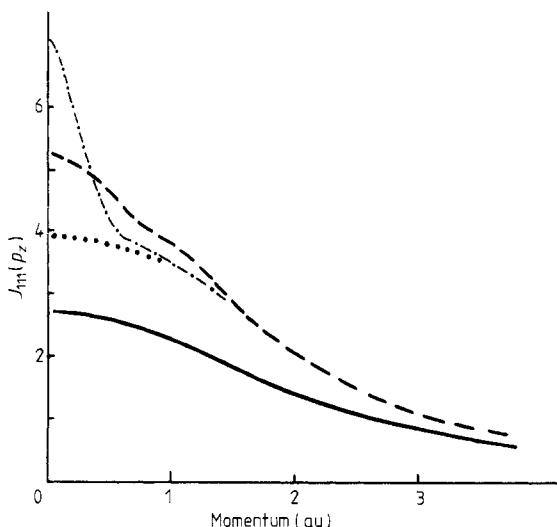


Figure 7. The free-atom and solid-state Compton profiles of iron. The free-atom profile (---), taken from Biggs *et al* (1975), is separated into $1s^2 2s^2 2p^6 3s^2 3p^6$ core (—) and $3d^6 4s^2$ valence contributions (· · ·). The solid-state profile for the [111] crystal orientation is denoted by (—) and is taken from the LCAO calculation of Rath *et al* (1973).

the Compton profiles of free-atom and crystalline iron are shown. Not only do the eight 3d⁶4s² electrons dominate the 18 core electrons in the low momentum profile but also the peak value for the solid is very different (~30% less) than that for the free atom. Moreover it would vary by small but discernible amounts (a few per cent) from one band theory model to another: it is only in the high momentum tails, where core contributions dominate, that the curves merge. In contrast, x-ray form factors calculated on the basis of the same free-atom and solid-state models differ so little—2% at the first Bragg peak and less at higher $\sin \theta / \lambda$ —that graphical presentation is inappropriate: they are listed for comparison in table 1. Even in scattering experiments with gaseous targets (Bonham and Fink 1980), where the continuous form factor curve can be determined, the intrinsic sensitivity to the valence density distribution is less than that of the Compton profile.

Table 1. Free-atom and solid-state form factors for iron.

Reflection	Solid-state form factor†			Free-atom relativistic Hartree-Fock form factor‡
	Core	Valence	Total	
000	18	8	26	26
110	15.14	3.24	18.38	18.44
200	13.14	1.94	15.08	15.24
211	11.69	1.35	13.04	13.14
220	10.62	0.93	11.55	11.62
310	9.80	0.62	10.42	10.53
222	9.17	0.45	9.62	9.67
321	8.68	0.30	8.98	9.02

† Taken from Doyle and Turner (1968).

‡ Taken from Tawil and Callaway (1973).

2.1. Wavefunctions in momentum space

The Schrödinger equation, which is normally solved to yield $\psi(\mathbf{r})$ and hence $\rho(\mathbf{r})$, could equally well be re-cast to yield the wavefunction $\chi(\mathbf{p})$ and hence $n(\mathbf{p})$, where $|\chi(\mathbf{p})|^2 = n(\mathbf{p})$. In that case it would be written

$$(p^2/2m - E)\chi(\mathbf{p}) + V(p)\chi(\mathbf{p}) = 0. \quad (2.2)$$

This is an awkward integral equation because $V(p)$ is the Fourier transform of the Coulomb potential $V(r)$. In this form it has been solved for hydrogen (Fock 1935), helium (McWeeny and Coulson 1949) and the hydrogen molecular ion (McWeeny and Coulson 1949). The problems are daunting and direct solutions for more complex systems are considered impracticable. However, Dirac (1926) first pointed out that an indirect approach followed from the Fourier transform relationship between $\psi(\mathbf{r})$ and $\chi(\mathbf{p})$, i.e. determine $\psi(\mathbf{r})$ by an habitual method and then transform to give

$$\chi(\mathbf{p}) = \left(\frac{2\pi}{\hbar} \right)^{-3/2} \int \psi(\mathbf{r}) \exp \left(-i \frac{\mathbf{p} \cdot \mathbf{r}}{\hbar} \right) d\mathbf{r}. \quad (2.3)$$

Where $\psi(\mathbf{r})$ has an algebraic form, the transformation can be obtained analytically. Podolsky and Pauling calculated the transforms for the hydrogenic and Slater type

(nodeless) orbitals in 1929. For example, if

$$\psi(r) = \left(\frac{\gamma^3}{\pi}\right)^{1/2} \exp(-\gamma r)$$

then

$$\chi(p) = \left(\frac{8\gamma^5}{\pi^2}\right)^{1/2} \frac{1}{(p^2 + \gamma^2)^{3/2}}$$

The larger γ the more contracted $\psi(r)$ and $\rho(r)$ and the more expanded $\chi(p)$ and $n(p)$. This aspect of complementarity is, of course, summarised by the Heisenberg uncertainty principle; for the above wavefunctions the calculation of the standard deviations yields $\sigma_r \sigma_p = \sqrt{3\hbar}$. Just as there is a shell structure in position space whereby different one-electron orbitals are characterised by increasing values of $\langle r^2 \rangle$ from K through L to M, etc, so there is a reciprocal tendency in momentum space with $\langle p^2 \rangle$ decreasing from K to M as is illustrated in figure 8 for argon. Similarly as $\langle r^2 \rangle$ decreases across a row of the periodic table, so $\langle p^2 \rangle$ increases (see figure 9).

If the wavefunction is assumed to be separable into radial and angular parts the Dirac-Fourier transformation preserves the symmetry and is independent of spin, i.e. only the radial part needs to be transformed. Thus, in the Hartree-Fock scheme where the wavefunction of an N -electron system is written as the antisymmetrical determinant of the one-electron wavefunctions $\psi_i(r_i)$ (or a multiconfigurational sum of such determinants) the momentum wavefunction is the determinental product of the individually

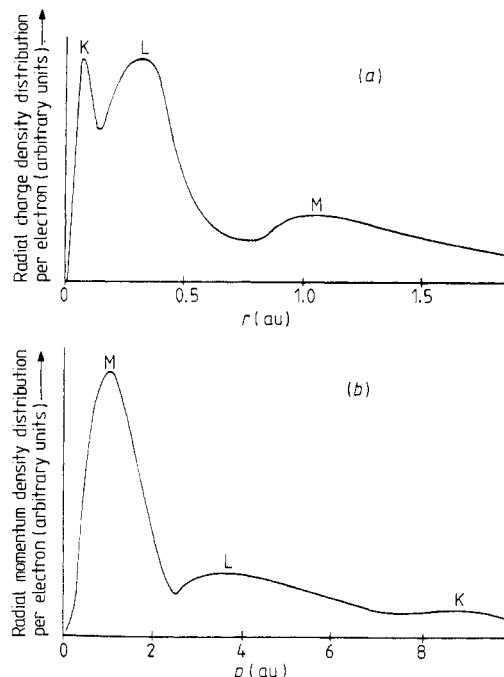


Figure 8. The radial electron density distributions $4\pi r^2 \rho(r)$ and $4\pi p^2 n(p)$ in argon, (a) in coordinate space and (b) in momentum space: both representations show the characteristic K, L and M shell structure. The atomic unit (au) of length is the Bohr radius (0.53×10^{-10} m) and the atomic unit of momentum is 2.0×10^{-24} N s. The vertical scales are arbitrary.

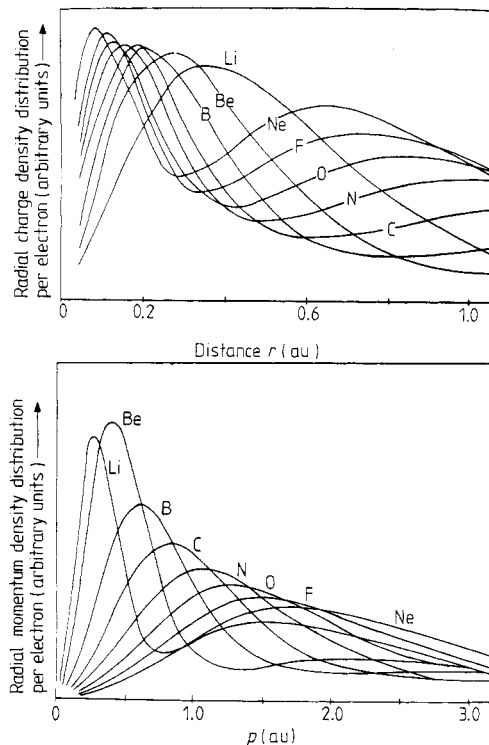


Figure 9. The radial electron density distribution (a) $4\pi r^2 \rho(r)$ and (b) $4\pi p^2 n(p)$ for elements in the first row of the periodic table. The effect of the Fourier relationship between coordinate and momentum space distributions is evident in the complementary nature of these curves. Densities were calculated from the wavefunctions of Clementi (1965) and unpublished tabulations provided by P J Brown and A Harvey. The vertical scales are arbitrary.

transformed orbitals $\chi_i(p_j)$. All the familiar techniques used to obtain real space wavefunctions, taken one stage further, can be used to produce momentum space wavefunctions of identical quality.

The properties of the ubiquitous Fourier transform are well catalogued and it is easy to develop intuition in the reciprocal space. For example, the incorporation of relativistic effects into the wave equation through the introduction of a velocity-dependent mass sucks electrons in towards the nucleus: the result is that $\psi(r)$ contracts and $\chi(p)$ expands (Mendelsohn *et al* 1973). The effect is most pronounced for the core electrons of heavy elements but the effects propagate out through the shells because of the orthogonality requirement incumbent on the one-electron orbitals. For Pb, $J(0)$, the Compton peak, drops by $\sim 6\%$ and the high momentum tail increases by $\sim 12\%$. The changes in the form factor at measurable values of $\sin \theta/\lambda$ are an order of magnitude smaller.

2.2: Momentum and kinetic energy in bonding

2.2.1. The virial theorem and cohesion. In equation (2.2) the momentum space wave equation, the potential operator, $V(p)$, is an intractable integral whereas the kinetic energy operator is a simple multiplicative factor. The expectation value of kinetic

energy is just

$$\frac{1}{2m} \int p^2 n(p) dp$$

which is also directly obtainable as the second moment of the Compton profile:

$$\frac{3}{2} \int_0^\infty q^2 J(q) dq \quad \text{in an isotropic system}$$

or

$$\sum_{i=x,y,z} \frac{1}{m} \int_0^\infty p_i^2 J(p_i) dp_i \quad \text{for an anisotropic system.} \quad (2.4)$$

Kinetic energy is important because, for systems subject only to Coulomb interactions, the virial theorem equates it to the total electronic energy (with a change in sign). Nuclear motion can be ignored since the associated kinetic energy is many orders of magnitude lower than that of the electron distribution. Thus total energy minimisation as a variational principle for the refinement of $\psi(r)$ corresponds to kinetic energy maximisation. The virial equality only holds for the exact solution but, generally speaking, the better the wavefunction the broader the Compton profile because the greater second moment equates with a bigger kinetic energy (equation (2.2)) and thus a lower total energy. This simple argument explains why the Compton profile of metallic iron in figure 7 is broader than the free-atom profile; the larger variance represents the cohesive energy.

Roux and Epstein (1973) suggested that the departure from virial equality can be used as a measure of the quality of a model's momentum representation. This test often exposes inadequacies in the calculation of $n(p)$. Weiss (1978) used the virial relationship to deduce cohesive energies from the Compton profiles predicted by band theories: in some instances the inadequacy of the band model was exposed by the fact that the cohesive energy not only had the wrong magnitude but also the wrong sign. Whilst it is a keen test of theory the determination of cohesive energies experimentally by this route is very difficult (Holt and Cooper 1980) because the p^2 weighting of the high momentum tails magnifies systematic errors alarmingly.

2.2.2. Diatomic bonds. The role of kinetic energy, and by implication momentum, in bond formation has been studied in detail by Feinberg and Rudenberg (1971) and Epstein and Tanner (1977) for diatomic molecules. It is instructive to compare their approach with the conventional one.

A simple model wavefunction for a molecular orbital might be written as a linear combination of atomic orbitals, $\psi_a(\mathbf{r})$, as

$$\psi(\mathbf{r}) = (2 + 2S)^{-1/2} [\psi_a(\mathbf{r}) + \psi_a(\mathbf{r} - \mathbf{R})] \quad (2.5)$$

where \mathbf{R} is the internuclear separation and S is the overlap integral. This expression immediately produces a bond density from the overlap term

$$\frac{\psi^*(\mathbf{r})\psi(\mathbf{r} - \mathbf{R})}{1 + S}$$

in the internuclear region. The corresponding momentum density is

$$\chi^2(\mathbf{p}) = \chi_a^2(\mathbf{p})(1 + \cos \mathbf{p} \cdot \mathbf{R})(1 + S)^{-1} \quad (2.6)$$

where $\chi_a(\mathbf{p})$ is the Fourier transform of $\psi_a(r)$. Thus in momentum space, which is single-centred, the build up in charge density is in the direction perpendicular to the bond, i.e. when $\mathbf{p} \cdot \mathbf{R} = 0$ and the density distribution is modulated with period $2\pi/R$. Feinberg and Rudenberg charted the process of bond formation by calculating energy expectation values as the interatomic separation reduces from infinity to R . They showed that the increase in kinetic energy which must accompany total energy minimisation is derived from an isotropic contraction of the charge density around each nucleus. This effect is as important as the more familiar lowering of potential energy through the accumulation of charge in the internuclear region.

In practice, because experiments cannot be performed on isolated or orientated molecules, it is difficult to observe these effects: measurements on gases and liquids only yield the spherical part of the bonded density distribution. There is rarely a unique direction in crystalline solids and the anisotropy is greatly diminished by the inherent averaging. A notable exception is the γ -ray study of single-crystal urea by Reed *et al* (1978) in which the anisotropic C=O bond momentum distribution was studied.

2.2.3. Solids. In a three-dimensional solid the full force of band theory is brought to bear upon the calculation of energies, Fermi surfaces, etc. The calculation of the momentum density, which has as a prerequisite the calculation of the band wavefunctions, is a more daunting prospect.

For alkali metals the free-electron approximation may be a reasonable starting point: that yields a uniform spherical density of states in k and hence p space ($p = \hbar k$ in this approximation):

$$n(\mathbf{p}) = \text{constant for } |\mathbf{p}| \leq p_F$$

$$n(\mathbf{p}) = 0 \quad \text{otherwise.}$$

This produces the characteristic parabolic Compton profile of figure 6. The introduction of the lattice potential destroys the identification of \mathbf{p} with \mathbf{k} and produces high momentum components $\mathbf{p} = \hbar(\mathbf{k} + \mathbf{G})$ where \mathbf{G} is a reciprocal lattice vector. The momentum eigenfunctions are then given by Fourier inversion of the Bloch functions, $u_k(\mathbf{r}) \exp(i\mathbf{k} \cdot \mathbf{r})$, (dropping $\hbar = 1$) as

$$\chi(\mathbf{k} + \mathbf{G}) = \int u_k(\mathbf{r}) \exp(-i\mathbf{G} \cdot \mathbf{r}) d\mathbf{r}.$$

For a nearly free-electron metal the Wigner-Seitz model, for example, predicts a conduction electron Compton profile consisting of the central parabola plus a series of much weaker parabolas centred at momenta corresponding to projections of the non-zero reciprocal lattice vectors onto the z direction.

The picture is further complicated by the introduction of the electron-electron interaction; its effect, which has been calculated in the random phase approximation by Daniel and Vosko (1960), is to promote some electrons to states just above the Fermi surface. The discontinuity in $n(\mathbf{p})$ at $\mathbf{p} = \mathbf{P}_F$ remains although it is reduced in height according to the parameter $e^2/\pi^2 P_F$, i.e. the interactions are progressively screened out in high-density electron gases. The correlations produce a characteristic tail on the Compton profile as shown in figure 6. This effect cannot be observed in the corresponding positron annihilation experiment: it is neutralised by the momentum-

dependent enhancement of the annihilation rate below the Fermi surface, and its suppression above it (Kahana and Carbotte 1965).

For most solids the free-electron model is not a good starting point and it is necessary to extract and transform the wavefunctions obtained by one of the standard band structure methods. This is not trivial and the wavefunction is inevitably obtained with lower accuracy than the band structure. However, there is a more fundamental objection: the calculations are invariably carried out in the local density approximation where Hohenberg and Kohn (1964), Kohn and Sham (1965) and Sham and Kohn (1966) have shown that only the charge density and the total energy can be precisely deduced. The solutions to the Kohn-Sham equations are pseudo-wavefunctions which require correction if they are transformed to produce momentum eigenfunctions. Bauer (1983) has recently shown how such a correction can be calculated within the framework of the local density approximation. The importance of this correction is discussed in § 5 in connection with transition-metal results.

2.3. Relationships between observables and density functions—the reciprocal form factor

In diffraction experiments the form factor, $f(\mathbf{k})$, is derived from the experimental scattering cross section and $\rho(\mathbf{r})$ reconstructed by transformation (equation (2.1)). In Compton scattering experiments one-dimensional projections of $n(\mathbf{p})$ —the directional Compton profiles—are derived from the experimental scattering cross sections (equation (1.5)) and $n(\mathbf{p})$ reconstructed by back projection (see § 2.5 below). Thus both density functions are, in principle, accessible. The Fourier transformation relates the wavefunctions, not the density distributions, and care must be exercised in applying complementarity arguments to the latter rather than the former.

The inter-relationships become clearer if, by analogy with equation (2.1) a reciprocal form factor, $B(\mathbf{r})$, is defined as

$$B(\mathbf{r}) = \int n(\mathbf{p}) \exp(-i\mathbf{p} \cdot \mathbf{r}) d\mathbf{p}. \quad (2.7)$$

This quantity, alternatively called the ‘ B function’, was introduced by Pattison *et al* (1977b); its Cartesian components are simply Fourier transforms of the directional Compton profiles:

$$\begin{aligned} B(0, 0, z) &= \iiint n(p_x, p_y, p_z) \exp(-ip_z z) dp_x dp_y dp_z \\ &= \int J(p_z) \exp(-ip_z z) dp_z. \end{aligned} \quad (2.8)$$

The similarity between the form factors is emphasised by rewriting them as autocorrelation functions:

$$f(\mathbf{k}) = \int \chi^*(\mathbf{p}) \chi(\mathbf{p} + \mathbf{k}) d\mathbf{p} \quad (2.9)$$

$$B(\mathbf{r}) = \int \psi^*(\mathbf{r}') \psi(\mathbf{r}' + \mathbf{r}) d\mathbf{r}'. \quad (2.10)$$

Both functions are subject to the normalisation rule $f(0) = B(0) = Z$, the number of electrons per atom.

The array of relationships is shown in a form that emphasises the symmetry between position and momentum space observables in figure 10; this diagram is attributed to Weyrich *et al* (1979).

The dominance of the core electron contribution to $f(\mathbf{k})$ can be interpreted (equation (2.9)) by noting that only electrons with high momentum components, i.e. core electrons, contribute to the overlap integral at intermediate and high \mathbf{k} values; bonding effects involve electrons with low momenta for which the overlap is significant only at small \mathbf{k} , usually around or below the first Bragg peak. In the reciprocal form factor (equation (2.10)) core electron overlap is restricted to small displacements, \mathbf{r} ; at intermediate and large displacements $B(r)$ is dominated by the valence electrons. In density functional language $B(r)$ involves off-diagonal components of the single-particle density matrix $\Gamma(\mathbf{r}|\mathbf{r}')$ and $f(\mathbf{k})$ is connected with off-diagonal terms of the inverse density matrix $\Gamma(\mathbf{p}|\mathbf{p}')$. Other combinations of terms can be studied by combining scattering and diffraction, e.g. by measuring the Compton scattering from standing wave fields created at the Bragg condition in crystals (Schülke 1981, 1982, 1983).

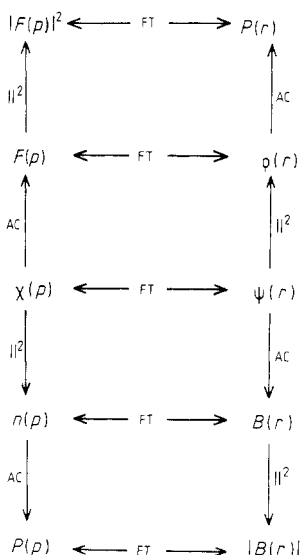


Figure 10. The relationship between various electron density functions in momentum and position space for one-electron wavefunctions. Fourier transformation is abbreviated FT and the double-headed arrows indicate reversibility. The operations of autocorrelation (AC) and squaring the modulus ($\| ^2$) are irreversible. The symbols have their usual meanings; $P(r)$, which is generally known as the Patterson function, and $P(p)$ are pair correlation functions.

The dominance of core over valence electrons in the form factor $f(k)$ has already been illustrated in the case of iron in table 1 where the free-atom and solid-state form factors are virtually identical above the first Bragg reflection. By contrast the reciprocal form factor for the free atom (Biggs *et al* 1975) and the metal (Rath *et al* 1973) diverge notably away from the origin ($z > 1 \text{ \AA}$, say) as is clear from figure 11. Differences ascribable to solid-state effects are evident through the intermediate and high z regions.

2.3.1. Some properties of the reciprocal form factor. The $B(r)$ representation possesses several advantages over the Compton profile from which it is derived, although the

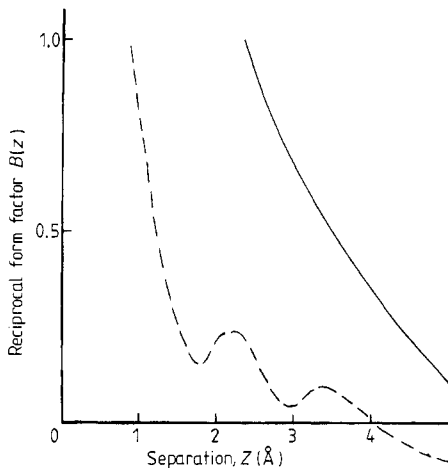


Figure 11. The reciprocal form factor of free-atom (—) and crystalline (---) iron. The data are derived from the same sources as for figure 7. Both curves coincide at $Z = 0$ since $B(0) = 26$ electrons for iron. Away from the origin they diverge strongly.

ideal information content is the same. On the practical side any slowly varying residual systematic errors in the data are restricted to the least interesting region, that near the origin of the $B(r)$ function. Furthermore the resolution broadening of the spectrum which convolutes the Compton profile is manifest in the reciprocal form factor as a more tractable multiplicative damping factor. In addition to these superficial advantages there is the considerable, albeit intangible, benefit of keeping the interpretation of experimental results on the more familiar territory of position space. Both the sign and size of the function convey information about bonding in a manner which can be more readily understood by chemists and physicists than the momentum space equivalent.

In crystalline solids the application of Bloch's theorem leads to some important properties of the reciprocal form factor. If the overlap integral (equation (2.10)) is written as a sum over the k states in each band ν , then

$$B(\mathbf{r}) = \sum_{\text{occupied bands}} \int \psi_{\nu,k}^*(\mathbf{r}') \psi_{\nu,k}(\mathbf{r} + \mathbf{r}') d\mathbf{r}'. \quad (2.11)$$

Schülke (1977, 1978) showed that when this expression is evaluated for any $\mathbf{r} = \mathbf{R}_L$, a translation vector of the real lattice, it reduces to

$$B(\mathbf{R}_L) = \frac{2}{V_{BZ}} \int_{BZ} n_\nu(k) \exp(-ik \cdot \mathbf{R}_L) dk \quad (2.12)$$

where the integration is over the volume, V_{BZ} , of the Brillouin zone and $n_\nu(k)$ simply describes the occupancy of the k th state in the ν th band, i.e. it drops from unity to zero at the Fermi surface.

This result, which is valid within the one-electron approximation, has two important consequences. Firstly, in a conductor the coefficients $B(\mathbf{R}_L)$ form a Fourier series expansion of the function $n(k)$ which simply defines the Fermi surface. This result is equivalent to the theorem of Lock *et al* (1973) which is used to reconstruct Fermi surfaces from positron annihilation angular correlation data (see also West 1980). In that formulation the angular correlation profiles are folded (convoluted) directly and

it must be assumed that the positron wavefunction can be taken to be constant. Then the high resolution of the positron lineshape (much higher than the attainable resolution of the Compton lineshape) essentially means that many high-order coefficients $B(R_L)$ can be determined (the damping function is very broad) and a good reconstruction of the Fermi surface obtained. Reconstructions have been made with Compton data (Schülke (1978) on lithium) but the resolution is limited. At a more modest level the measured low-order coefficients, which are accurately predicted from the known Fermi topology, can provide a check on the validity of the one-electron approximation. Any discrepancy will be related to the height of the break in the occupation function $n(k_F)$ at the Fermi surface.

For insulators there is no Fermi surface and Fourier inversion of equation (2.12) should produce a flat distribution, as indeed it does for Compton data. For positron data the discrepancies are attributable to the non-uniform positron wavefunction (Beardsley *et al* 1975). Rewriting equation (2.12) in terms of Wannier functions $\varphi(r)$ yields

$$B(R_L) = \sum_{\text{occupied bands}} \int \varphi_\nu^*(\mathbf{r}') \varphi_\nu(\mathbf{R}_L + \mathbf{r}') d\mathbf{r}' \quad (2.13)$$

and since Wannier functions at different lattice sites are orthogonal, all $B(R_L)$ are equal to zero (again within the one-electron approximation). The main value of this result is not in the determination of lattice parameters but in the checks on experiment and theory that it affords for insulators. In the case of experimental data the zero crossing points of $B(r)$ will not be shifted by the resolution damping factor and their correct location corroborates the data processing procedure; see, for example, Pattison and Schneider (1978) on graphite and diamond. In the case of model calculations in which the wavefunctions are only approximately orthogonalised the location of lattice zeros is a test of the extent of the orthogonalisation (see Pattison and Weyrich 1979, Mackinnon and Kramer 1980). This is exemplified in figure 12 (taken from Pattison and Weyrich) which shows $B_{111}(z)$ of LiH for calculations with orthogonalisation up to fourth (Berggren 1975) and forty-second (Aikala 1976a, b) nearest neighbours. Only the latter shows correctly located zeros.

Information about the bonding is obviously contained in the sign and size of the oscillations between the lattice zeros of the reciprocal form factor. Here an elementary model is sufficient to indicate the nature of the interpretation. Consider the simple LCAO diatomic bond of equation (2.4). The corresponding reciprocal form factor can be written as

$$B(\mathbf{r}) = \frac{(1+S)^{-1}}{2} [2B_a(\mathbf{r}) \pm B_a(\mathbf{r} - \mathbf{R}_B) \mp B_a(\mathbf{r} + \mathbf{R}_B)] \quad (2.14)$$

where $B_a(\mathbf{r})$ is formed from $\psi_a(\mathbf{r})$ according to equation (2.10) and the ambiguity of sign covers both bonding (+) and antibonding (-) interactions. Since $\psi_a(\mathbf{r})$ is confined to the region $|\mathbf{r}| < \frac{1}{2}\mathbf{R}_B$, $B_a(\mathbf{r})$ will be restricted to a region only slightly larger. Apart from the origin the reciprocal form factor will peak around $\mathbf{r} = \pm \mathbf{R}_B$, i.e. at the bond length. The sign of the extremum will depend on the nature of the wavefunctions but for 1s functions, for example, a positive maximum will correspond to bonding and a negative minimum to antibonding.

2.3.2. Reconstruction of the momentum density distribution. The derivation of the B function also forms an important intermediate step in the reconstruction of the full

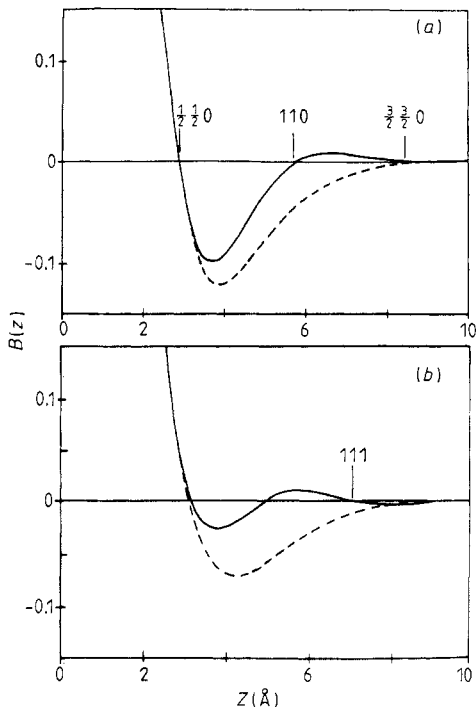


Figure 12. Theoretical reciprocal form factors for (a) [110] and (b) [111] directions in LiH. The broken curves are obtained from Compton profiles (Berggren 1975) derived from wavefunctions with orthogonalisation up to the fourth shell of neighbours. The full curves are from Aikala (1976a, b) where orthogonalisation up to the forty-second shell has been attained. The position of the zeros required by orthogonality are indicated and the difference between the two calculations in this respect is evident (from Pattison and Weyrich 1979).

three-dimensional momentum distribution function, $n(\mathbf{p})$. The method used is an adaptation (Hansen 1980) of one devised by Mijnarends (1974, 1977, 1979) for positron annihilation data. The first step is to construct the three-dimensional $B(\mathbf{r})$ function from a set of the $B(z)$ directional functions obtained by transformation of the Compton profiles. If the Compton profiles have been measured for a number of independent directions \mathbf{t} the reciprocal form factor, $B(\mathbf{t})$, can be written as an expansion over an equal number of lattice harmonic functions $h_j(\mathbf{t}/\mathbf{t})$

$$B(\mathbf{t}) = \sum_j b_j(\mathbf{t}) h_j(\mathbf{t}/\mathbf{t}) \quad (2.15)$$

and the simultaneous equations solved for the functions $b_j(\mathbf{t})$. Now if $n(\mathbf{p})$ is expanded in the same lattice harmonics

$$n(\mathbf{p}) = \sum_j n_j(\mathbf{p}) h_j(\mathbf{t}/\mathbf{t}) \quad (2.16)$$

the terms $n_j(\mathbf{p})$ are given in terms of spherical Bessel functions $J_{l_j}(pt)$

$$n_j(\mathbf{p}) = \frac{i^{l_j}}{\pi} \int_0^\infty b_j(t) J_{l_j}(pt) t^2 dt \quad (2.17)$$

where l_j is the order of the lattice harmonic h_j . In the cubic system the density is usually expanded up to the fourth harmonic; if the reciprocal form factor has been determined for more directions than this a least squares procedure can be used to refine the functions $b_j(t)$. The most ambitious study of this kind to date, as yet unpublished, is on LiOH. Preliminary accounts have been reported by Heuser and Weyrich (1981) and recently the full study was presented at the 1984 International Union of Crystallography Congress (Heuser-Hofmann and Weyrich 1984). In a marathon series of experiments 23 independent data sets were collected, a total of $\sim 10^9$ photons recorded in $\sim 10^7$ s from which all the sections of $n(\mathbf{p})$ and $B(\mathbf{r})$ have been reconstructed. The Li—OH bonds are parallel to the tetragonal axis and the build up of momentum density perpendicular to this direction is readily evident. Such accuracy and patient endeavour is unlikely to be equalled. A reconstruction of the momentum density in lithium from 10 directional Compton profiles measured on a focusing x-ray (Mo K α) spectrometer was reported at the same conference (Schülke *et al* 1984). The work of Hansen *et al* (1984) on the reconstruction of the momentum density in silicon is discussed in § 5.

In summary, the introduction of the reciprocal form factor as a meeting ground for experiment and theory has provided a refreshing impetus to the interpretation of data, especially for systems with localised electrons. The fact that the function involves real space variables as opposed to their momentum space counterparts means that it is of interest in its own right as well as a staging post *en route* to the momentum distribution function.

3. Theory of Compton scattering

In scattering experiments the total flux into the detector can be measured and the differential scattering cross section, $d\sigma/d\Omega$, deduced. Additionally when inelastic processes are involved the spectral distribution can be plotted and the double differential scattering cross section, $d^2\sigma/d\Omega d\omega$, obtained ($\omega = \omega_1 - \omega_2$ is the energy transfer—refer to figure 1 for the nomenclature). Compton scattering experiments are capable of yielding both quantities, but it is only under certain conditions that $d^2\sigma/d\Omega d\omega$ can be transformed into the Compton profile, $J(p_z)$, given by equation (1.5).

Compton scattering will not occur at all from electrons with binding energies, E_B , greater than the energy transfer ω . At energies below or around this threshold plasmon and Raman transitions may be excited (Suzuki 1982) but it is doubtful whether information about the ground-state momentum distribution $n(\mathbf{p})$ can be extracted. Even at higher energies it is not obvious *a priori* that the Compton profile can be disentangled from the differential scattering cross section in the manner presumed in § 1. The object of this section is firstly the assessment of those approximations which are essential to the establishment of that link and, secondly, the introduction of important non-classical effects. The actual derivations, especially in the full quantum electrodynamical theory, are complicated and will certainly be avoided. The quantisation of the field and the inclusion of electron spin (for a stationary electron) is dealt with comprehensively by Jauch and Rohrlich (1976); this discussion below will be couched for the most part in terms of the more familiar semi-classical approach.

3.1. Scattering in the Born approximation

The theory of Compton scattering is normally developed within the weak coupling limit commonly referred to as the Born approximation. In this approximation the

differential scattering cross section can be written as the product of two terms, one characterising the nature of the interaction and the other a generalised scattering factor $S(\mathbf{K}, \omega)$ describing the target. Then

$$\frac{d\sigma}{d\Omega} = \left(\frac{d\sigma}{d\Omega} \right)_0 S(\mathbf{K}, \omega). \quad (3.1)$$

For x-rays $d\sigma/d\Omega$ is the Thomson cross section $(e^2/mc^2)^2 |\mathbf{\epsilon}_1 \cdot \mathbf{\epsilon}_2|^2$ where $\mathbf{\epsilon}_1$ and $\mathbf{\epsilon}_2$ are the photon polarisation vectors. This cross section is somewhat less than 1 b (10^{-28} m^2) which is certainly small enough for the scattering to be termed weak. The situation does not change dramatically at higher energies where the Klein-Nishina expression (equation (1.3)) must be used (in fact $d\sigma/d\Omega$ decreases away from the straight-through direction).

For electron scattering the characteristic term is the Rutherford cross section $4|\mathbf{K}|^{-4}$, which is typically four orders of magnitude larger than the Thomson term. Even so, most electron scattering experiments can be treated within the first Born approximation. The problem of exchange arises; this is, of course, particular to the electron experiments and leads to the replacement of the Rutherford term by the Mott (1930) cross section or, in the relativistic case, the Møller (1932) cross section, both of which principally change the angular variation.

Returning to photon scattering the perturbation of the electron by an electromagnetic wave can be described by $\mathbf{p} \cdot \mathbf{A}$ and \mathbf{A}^2 terms (\mathbf{A} is the vector potential) in the Hamiltonian. If, as is usually the case, the incident photon energy is substantially greater than the electron binding energies Compton scattering in the non-relativistic limit arises from the \mathbf{A}^2 term. First-order time-dependent perturbation theory gives the same result as the first Born approximation in a stationary state treatment and the spectral distribution is given by the Fermi golden rule as

$$\frac{d^2\sigma}{d\Omega d\omega} = \left(\frac{d\sigma}{d\Omega} \right)_0 \frac{\omega_2}{\omega_1} \sum_f \left| \left\langle f \left| \sum_j \exp(i\mathbf{K} \cdot \mathbf{r}_j) \right| i \right\rangle \right|^2 \delta(E_2 - E_1 - \omega) \quad (3.2)$$

where the delta function restricts the summation to those states accessible with energy conservation: the Born operator is summed over the coordinates \mathbf{r}_j of the j target electrons. The prefactor, ω_2/ω_1 , in equation (3.2) has appeared in diverse places raised to various powers, squared in the original work of Waller and Hartree (1929) and cubed in Compton and Allison (1935); the former is usual in perturbation theory treatments of x-ray scattering by free electrons. The confusion has now been removed by Ribberfors and Berggren (1982) who have shown that in the relativistic treatment of scattering by bound electrons the correct choice of flux factor leads unambiguously to a linear prefactor.

The Compton profile can now be derived after one further approximation.

3.1.1. The impulse approximation. Known to electron spectroscopists as the binary encounter approximation this is the assumption that effectively removes the potential energy terms from the energy conservation condition (see § 1.2). Essentially, if the interaction is restricted to the projectile—photon or electron—and target electron, i.e. a binary encounter, it must be impulsive. Then the remaining electrons are truly spectators and their distribution does not relax before the recoiling electron has escaped. This will only occur if the energy transfer greatly exceeds the one-electron binding energies. Since it has already been assumed that $\omega_1 \gg E_B$ this more restrictive condition implies that high-angle scattering is involved (see equation (1.2)). The time the photon spends probing the electron distribution ($\sim \hbar/\omega$) is so short that the potential energy

$V(\mathbf{r})$ is constant for the duration and thus cancels out in the conservation equation. This would justify the simplistic approach adopted earlier (§ 1.2) in which the target is treated as an assembly of free electrons with a momentum distribution $n(\mathbf{p})$ prescribed by the potential $V(\mathbf{r})$ through the Schrödinger equation.

With the nomenclature of figure 1 energy conservation as expressed by the delta function in equation (3.2) is precisely as given by equation (1.4) (adopting atomic units) specifically dropping $\hbar = 1$, viz:

$$\omega = \frac{|\mathbf{K}|^2}{2m} + \frac{\mathbf{K} \cdot \mathbf{p}}{m}.$$

The summation for each value of ω is therefore over all initial states with a fixed z component momentum, i.e. a sum over states in the p_x, p_y plane. Now if, in the spirit of the impulse approximation, $|\mathbf{K}|^2 \gg |\mathbf{p}_i|^2$ the final electron state can be written as a continuum plane wave, $\exp(i\mathbf{p}_2 \cdot \mathbf{r}_j)$, and the matrix element becomes

$$\sum_j \left| \int \psi_i(\mathbf{r}_j) \exp[i(\mathbf{K} - \mathbf{p}_z) \cdot \mathbf{r}_j] d\mathbf{r}_j \right|^2$$

which, since $\mathbf{p}_2 = \mathbf{K} + \mathbf{p}_1$ simply reduces to $\sum_j |\chi_i(\mathbf{p}_j)|^2$ the one-electron momentum density, where $\chi_i(\mathbf{p}_j)$ is the Fourier transform of $\psi_i(\mathbf{r}_j)$.

The cross section is now

$$\frac{d^2\sigma}{d\Omega d\omega} = \left(\frac{d\sigma}{d\Omega} \right)_0 \frac{\omega_2}{\omega_1} \frac{m}{|\mathbf{K}|} \int_{p_x} \int_{p_y} n(p_x, p_y, p_z) dp_x dp_y. \quad (3.3)$$

Clearly the Compton profile integral of equation (1.5) can be extracted from the spectral distribution, the transformation from energy to momentum scales being accomplished by the equation

$$\frac{p_z}{mc} = (\omega_1 - \omega_2) \pm \frac{\omega_1 \omega_2}{mc^2} (1 - \cos \varphi) (\omega_1^2 + \omega_2^2 - 2\omega_1 \omega_2 \cos \varphi)^{-1/2}. \quad (3.4)$$

(The choice of positive and negative momenta, measured from the shifted Compton peak, is arbitrary.)

The derivation is similar for electrons; in that case the energy to momentum transformation is

$$p_z = \frac{k_2(k_2 - k_1 \cos \varphi)}{(k_1^2 + k_2^2 - 2k_1 k_2 \cos \varphi)^{1/2}} \quad (3.5)$$

where k_1 and k_2 are the incident and scattered wavenumbers.

3.1.2. Validity of the impulse approximation. The deviations from this approximation have been assessed by Eisenberger and Platzman (1970) who calculated the influence of $V(r)$ on moments of the spectral distribution, specifically moments of $S(\mathbf{k}, \omega)$. They found that the first two moments are truly independent of $V(r)$: the term first appears in the third moment to the order of binding energy²/recoil energy; thus, when this term is small the corrections should be relatively minor.

These predictions have been borne out in ‘exact’ calculations for target electrons in truly hydrogenic potentials by Mendelsohn and Biggs (1973) and Bloch and Mendelsohn (1974) for K and L shell electrons, respectively. In these calculations the final state of the electron is a continuum state of the central potential rather than a plane

wave. They show that the Compton peak may move slightly to higher or lower energies and the lineshape may change, as is illustrated in figure 13 for 2p electrons in boron. However the overall effect, when all electrons present are included, is small even at x-ray energies.

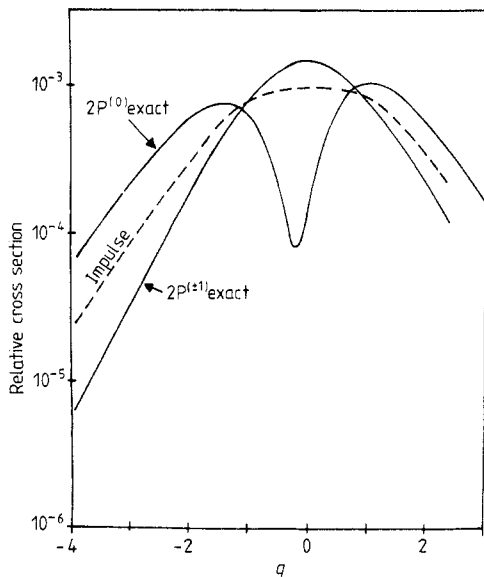


Figure 13. An example of deviations from the impulse approximation as exemplified by an 'exact' calculation with a hydrogenic potential for the 2p electrons in boron. In this calculation the incident photon energy is 20 keV and the scattering angle 180°. There is a clear difference between the 'exact' and 'impulse' cross sections but the amount is exaggerated by the logarithmic scale. In a real target atom all the 2p states would be populated which would tend to wash out the difference, as would the superposition of other electron contributions (from Bloch and Mendelsohn 1974). —, 'exact'; - - -, 'impulse'.

Defects in the peak shift have been observed with difficulty in x-ray experiments (Weiss *et al* 1977) but in γ -ray experiments when the average energy transfer is much larger, the most likely effect is a sharp cut-off in the high-energy profile tail when the energy transfer drops below the K or L shell binding energy. For example, with $\omega_1 = 412$ keV (the energy of γ -ray emission from ^{198}Au) and $E_B = 81$ keV (the binding energy of a K shell electron in gold), this cut-off occurs at 325 keV, i.e. at an electron momentum of 80 au. Here only K and L electron contributions remain. The spectrum obtained by Pattison and Schneider (1979a, b) in this region is shown in figure 14. The discontinuity is clearly visible and is well matched by a relativistic Hartree-Fock calculation (Biggs *et al* 1975) of the profile. The good agreement also strongly supports the relativistic cross section derived by Ribberfors (1975). The height of the discontinuity is indeed a good check of the wavefunction and Pattison and Schneider suggest that if the scattering angle could be varied the K shell contribution could be isolated at a series of electron momentum values. The method might be adapted to provide very precise information about the K shell scattering cross section; current calculations of absolute values vary enormously (Rullhusen and Schumacher 1976).

In general, the breakdown of the impulse approximation in photon experiments is well understood; it can usually be avoided or its consequences rendered negligible so that $J(p_z)$ can be extracted. In practice, the problem is not one of deviation from the idealised lineshape but a failure of the usual normalisation methods which are based

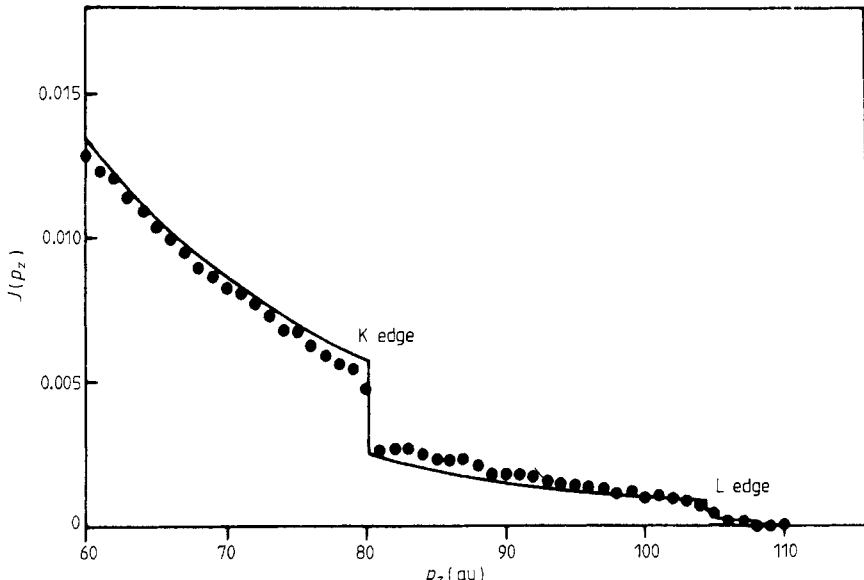


Figure 14. The high momentum tail of the Compton profile of gold (\cdots) measured with 412 keV radiation by Pattison and Schneider (1979a, b). The superimposed curve is the relativistic Hartree-Fock profile calculated by Biggs *et al* (1975). At the K edge the Compton profile has only 0.05% of its height at the peak.

on the fact that $J(p_z) dp_z = N$, the number of electrons per atom—but only if each electron contributes fully.

At first sight the situation appears worse in electron scattering where energy transfers are typically as low as 500–1000 eV, but this is not so for two reasons. Firstly, experiments are necessarily restricted to gases to avoid overwhelming multiple scattering and this normally implies molecules with low Z number, i.e. small binding energies. Secondly, within the Born approximation normalisation of the entire spectrum including the elastic line is guaranteed by the Bethe sum rule, irrespective of the validity of the binary encounter approximation. On the other hand (see Barlas *et al* 1977, 1978) because the energy resolution of electron spectrometers is so high (a few eV) small defects in peak positions can be measured and studied as a function of the momentum transfer (Rueckner *et al* 1978). Gasser and Tavard (1981a, b, c) have calculated the impulse corrections by making a series expansion of the Born operator. The terms then obtained are overlap integrals which involve the displacement of the recoiling electron during the collision. By this approach they can explain why the peak shift is always towards lower energy transfers for s orbitals but can be of either sign for p functions. This resolves the confusion over the sign of defects in the Compton shift which has reigned since the first calculations by Bloch (1934). Their results are in good agreement with those based on solutions for the hydrogenic potential.

Measurements of the defect in the Compton shift made with x-rays and electrons are collected together in table 2 which is adapted from Gasser (1980).

3.2. Relativistic effects

3.2.1. Spin-independent effects. The transition from a non-relativistic to a relativistic treatment of the scattering is unavoidable once ω_1 becomes an appreciable fraction of

Table 2. The Compton defect: summary of results (by convention, a negative sign for the defect indicates that the peak shift is less than predicted). Data from Gasser (1980).

Sample	Radiation	Defect		
		Value (eV)	% of Compton shift	Reference
Beryllium	X-rays	-5	-0.5	Philips and Weiss (1968)
Lithium	X-rays	-10 ± 3	-1	Weiss <i>et al</i> (1977)
Polyethylene	X-rays	-10 ± 3	-1	Weiss (1965)
Aluminium	X-rays	-10 ± 7	-1	
Helium	Electrons	-5.4 ± 1	-0.5	
Molecular hydrogen	Electrons	-4.1 ± 2.4	-0.4	Rueckner <i>et al</i> (1978)
Neon	Electrons	+14.3 ± 1.5	+0.9	
Nitrogen	Electrons	+2.8 ± 1.0	+0.2	
Ammonia	Electrons	5	+0.5	Lahmann-Bennani <i>et al</i> (1979)

mc^2 . It is not merely a matter of replacing the Thomson cross section by the Klein-Nishina expression (equation (1.3)) in equation (3.3). Quantisation of the radiation field not only complicates the algebra—the scattering matrix must be summed over many intermediate states—but also introduces additional terms which arise from electron spin. It is then not obvious that the Compton profile can be extracted, intact, from the cross section after the fashion of the semi-classical treatment; the Compton profile may not be a measurable quantity.

Eisenberger and Reed (1974a) and Manninen *et al* (1974) considered the scattering from a system of free electrons with momentum distribution $n(\mathbf{p})$ and no net spin in the spirit of the previous analysis. The cross section now contains an integral of $n(\mathbf{p}) \cdot X(\mathbf{p})$, where $X(\mathbf{p})$ is a flux factor. In the limit that $\varphi \rightarrow 180^\circ$ and terms $\sim p_i^2/mc^2$ can be neglected. The flux factor $X(\mathbf{p})$ is essentially constant (i.e. has no p variation). The analysis then produces a double differential cross section analogous to equation (3.3); the derivation is summarised in the Appendix of Manninen *et al* (1974).

It was not clear to what extent experiments performed at moderately high scattering angles (150 – 170°) on real systems deviate from these limits. Ribberfors (1975) showed that the Compton profile could be extracted from such data by a rapidly converging iterative procedure if $n(\mathbf{p}) \cdot X(\mathbf{p})$ was integrated successively by parts. Indeed for experiments carried out at angles above $\sim 165^\circ$ the corrections are so small that the leading term assumed by Manninen *et al* is adequate. The importance of Ribberfors' work is that it clearly validates the conventional assumptions.

In electron scattering experiments, where the energy of the source can be chosen at will, both relativistic and exchange corrections can be minimised and then expressed as separable multiplicative factors (Bonham and Fink 1974) leaving the Compton profile integral intact.

3.2.2. Spin-dependent effects. Platzman and Tzoar (1970) showed how the matrix operator, M_{jk} , in the relativistic cross section can be split into spinless and spin-dependent terms, i.e.

$$\mathbf{M}_{jk} = \mathbf{A}_{jk} + i\mathbf{B} \cdot \mathbf{S}_{jk}$$

where \mathbf{S}_{jk} is the electron spin matrix. Thus, besides the A^2 term which leads to the replacement of the Thomson by the Klein-Nishina cross section there are $iA(\mathbf{B} \cdot \mathbf{S})$

and B^2S^2 terms present. Now since $B \sim (\omega_1/mc^2)A$ the B^2 term is generally ignored in x-ray Compton scattering experiments where $\omega_1 \ll mc^2$. The contribution of the B^2 term has, however, been detected by DeBergevin and Brunel (1972) in x-ray diffraction studies ($\omega_1/mc^2 \sim 1/50$) of the antiferromagnet NiO by selecting scattering vectors corresponding to the magnetic superlattice reflections. In this case the A^2 terms (normal lattice reflections) are zero at these positions and the spin-dependent term is not submerged by the background. There do not appear to have been any attempts to repeat such experiments at higher photon energies.

The cross term $iA(\mathbf{B} \cdot \mathbf{S})$ in $|M|^2$ appears to be imaginary; it can only make a real contribution to the scattering if the polarisation product $\epsilon_1 \cdot \epsilon_2$ is complex, i.e. if the radiation is circularly polarised. In an experiment in which this is so, but the polarisation of the scattered beam goes unmeasured, the additional term in the cross section for a stationary electron with spin, S , will be

$$\frac{d\sigma_s}{d\Omega} = \left(\frac{e^2}{mc^2} \right)^2 \left(\frac{\omega_2}{\omega_1} \right)^2 \left(\frac{1 - \cos \varphi}{mc} \right) \mathbf{S} \cdot (\mathbf{k}_1 \cos \varphi + \mathbf{k}_2) \quad (3.6)$$

according to Lipps and Tolhoek (1954). Since $k_1/mc \sim \omega_1/mc^2$ the term contributes $\sim f_m \omega_1/mc^2$ where f_m is the fraction of electrons with unpaired spins. The magnitude and angular variation of the magnetic scattering is compared with the unpolarised scattering in figure 15 where it can be seen that if circularly polarised radiation can be produced an appreciable effect will be observed at high scattering angles and short wavelengths.

This scattering property has been widely used to analyse the polarisation state of γ rays emitted after β decay (Steffen and Frauenfelder 1965). The intensity of scattering

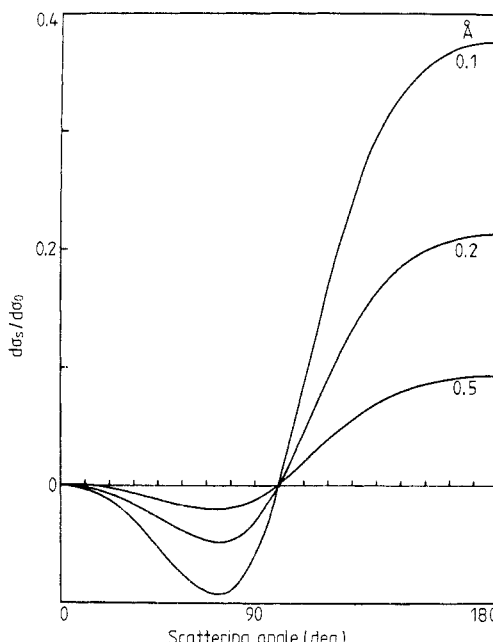


Figure 15. The spin-dependent Compton cross section $d\sigma_s/d\Omega$ expressed as a fraction of the spinless cross section $d\sigma/d\Omega$ and plotted as a function of scattering angle for three wavelengths of circularly polarised radiation for the case when the electron spin is parallel to the incident γ -ray.

from a magnetised iron 'analyser' is measured before and after reversal of the magnetic field; the fractional change in flux is used to predict the sense and degree of circular polarisation.

In theory the Compton profile of unpaired spin electrons can be deduced from the spectral distribution of scattered circularly polarised radiation, the A^2 term being removed by subtraction of the profile obtained with the magnetic field or sense of polarisation reversed. This is potentially a most interesting development in Compton scattering studies because it would make the study of charge density in magnetic materials much more specific. The problem is to develop a sufficiently intense source of circularly polarised photons. Heroic experiments of this kind with weak radioisotope sources have been pioneered by Sakai and Ono (1976) who obtained a magnetic Compton profile of iron. Holt and Cooper (1983) have proposed the use of synchrotron radiation but experiments are yet to be performed. The technique is discussed further in § 4.2.2 below.

4. Experimental methods

The Compton cross section is low ($\sim 1b$) and the line broadening modest ($\sim 5\%$). Therefore the experimental requirement is for an abundant source of photons and an efficient energy-dispersive detection system.

The combination of an x-ray tube source and a crystal spectrometer was a natural choice in the era preceding the development of energy-dispersive semiconductor detectors. The technology of x-ray production was well developed by DuMond's time in response to the burgeoning demand from x-ray crystallographers. High-resolution spectroscopy was possible although efficient photon detection awaited the development of the scintillation counter. Then, as now, x-ray tubes and generators provided characteristic radiation in the energy range 5–25 keV which is suited to crystallographic work. Unfortunately at these energies the Compton cross section is much smaller than that for photoelectric absorption in all but the lightest elements. It is, for example, unrealistic to contemplate experiments with Mo $K\alpha$ radiation (17.6 keV) on anything heavier than aluminium—the typical measurement time would be one month. Even if higher intensities can be realised by using focusing optics and bright synchrotron sources the study of heavier elements would be jeopardised through the failure of the impulse approximation. Only 'difference experiments', in which the dubious core contributions and other systematic errors subtract out, would be possible.

Although x-ray tubes with heavy-metal anodes would increase the incident energy there is little commercial pressure for this development. Tungsten ($E_{K\alpha} = 59$ keV) is the only exception but here the tubes are often powered by 60 kV generators so that only bremsstrahlung radiation is produced, or incorporated into very high-voltage medical/industrial radiography units. In view of the proven value of high-energy diffraction (Freund 1979) for making extinction-free intensity measurements, and for studying the degree of perfection of thick crystals, it is surprising that development in this area is only now being considered. X-ray tubes are not, however, ideal sources: the characteristic line may be intense but it is a $K\alpha_1\alpha_2$ doublet (or the weaker $K\beta$ multiplet) superimposed on a bremsstrahlung background. Monochromatisation would involve a prohibitive loss of intensity if a flat crystal analyser were used.

This leaves radioisotopes as the only potentially monochromatic sources of higher ($E_\gamma > 50$ keV) radiation. Unfortunately the intrinsic flux is three or four orders of

magnitude lower than the x-ray source (the characteristic emission of a 1 kW tube is 10^{13} - 10^{14} photons s $^{-1}$ whereas 1 curie is 3×10^{10} photons s $^{-1}$). Prior to the development of semiconductor detectors there was no method of off-setting this weakness, but an efficient detector which offers simultaneous acquisition and good energy resolution of a γ -ray spectrum provides the necessary gain in speed when compared with the point-by-point recording of a flat crystal Bragg spectrometer. In this γ spectrometer there are no moving parts and the only problem is to obtain a suitable isotope source. It is now accepted as the standard technique against which all developments should be measured. A survey of the methods in current and recent use is compiled in table 3.

4.1. Crystal spectrometers

All previous reviews have dwelt upon the use of flat crystal Bragg spectrometers for the energy analysis of Compton scattered radiation: today they merit far less attention. If the incident beam is left unmonochromated x-ray tubes with a small spot size (diffraction tubes) are not ideal, a broad source, producing a beam divergence of a few degrees, can be tolerated in back-scattering geometries with a gain in the total intensity of the output. Parallel plate Soller-slit collimators ($\sim \pm 1/10^\circ$ divergence) are then used on the spectrometer, the flat analysing crystal (usually LiF) and the detector being scanned in the $\theta:2\theta$ mode. The resolution depends upon the chosen Bragg reflection of the analyser ($\Delta\lambda/\lambda = \cot\theta \Delta\theta$) as does the intensity. With Mo K α radiation LiF 400 is the usual compromise yielding an instrumental momentum resolution ~ 0.15 au which, by comparison with γ -ray experiments, must be accounted as good. However, the abysmal count rate (~ 1 CPS at the Compton peak) together with the confusion of K $\alpha_1\alpha_2$ profiles and the presence of bremsstrahlung background prevents the realisation of any advantage from the comparatively good resolution. It is no surprise that this method has been abandoned.

4.1.1. Focusing spectrometers. The intensity of conventional x-ray sources cannot be increased by more than one order of magnitude and therefore efforts have been concentrated on improving the efficiency of data collection (and hence the attainable resolution and statistical accuracy) by recording the entire spectrum simultaneously. In x-ray fluorescence analysis this has been achieved by replacing the crystal spectrometer with a silicon detector. This is not the answer here: the resolution (~ 150 eV at 6 keV) may be adequate to differentiate neighbouring elements but it is an order of magnitude too coarse for the analysis of the Compton lineshape.

The solution, implemented 50 years ago by DuMond and Kirkpatrick (1930) (see figure 3), is to use focusing optics with a curved crystal monochromator and analyser. They were hampered by the inefficiency of film recording; the contemporary breakthrough has come from the development of position-sensitive proportional counters which have a high quantum efficiency in the x-ray region ($\sim 50\%$ for Cu K α) and acceptable spatial resolution ($\sim \pm 0.1$ mm) in at least one dimension. There is every prospect that these figures of merit will improve.

A focusing Compton spectrometer that uses a 1 kW Cu anode x-ray tube and a position-sensitive detector has been constructed by Pattison *et al* (1981a). A curved quartz 1011 monochromator crystal was used to isolate the Cu K α_1 incident beam and a germanium 333 curved analyser (both crystals Johansson-type) focused the scattered radiation onto a xenon-filled position-sensitive detector of the backgammon type. Even

Table 3. Photon sources in current or recent use for momentum studies.

(a) γ -ray sources						Comment/reference
Isotope	γ -ray	Half-life	Strength	Laboratory		
^{123m}Te	159	102 d	~1 Ci	Bell Laboratories, USA		Use discontinued: Source material expensive and impure (Eisenberger and Reed 1972)
^{51}Cr	320	28 d	~45 Ci	Institut für Festkörperforschung, Jülich, West Germany		Not in current use (Lässer <i>et al</i> 1979)
^{137}Cs	662	30 yr	1–10 Ci	University of Louisville, USA		Difficult to shield. Use discontinued for momentum studies (use for Compton densitometry) (DuBard 1978)
^{241}Am	60	425 yr	1–5 Ci	Warwick University, UK Dortmund University, West Germany Konstanz University, West Germany Helsinki University, Finland Ioannina University, Greece Warwick University, UK		Cheap and long-lived: high self-absorption (see, for example, Weyrich 1975, Cooper <i>et al</i> 1978, Bonse <i>et al</i> 1979)
^{198}Au	412	2.7 d	100–250 Ci	Inst. Phys. Bhubaneswar, India Warwick University/Rutherford Laboratory, UK		Only feasible near neutron reactor, frequent replenishment required (Holt <i>et al</i> 1979, Pattison and Schneider 1979a, b)
^{57}Co ^{191}Os	122 129	120 d 15 d	10 mCi	Hahn-Meitner Institute, Berlin Institute of Physics and Chemical Research, Japan		Cooled sources used to produce circularly polarised photons for magnetic Compton scattering (Sakai and Ono 1976, Sakai <i>et al</i> 1984)
(b) X-ray/synchrotron sources						
Mo K α	17.6 keV 17.6 keV		2 kW 30 kW	Konstanz University, West Germany Dortmund University, West Germany		Pattison and Weyrich (1984) Compton scattering at the Bragg position (Schulke <i>et al</i> 1984)
Cu K α	8 keV		1 kW	Hahn Meitner Institute, Berlin		Focusing crystal spectrometer (Pattison <i>et al</i> 1981a, Patterson and Weyrich 1984)
LURE-DCI synchrotron	10 keV		See table 4 for flux comparisons	Orsay, France		Focusing crystal spectrometer (Loupias <i>et al</i> 1980)

in this prototype a Compton peak count rate of ~ 1 CPS per 1 eV channel was obtained at a resolution of 6 eV. This corresponds to a momentum resolution of 0.07 au which is clearly superior to the older x-ray methods. Another recently constructed focusing spectrometer (Pattison and Weyrich 1984) reverts to a scintillation detector to increase the count rate to ~ 100 CPS at 0.25 au resolution.

The intrinsic collimation of synchrotron radiation renders it an ideal source for focusing spectrometers. The divergence of the beam ($\sim 1/10$ mrad at x-ray energies) neatly matches the width of the rocking curves of perfect silicon and germanium; thus monochromatisation can be achieved with a minimal loss of intensity. Such an instrument is in use at the LURE-DCI synchrotron facility in Orsay, France and operates in the energy range 5–15 keV (Loupia *et al* 1980): it is shown in figure 16. There is no doubt that, despite the limited availability of hard synchrotron radiation, this approach will be exploited as the only practicable method of simultaneously achieving high resolution (~ 0.05 au) and good statistical accuracy in Compton experiments on light materials. The high-energy resolution of such an instrument and the ‘tuneability’ of the source makes it ideal for studies of Raman and plasmon as well as Compton scattering.

The figure of merit of x-ray and synchrotron machines are compared with the γ -ray alternative in table 4 in the next section.

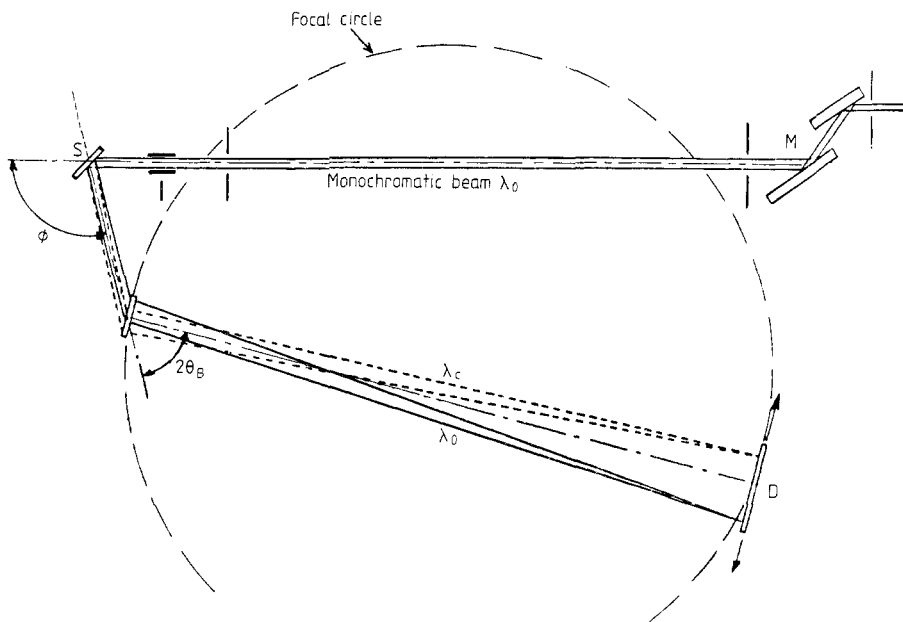


Figure 16. Schematic diagram of the focusing Compton spectrometer installed on the LURE-DCI synchrotron ring. The white beam is monochromated (an energy around 10 keV is selected) by the channel-cut silicon monochromator, M, and the collimated beam passes through an ionisation chamber monitor (I) to the sample S. The curved crystal analyser (a silicon 220 crystal) and the multiwire position sensitive detector D are kept in position on the focusing circle by a series of linkages between the parts (from Loupias and Petiau 1980).

4.2. γ -ray spectrometers

The method centres around the behaviour of dispersive semiconductor detectors. The width, ΔE , of the instrumental broadening function of such a device obeys the equation $(\Delta E)^2 = \alpha^2 + \beta E$. The first term represents a noise contribution, which is minimised by cooling the primary electronics to liquid-nitrogen temperatures, and the second term relates to the statistics of electron-hole production in the crystal, and charge collection at the electrodes. From equation (1.8) it can be shown that the Compton linewidth increases with photon energy in a linear fashion for energies well below mc^2 . Therefore the ratio of the linewidth to the resolution width steadily improves as evidenced by their ratio as plotted in figure 17(a); at low energies the optimum values occur at $\varphi = 180^\circ$, at high energies the peak moves to lower angles. These ratios of 4–5 compare poorly with values ~ 20 for the focusing crystal spectrometers; moreover, little improvement in detector performance can be expected. The resolution would be barely acceptable were it not for two mitigating factors: they are used in conjunction with monochromatic sources bereft of white background, and high statistical accuracy can be routinely obtained— 10^7 counts under the Compton line is typical.

There is little point in increasing the photon energy above mc^2 , for one thing the broadening of the profile due to the beam divergence becomes more severe (see figure

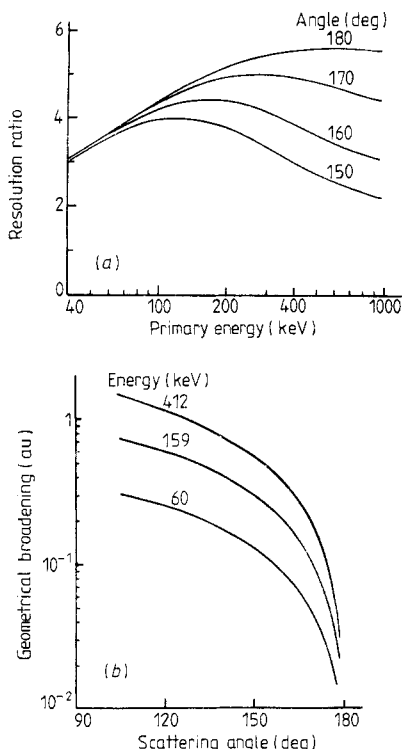


Figure 17. Resolution in the γ -ray Compton experiment. (a) The upper figure indicates the resolution of Compton scattering experiments as a function of energy for various angles of scattering. The resolution ratio is the ratio of the Compton line width (taken as 2 au full width at half-maximum) to the width of the detector resolution function when expressed in the same units. (b) The lower figure shows the extra broadening of the Compton profile which arises from a beam divergence of $\pm 1^\circ$ in the scattering plane (data taken from DuBard (1978)).

17(b)) and a higher scattering angle or a more tightly collimated (and hence less intense) beam must be selected. At high scattering angles the shielding of the detector from the source becomes extremely difficult if short path lengths (minimum $1/r^2$ losses) are to be retained. Source and detector are inevitably in close proximity as is illustrated in figure 18 which shows the present author's ^{198}Au 412 keV spectrometer. At these energies lead is a poor absorber and denser tungsten alloys are commonly used to provide compact effective shielding.

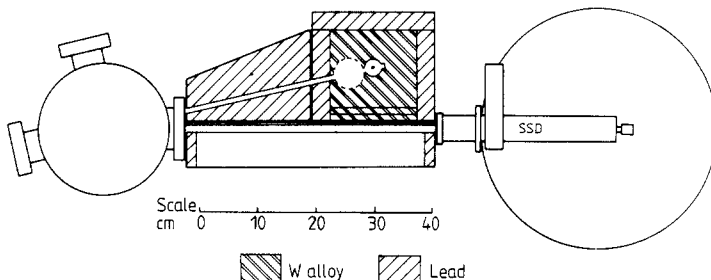


Figure 18. Schematic diagram of a typical Compton γ -ray spectrometer, illustrating the compromise between high scattering angles, short beam paths and adequate shielding. In this design tungsten alloy is used to replace lead in the region immediately surrounding the source for effective shielding of the ^{198}Au 412 keV radiation. The sample chamber is to the left, and the solid-state detector (SSD), to scale, to the right. Source strengths of the order of 100–300 Ci are typical for ^{198}Au . Other isotopes used for Compton scattering are generally produced with a lower activity (see table 3).

4.2.1. Source selection. The choice of the source is virtually the only variable in the γ -ray experiment. What criteria should it satisfy?

(a) A high specific activity and low self-absorption so that high intensity and small beam divergence can be simultaneously achieved.

(b) The source must be monochromatic to the extent that there are no other lines of significant intensity near the chosen one—that would produce overlapping profiles—or in the energy range where the profile will appear. Any high-energy (>1 MeV) contamination is to be avoided since it will multiply scatter into the detector through the shielding.

(c) The isotope to be irradiated must be available in adequate quantities at an affordable cost! If the cross section for (n, γ) activation is low the irradiation cost may also be considerable.

In practice there are very few sources from which to choose; none of them is ideal as can be judged from the selection summarised in table 3. The popular choice is ^{241}Am ($E_\gamma = 60$ keV) which has low specific activity and high self-absorption but is cheap and long-lived ($T_{1/2} = 450$ yr) (see Bonse *et al* 1979) for a description of a typical system. Compton studies with ^{241}Am are limited to the first transition-series elements by photoelectric absorption and impulse approximation considerations. In addition the detector resolution at this comparatively low γ -ray energy is relatively poor (see figure 17(a)). There has been intermittent use of $^{123}\text{Te}^m$ ($E_\gamma = 159$ keV, $T_{1/2} = 107$ d, see Eisenberger and Reed (1972)) but the initial isotope is difficult to obtain with high purity; ^{51}Cr ($E_\gamma = 320$ keV, $T_{1/2} = 27$ d, see Lässer *et al* (1979)) has also been tried. Their ^{51}Cr Compton spectrometer was used for studies of the α/γ transition in cerium

(Kornstadt *et al* 1980) and single-crystal studies of palladium (Podloucky *et al* 1979) but no ^{51}Cr sources are in current use.

A measure of the paucity of sources is afforded by the use of an isotope which has a half-life as low as 2.7 d. ^{198}Au ($E_{\gamma} = 412 \text{ keV}$) was originally used for γ -ray diffraction studies at the Institut Laue-Langevin, Grenoble (Schneider 1974). It has a high specific activity and source strengths up to 250 Ci are attainable, but the spectrometer must be sited near the neutron reactor where the isotope is produced by an (n, γ) reaction in the naturally occurring isotope ^{197}Au . The apparatus shown schematically in figure 18 was built by the present author's group for use at the Rutherford Appleton Laboratory which is in close proximity to the AERE Harwell reactors (Holt *et al* 1979): a similar instrument is sited at the Hahn-Meitner Institute, Berlin (Pattison and Schneider 1979a, b). For scattering through angles between 165–170° the Compton line is centred around 160 keV and a $^{123}\text{Te}^m$ radioisotope ($E_{\gamma} = 159 \text{ keV}$) can be conveniently used to provide a suitable resolution measurement.

Recently I K MacKenzie (private communication) has suggested the use of weak point sources of high specific activity in a very compact spectrometer with beam paths of the order of a few centimetres. In such an arrangement the use of very small samples would be possible; this could simultaneously remove the problem posed by the need to grow large single crystals and dramatically reduce the difficulties produced by multiple scattering.

A detailed review of γ -ray source properties has been published elsewhere (Cooper 1979). The x-ray and γ -ray spectrometers are compared in table 4.

4.2.2. Circularly polarised γ -ray sources. The possibility of isolating the Compton scattering from just those electrons with unpaired spins was introduced in § 3.2.2. The first measurements of this kind were made by Sakai and Ono (1976, 1977). They utilised the inequality in left- and right-handed circular polarisation produced from oriented ^{57}Co nuclei ($E_{\gamma} = 122 \text{ keV}$) aligned in the 30 T internal field of the iron host metal. Unfortunately nuclear orientation requires temperatures around 50 mK which they maintained by repeated adiabatic demagnetisations—a total of 40 in the 139 h measurement period. The average degree of circular polarisation was $\sim 50\%$. Because of limited cooling power the source strength was limited by self-heating effects to a mere 10 mCi; the statistical quality of the data was accordingly low.

Recently Sakai *et al* (1984) have identified a different isotopic source, ^{191}Os , which after β decay to $^{191}\text{Ir}^m$ ($T_{1/2} = 15 \text{ d}$) produces a 129 keV γ ray: this can be used at operating temperatures up to 100 mK and still yield an acceptable degree of circular polarisation. Using a 40 mCi source, they produced the results shown in figure 19 from a ferromagnetic iron specimen. The experiment is still far from straightforward but these results are sufficiently accurate to provide a sensible test of spin-polarised momentum densities. Larger sources could be used with more powerful $^3\text{He}/^4\text{He}$ dilution refrigeration (a 20 mCi ^{191}Os source dissipates 18 μW).

An alternative approach, with comparable but different difficulties, is to extract circularly polarised photons from synchrotron radiation (Holt and Cooper 1983). The source is viewed at a small angle ($\sim 1/10 \text{ mrad}$) to the orbital plane; the electron orbit must therefore be very stable. Although the experiment has yet to be performed current indications are that beam stability should be adequate. 'Wiggler' magnet configurations which produce high-energy photons should provide sufficient flux at photon energies $\sim 30\text{--}40 \text{ keV}$ to permit a realistic experiment.

Table 4. Figures of merit† for γ -ray and x-ray experiments.

Method	Energy (keV)	Peak to background ratio	Momentum resolution (au)	Integrated count rate (cps) (approx)	Reference
$^{241}\text{Am} + \text{SSD}$	~59.5	500:1	0.55	20	Manninen and Paakkari (1978)
$^{198}\text{Au} + \text{SSD}$	412	500:1	0.40	10	Pattison and Schneider (1979a,b)
Mo x-ray tube plus flat crystal spectrometer	17	5:1	0.25	10	Cooper and Pattison (1974)
Cu x-ray tube plus curved crystal spectrometer	8	15:1	0.07	1	Pattison <i>et al.</i> (1981a)
Synchrotron radiation plus curved crystal spectrometer	~10	100:1	0.15 achieved 0.05 theoretical	1 4	Louprias and Petiau (1980)

† The data presented here relate to a 0.2 mm thick aluminium sample. This table is adapted from Loupias and Petiau (1980).

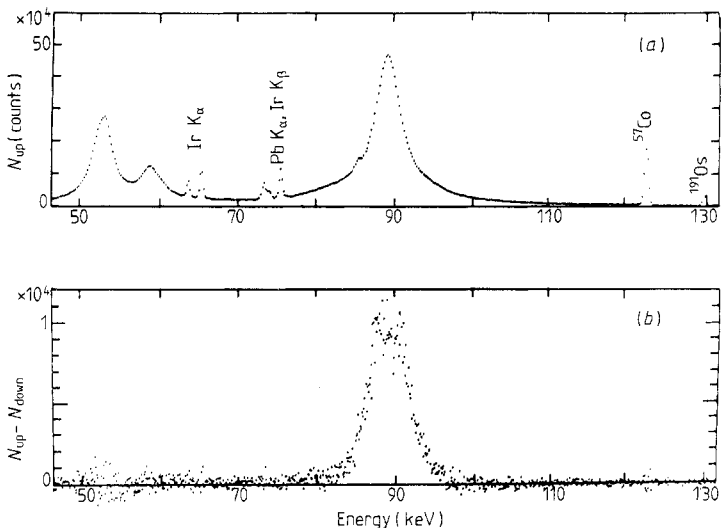


Figure 19. Compton scattering from ferromagnetic iron with circularly polarised photons. (a) shows the spectrum of Compton scattering (centred around 90 keV) and x-ray fluorescence produced by a 40 mCi ^{191}Os source which has a half-life of 15 d and is cooled to 100 mK. The 122 keV line from a ^{57}Co source has been superimposed for calibration. (b) shows the difference Compton profile due to reversal of the magnetisation of the sample after 167 h of measurement. The magnetic Compton profile accounts for 2.6% of the intensity of the unpolarised profile. The statistical accuracy is limited by the source strength which in turn is limited by the cooling capacity of the $^3\text{He}/^4\text{He}$ dilution refrigerator (from Sakai *et al* 1984).

4.3. Data analysis

The cynical comment that ‘all Compton profiles look alike’ can be rebutted but it does underscore the fact that physically interesting effects only change the lineshape by small amounts. Accordingly, both random and systematic errors must be reduced to a very low level. This is the forte of the γ -ray method; random errors as low $\pm 1/5\%$ $J(0)$ are routinely obtained and reproducibility is close to this limit. The point is illustrated in figure 20 where two data sets on vanadium, obtained in different laboratories, are shown to be strictly comparable.

Systematic errors require various levels of attention. Corrections for the energy variation of absorption, detector efficiency, etc, are straightforward but more care is required, for example, in locating the correct peak ($p_z = 0$) position since the lineshape will be critically affected through the normalisation procedure. At the top of the scale the two thorniest issues are resolution broadening and multiple scattering.

Deconvolution and its perils are hardly restricted to this experiment but the rather poor resolution of the γ -ray experiment exacerbates the situation. There are two schools of thought: the first believes in a full deconvolution according to one or other of the prescriptions for series termination, and then acknowledges the imperfect nature of the business by convoluting the theory with a residual instrument function (Paatero *et al* 1974). The other, more cautious, approach merely restricts the deconvolution to stripping the low-energy tail of the resolution function and smoothing the data, leaving the theory to be convoluted with a Gaussian.

The most imponderable problem is multiple scattering. Although Compton scattering is a weak process multiple scattering can account for $\sim 30\%$ of the integrated

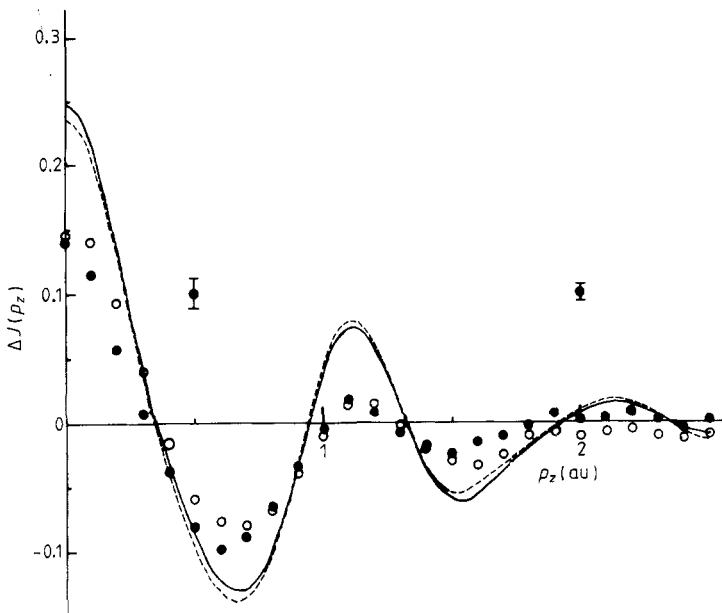


Figure 20. Reproducibility of γ -ray Compton data. This figure shows two independent sets of processed data for the directional profile difference $J_{110}(p_z) - J_{100}(p_z)$ in single-crystal vanadium. Points marked ● were obtained at the Rutherford Appleton Laboratory and those indicated ○ at the Hahn-Meitner Institute with ^{198}Au 412 keV γ -ray sources. The error bars are appropriate to both data sets which have been corrected for multiple scattering. Absolute values of the differences are shown; the spherically averaged profile peak height is ~ 5.1 at the origin. The graph also shows the anisotropy predicted by LCAO (full curve) and APW (broken curve) band calculations. Characteristically theory overestimates the scale of the experimental anisotropy (from Rollason *et al* 1981).

intensity, though a figure of 10% would be more typical. Its spectral distribution will be much broader than for single scattering and will therefore, if uncorrected, smear out the lineshape. The problem was first pointed out by DuMond (1930) but was largely ignored in the era of x-ray experiments when larger and larger samples were used to increase the intensity.

In an absorbing sample multiple scattering is proportional to the effective thickness, reaching saturation when $t > \mu^{-1}$. The strategy of using very thin samples is usually rejected because of the inordinately long measurement times. Instead measurements on thick samples are corrected by Monte Carlo simulation of the scattering process (see, for example, Felsteiner *et al* 1974). The programmes are somewhat unwieldy with upwards of half a million scattering events followed in each iterative simulation in order to establish the spectral correction. It is much easier to calculate the total amount of multiple scattering because the Klein-Nishina cross section for a stationary electron can be substituted for the complex momentum-dependent expression. This single figure is sufficient to renormalise Compton difference profiles and it can be used to provide a suitable linearising parameter for experimentally based extrapolation methods such as that proposed by Felsteiner and Pattison (1980).

Multiple scattering can now be confidently removed by either method with a residual uncertainty no greater than that associated with the more routine corrections. Absolute profiles can be quoted with an error tag of $\pm \frac{1}{2}\%$ $J(0)$ at low momenta, while the directional profiles can be two or three times more accurate.

4.4. Electron spectroscopy

4.4.1. Compton scattering. Electron Compton scattering enjoys two practical advantages over its photon counterpart. Firstly, the source energy (from an electron gun) can be chosen almost at will; there is no restriction to natural x-ray or γ -ray lines and the monochromaticity is higher. Secondly, electron velocity analysers (magnetic prism spectrometers) afford exemplary resolution: ~ 1 eV against a Compton linewidth of ~ 100 eV. This is incomparably better than the equivalent photon experiment. On the debit side the high cross section necessitates the use of dilute gas samples, the entire electron beam trajectory being in vacuum. The rapid angular variation of the Rutherford cross section ($\alpha \operatorname{cosec}^4 \varphi/2$) means that the scattering angle must be defined to better than $\frac{1}{100}^\circ$, thereby undermining the experiment's inherent intensity advantages.

In a typical experiment an electron beam of flux 10^{15} s^{-1} at an energy between 30–50 keV is scattered through a well-defined angle between $10\text{--}15^\circ$ from a 1 Torr gas jet target in a spectrometer evacuated to between $10^{-6}\text{--}10^{-4}$ Torr and shielded from the Earth's magnetic field (see the review of Barlas *et al* (1978)). The technique has recently been adapted to use electron microscopes fitted with velocity analysers and solid thin-film targets. The conventional tilt coils can be used to establish a $\sim 5^\circ$ scattering angle for a 100 keV beam (see Williams *et al* 1981, 1984, Williams and Thomas 1983).

4.4.2. Electron coincidence spectroscopy. One general disadvantage of the Compton experiment is that no information about the recoil electron is recorded. In photon experiments the only step in that direction has been to record the scattered beam in coincidence with K-shell x-ray fluorescence, thereby isolating the $1s^2$ core contribution (Fukamachi and Hosoya 1972). With dilute gas targets it is possible to detect both recoil and scattered electrons in coincidence and thus determine all momentum components. The price to be paid is a drastically reduced count rate and increased experimental complexity.

The advantages of this experiment are even greater than might at first be supposed because electrons can be 'picked-off' shell by shell. Consider the scattering geometry sketched in figure 21. If the target electron were initially at rest the three vectors k_1 , k_2 and k'_2 would be coplanar and conservation of energy and momentum would dictate that k_2 , k'_2 are perpendicular. If scattering events with $\theta_A = \theta_B = 45^\circ$ are selected for coincidence the energy of incident beam, E_1 , is equally divided between the two exiting electrons: detectors (velocity analysers) tuned to the energy $E_1/2$ should pick up these beams. However, this analysis neglects the target binding energy. In fact, no coincidences would be recorded until the incident energy had been increased by a specific amount equal to a target electron binding energy. Then the momentum distribution of a group of electrons characterised by that unique binding energy could be measured either by varying $\theta_A (= \theta_B)$ with $\eta = 0$ or by varying η with θ_A and θ_B fixed.

In the coincidence spectrometer described by Brion *et al* (1980) the momentum resolution at 400 eV is 0.05 au and at 1200 eV it is 0.08 au. The differentiation by binding energy is appropriate not only in isolated atoms with their one-electron shells, but also in molecules. This is illustrated in figure 22 taken from the work of Brion *et al* (1980): the upper diagram shows how the coincidence count rate varies as the source energy is 'tuned-in' to equal the binding energy of various molecular orbitals in the molecule HF. Peaks corresponding to the removal of electrons from 1π , 3σ and 2σ orbitals occur at the energies predicted by conventional photoelectron spectroscopy.

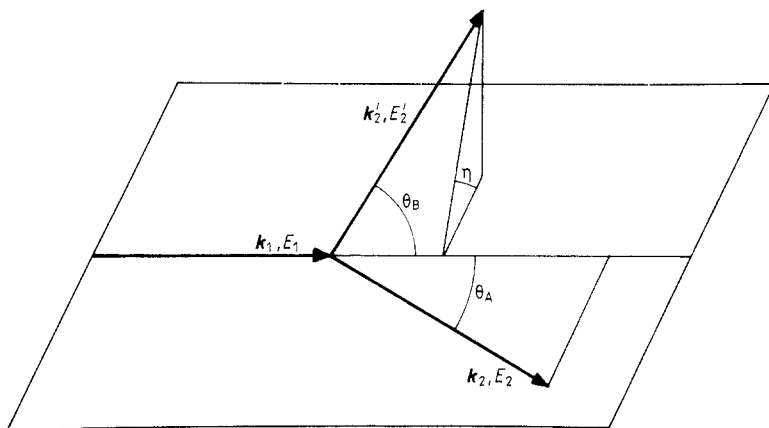


Figure 21. Geometry of the e^-2e^- reaction. In the actual apparatus an incident collimated monochromatic beam (k_1, E_1) is scattered by a gas target. The scattered and recoil beams ($k_2, E_2; k'_2, E'_2$) are detected by cylindrical mirror analysers coupled to channel electron multipliers. Their energy resolution is $\sim 1\%$ and the resolving time of the coincidence circuit is ~ 10 ns. In the symmetric coplanar geometry the experiment is performed by setting $\eta = 0$ and varying $\theta_A (= \theta_B)$. In the non-symmetric geometry $\theta_A = \theta_B = 45^\circ$ and η is varied.

The lower diagrams (figure 22(b)) then show the radial momentum distribution for the 3σ and 1π orbitals. The latter shows clearly that the molecular orbitals of Snyder and Basch (1972) are too extended in momentum space; the one-particle Green function calculation gives much better agreement.

A more striking example is afforded by very recent work (Cook *et al* 1984) on the heavy gas xenon. The $5p_{3/2}$ and $5p_{1/2}$ one-electron momentum distributions have been measured with sufficient accuracy to show that they are indeed different. The momentum density distributions are shown in figure 23. Non-relativistic theories predict identical distributions, but the relativistic splitting is quite clear and is well described by a single-configuration Dirac-Fock wavefunction. Although these experiments are complex and necessarily restricted to gaseous targets their information content is very high.

Finally, and somewhat amusingly, the method has been applied by Lohmann and Weigold (1981) to provide the first direct measurement of the electron density distribution in atomic hydrogen. The unique energy tuning property enables atomic events to be selected from the predominant recombined molecular species. Although such evidence is long overdue it is thankfully in good agreement with the analytical expression taught to every physics student as the bedrock of quantum mechanics!

5. Recent studies

5.1. General considerations

Some of the work of the past decade has already been described where it has served to illustrate improvements and innovations in the interpretative and experimental techniques, or provide a benchmark for the current state of the art.

It is possible to discern two separate but interwoven threads of development within the last few years and they provide the basis for this section. In the first place there

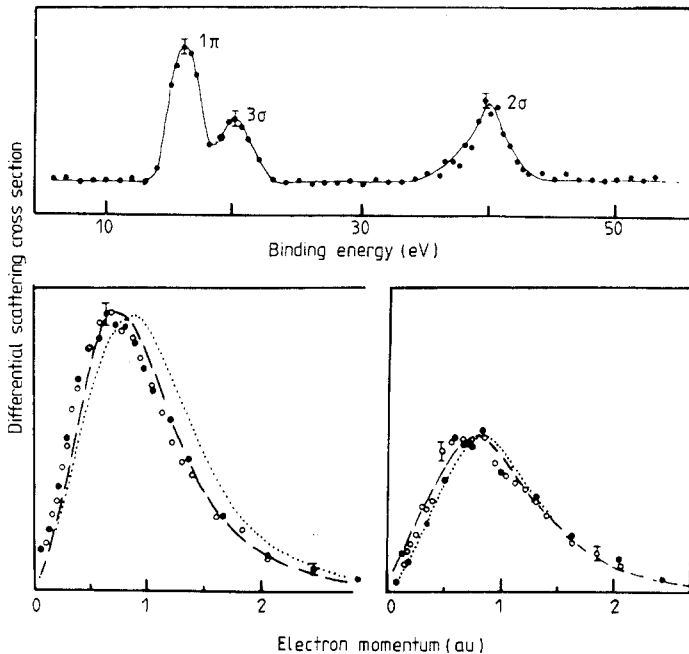


Figure 22. Electron coincidence spectra of gaseous hydrogen fluoride. The upper diagram shows how the coincidence count rate peaks when the source is 'tuned-in' to the binding energy of different molecular orbitals (specified here by the remaining hole state).

The two lower diagrams show the momentum distributions of two orbital groups measured with the non-coplanar symmetric geometry ($\theta_A = \theta_B$, $\eta = 0$ in figure 21) at source energies corresponding to the 1π (left) (16.1 eV) and 3σ (right) (19.9 eV) separation peaks. The results were obtained at two source energies, 1200 eV (●) and 400 eV (○). Also shown are the distributions predicted by Green function (---) and molecular orbital (···) calculation (from Brion *et al* 1980).

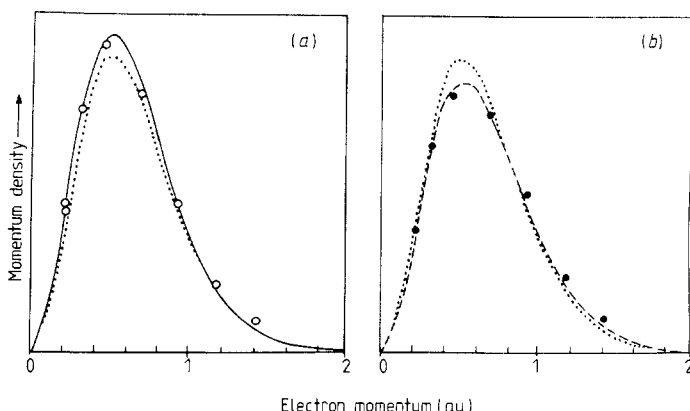


Figure 23. The electron momentum density distribution for (a) the $5p^{3/2}$ (○) and (b) $5p^{1/2}$ (●) orbitals of atomic xenon as deduced from $e, 2e$ coincidence experiments with a 1200 eV electron source. The relativistic density distributions (—) in each case are different whereas the non-relativistic prediction (···) is the same. The data are clearly closer to the relativistic calculations (from Cook *et al* 1984).

has been a rapid exploration of the use of the reciprocal form factor, $B(z)$, especially in 'bonded' systems where discussion in terms of the overlap of localised wavefunctions is apt. The partial segregation of core and valence contributions when the separation z is of the order of the bond length (see equation (2.14) and § 2.3.1) highlights the latter in a manner not apparent in the original profile. The role of the reciprocal form factor in atoms and molecules has been examined and promoted by Weyrich, Pattison and Williams both singly and collectively (see, for example, Weyrich *et al* 1979).

In the second place very accurate results on metallic solids have been used, not only to discriminate between rival band theories, but also to challenge the underlying approximations within which such calculations are performed—specifically the local density approximation. In general in these delocalised systems the analysis proceeds in terms of the momentum representation, i.e. the directional Compton profiles and their differences, rather than the $B(r)$ formulation.

The measurements on metals suffer two disadvantages by comparison with insulators. Firstly, at the purely practical level it is often more difficult to grow large single crystals of the former. Secondly, the momentum distribution of a conductor is characterised by Fermi surface discontinuities which will be largely washed out by the modest experimental resolution; sharp features are not anticipated in the momentum density of an insulator and consequently the limited resolution is less of a problem.

Since the Compton profile integral is a one-dimensional projection of the entire electron momentum distribution it is inevitably difficult to extract those features which differentiate the material from its parent atoms. In electron scattering experiments the problem is compounded by the spherical averaging in the gas target and it is only the very high resolution and good statistical accuracy which saves that situation. γ -ray experiments, where these conditions are much less favourable, are now rarely performed on powders or polycrystals: single-crystal studies are strongly preferred. The directional Compton profiles can then be compared with theory on an absolute basis or, with greater certainty, on a relative basis by forming directional differences, $\Delta J(p) = J_{hkl}(p_z) - J_{h'k'l'}(p_z)$. The latter not only eliminates the isotropic part relating to the closed shell which is of little interest, but also minimises residual systematic errors from the individual profiles.

More ambitiously, if many directional profiles are measured it is possible to reconstruct the three-dimensional momentum distribution or sections through it. The reciprocal form factor is a necessary stage in that reconstruction process (see § 2.3.2). There are thus three possible levels for data interpretation which correspond to increasing levels of sophistication:

(a) directional difference Compton profiles and reciprocal form factors, $\Delta J(p)$ and $\Delta B(z)$,

(b) absolute Compton profiles and reciprocal form factors $J(p_z)$ and $B(z)$,

(c) reconstructed distributions $n(p_x, p_y, p_z)$ and $B(x, y, z)$.

All these feature in the following survey of recent studies which is summarised in tables 5, 6, 7 and 8.

5.2. Ionic solids

5.2.1. LiH. Lithium hydride is, of course, the simplest ionic material and its charge density has been extensively studied. The theoretical reciprocal form factor, shown earlier in figure 12 (taken from Pattison and Weyrich 1979), was cited as an illustration of how the model orthogonalisation could be tested by locating the zeros in $B(z)$. In

fact it shows much more. The atomic wavefunctions for Li^+ and H^- ions are 1s functions, i.e. they are necessarily positive and a superposition of free ions would yield $B(z) > 0$ for all z . The zeros must arise when Bloch functions are constructed, but the large negative area between 3–5 Å contains additional information. It indicates an antibonding interaction between the H^- ions which have a nearest-neighbour separation of 2.9 Å along [110]. The lobe is not, in fact, pronounced in the other symmetry directions. This confirms the earlier observation of Berggren and Martino (1971) that it is not the $\text{Li}^+ - \text{H}^-$ but the $\text{H}^- - \text{H}^-$ interaction that dominates the solid-state wavefunction, despite the acknowledged ionic character of the material. The effect is so strong that it dominates the spherical average of $B(z)$ and was apparent in the experiments which were unfortunately limited to powder samples.

5.2.2. MgO . Magnesium oxide is similar to LiH in having much larger overlap matrix elements than classical ionic materials such as LiF. Single-crystal measurements and cluster calculations have been performed by Aikala *et al* (1982) using a 5 Ci annular ^{241}Am source and recently APW calculations by Podloucky and Redinger (1984) have appeared.

The O^{2-} ion must be stabilised by the crystalline field. At the simplest level that field can be simulated by a hollow charged sphere—the Watson sphere—with its radius equal to the nearest-neighbour separation. This isotropic free-ion model is capable of predicting the x-ray form factors, although Vidal-Valet *et al* (1978) found some evidence for the delocalisation of one O^{2-} electron and a charge transfer from [111] to [100]. It provides a very poor fit to the Compton data because the wavefunctions are not orthogonalised. Aikala *et al* consider cluster calculations which achieve varying degrees of orthogonalisation and the LCAO band calculation of Pantelides *et al* (1974). All these models predict a momentum density asphericity, as revealed by the directional difference profiles $\Delta J(\mathbf{p})$, which shows oscillations with a period characteristic of the reciprocal lattice structure. In all cases the amplitude of these oscillations is overestimated. The anisotropy does not appear to be especially sensitive to the quality of the O^{2-} ion representation.

A more enlightening comparison can be made when the reciprocal form factors are calculated. Along [110] and [100] the orthogonalised Watson sphere calculations are very similar and consistently lie one to two standard deviations above the experimental curves. The LCAO and APW calculations are notably better for the [110] and [111] directions, being generally within one standard deviation of the data. However, there is a considerable discrepancy in the [100] direction as is shown in figure 24 where the band contributions are analysed. In the theoretical curves for $B_{100}(z)$ (and $B_{110}(z)$) it is the p-like oxygen function which produces the negative overlap region; the s-band overlaps are necessarily positive. The minimum in $B_{100}(z)$ between 3.5 and 4.0 au is at best reproduced as a ledge in the APW calculation which uses the local density approximation of Hedin and Lundqvist (1972). The LCAO calculation (Hartree-Fock plus non-local exchange) is rather worse at describing this minimum.

It is to be expected that the [100] Mg—O nearest-neighbour direction should be the most difficult to describe although the degree of disagreement is surprising. Seth *et al* (1977) in their study of TiC noted similar anomalies in the [100] profiles of other materials with the rock-salt structure.

5.2.3. Li_3N . Lithium nitride is of interest because of its behaviour as an ionic conductor. Hexagonal layers of lithium are sandwiched between Li_2N layers and electrical conduction

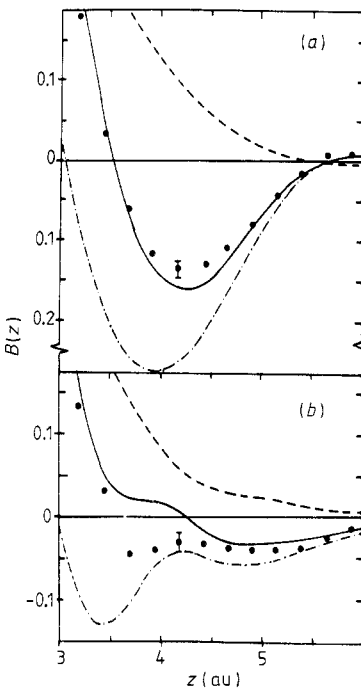


Figure 24. The $B(z)$ function in MgO along (a) [110] and (b) [100] directions. The experimental results (●) are due to Aikala *et al* (1982) and the theoretical prediction (—) is the APW calculation of Podloucky and Redinger (1984) damped by the experimental resolution. The theoretical curves have been split into the oxygen p band (---) and s band (—·—) contributions. The theory does not reproduce the experiment along the [100] nearest-neighbour direction (from Podloucky and Redinger 1984).

tivity is much greater perpendicular to the c axis than parallel to it. The x-ray diffraction results of Schwartz and Schultz (1978) can be explained with a model in which N^{3-} ions are embedded in Watson spheres, but this closed-shell ionic model is at odds with the Compton data of Pattison and Schneider (1980) which show significant anisotropy. Incidentally the fact that the crystals are coloured also conflicts with a closed-shell configuration.

In terms of the reciprocal form factor the anisotropy has contributions from separations z , in excess of the 2 Å which characterises the Li–N nearest neighbours and this is thought to arise from the overlap of more distant polarisable N^{3-} ions. Inspection of the individual reciprocal form factors reveals the most significant feature to be a negative dip around $z = 3$ Å along the [11̄20] direction. Neighbouring nitrogen ions lie along this basal plane direction at a separation of 3.6 Å and they cause the large antibonding interaction.

The apparent contradiction between the isotropic form factor and the anisotropic Compton profile is merely a reflection of the different extent to which overlap terms contribute to $\rho(\mathbf{r})$ and $n(\mathbf{p})$. Anisotropy in the profile scales linearly with overlap whereas its contribution to the form factor is faster than the second power. Consequently, when the overlap is small its effect in the momentum density exceeds that in the charge density. This argument was first proposed by Reed *et al* (1974) in their analysis of a γ -ray Compton study of LiF. It was reinforced by a theoretical study of

molecular fluorine by Snyder and Weber (1978) where an overlap charge of 0.03 electron (0.2% of the total) changed the Compton profile at the origin by some 13%.

Pattison *et al* (1984) have extended their γ -ray studies of this system by measuring Compton profiles in six directions in a 30° segment of the basal plane and used these data to reconstruct this section of the $B(r)$ function. The map shown in figure 25 is damped by the Gaussian resolution function which halves the peak heights at $z = 3.56 \text{ \AA}$. Nonetheless the negative lobe of $B_{110}(z)$ can be seen to be a broad crescent-shaped region peaked around the N—N direction, whilst a sharper positive incursion runs along the N—Li direction. The former feature arises from the diffuse nature of the 2s and 2p nitrogen orbitals while the latter is consistent with the overlap of a highly localised lithium 1s orbital and an sp^2 hybrid on the nitrogen site.

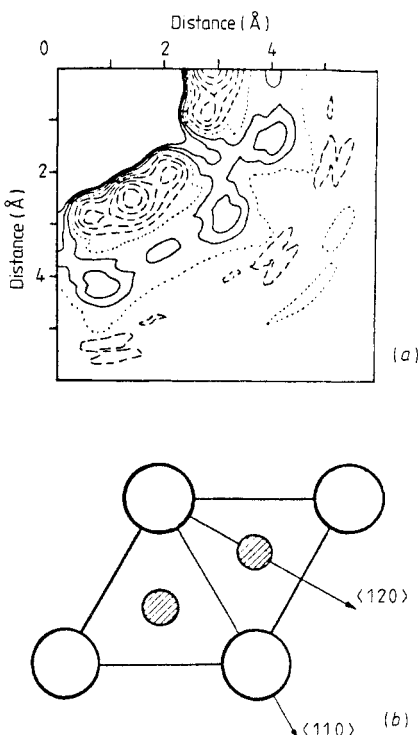


Figure 25. The two-dimensional reciprocal form factor reconstructed from six Compton profiles measured in the basal plane of Li_3N which is shown in plan form in the lower diagram (large circles, N; small circles, Li). The negative contours are shown as broken lines and the positive contours as continuous lines. The contour interval is 0.01 electrons and the experimental error is less than this. The anisotropy reflects the orthogonality requirements of the ionic orbitals centred on different sites, in particular the overlap of the diffuse anions (from Pattison *et al* 1984).

The extent to which the authors are able to analyse these results in terms of molecular orbital overlap—simulating the orthogonalisation of the solid—is indicative of the amount of chemical information in the $B(r)$ function. The relative ease with which features can be interpreted highlights the enormous value of the mapped two-dimensional $B(r)$ distribution as compared with a series of independently considered one-dimensional $B_{hkl}(z)$ functions.

Table 5. Recent Compton studies of ionic compounds.

Material	Nature of the investigation	References
LiF	Experiment: ^{123m}Te γ -rays, single crystal, $\Delta J(p)$ Theory: LCAO cluster with limited orthogonalisation	Reed <i>et al</i> (1974) Berggren (1975)
LiH	Experiment: ^{123m}Te γ rays, powder, $J(p)$ Experiment: ^{241}Am γ rays, powder, $B(z)$ Theory: LCAO cluster with Lowdin's orthogonalisation Theory: Heitler London approximation with Lowdin's symmetric orthogonalisation Theory: Hartree-Fock LCAO Theory: Tight binding	Reed (1978) Pattison and Weyrich (1979) Aikala (1976a, b) Kodama <i>et al</i> (1981) Dovesi <i>et al</i> (1984) Ameri <i>et al</i> (1981)
TiC	Experiment: ^{241}Am γ rays, single crystal Theory: LCAO	Seth <i>et al</i> (1977)
MgO	Experiment: ^{241}Am γ -rays, single crystal, $J(p)$, $B(z)$, $\Delta J(p)$, $\Delta B(z)$ Theory: LCAO tight binding Theory: APW local density approximation	Aikala <i>et al</i> (1982) Pantelides <i>et al</i> (1974) Podloucky and Redinger (1984)
Li_3N	Experiment: ^{198}Au γ -rays, Single crystals: $J(p)$, $B(z)$ $B(r)$ reconstructed Theory: Pseudopotential	Pattison and Schneider (1980) Pattison <i>et al</i> (1984) Kerker (1981)

5.3. Semiconductors

Tetrahedrally bonded semiconductors with the diamond structure have understandably received intensive attention from theoreticians and this work included calculations of Compton profiles at an early stage (e.g. Stroud and Ehrenreich (1968) on silicon). The fact that, with the possible exception of diamond, large single crystals of elements and compounds are readily available prompted early experiments that were at least statistically accurate, though multiple scattering could have been a problem. Eisenberger and Reed's (1972) study of C, Si and Ge stood for many years as the benchmark for subsequent experimental work; indeed, their results remain uncontradicted by recent more exhaustive experiments. In the mean time there has been a profusion of calculations ranging from Hartree-Fock (Wepfer *et al* 1974), SCF discrete variational method (Seth and Ellis 1977) and SCF-OPW (Krusius 1977) to pseudopotential (Nara *et al* 1979). Theoretical and experimental work is summarised in table 6.

The similarity between C, Si and Ge is evident in their isotropic Compton profiles which scale with the reciprocal lattice vector to define a universal curve. This emphasises the importance of the reciprocal lattice structure, in particular the Jones zone (or more correctly the first four Brillouin zones) containing the eight valence electrons. The behaviour of the directional difference profiles can be predicted qualitatively from this zone structure by simply filling the occupied regions with plane wave states. The extrema are correctly located, but the amplitudes of the oscillations are overestimated. Nara *et al* (1979) conclude that the Compton profile anisotropies are insensitive to the model potential but this is perhaps an overstatement in view of the fact the scale is consistently overestimated. More specifically Mackinnon and Kramer (1980) state that the Compton profile is insensitive to that part of the Hamiltonian

Table 6. Recent Compton studies of semiconductors.

Material	Nature of the investigation	References
C	Experiment: ^{123m}Te γ -rays, single crystals, $J(p)$	Reed and Eisenberger (1972)
Si		
Ge		
C	Theory: LCAO HFS discrete variational method, $J(p)$	Seth and Ellis (1977)
Si		
SiC		
Si	Experiment: ^{198}Au γ rays, single crystals; $B(z)$	Pattison and Schneider (1978)
Ge		
C	Theory: nearest neighbour LCAO density matrix	Schlüke and Kramer (1979)
Si		
Ge	Experiment: ^{241}Am γ rays	
C	Theory: molecular orbital models, $B(r)$	Pattison <i>et al</i> (1981b)
Si		
Si	Theory: pseudopotential, $J(p)$	Nara <i>et al</i> (1979, 1984)
Ge		
GaAs		
ZnSe		
Ge	Experiment: ^{241}Am γ rays, liquid samples	Itoh <i>et al</i> (1980b)
Se		
Se	Experiment: ^{241}Am γ rays, amorphous and polycrystalline	Kramer <i>et al</i> (1977)
	Theory: SCF OPW, local density formalism	Krusius (1977)
	Experiment: ^{241}Am γ rays and ^{198}Au γ rays	Krusius <i>et al</i> (1982)
	Theory: SCF OPW	
All tetrahedral semiconductors	Theory: LCAO $B(r)$ function	Mackinnon and Kramer (1979, 1980)

which governs sp hybridisation and the density of states: in that sense Compton spectroscopy is complementary to other spectroscopies.

The strongest feature in the $B(r)$ reconstruction for diamond and silicon is the negative region at the bond length along [111]. This arises because a 2p σ orbital on one atom overlaps with an identical but antiparallel orbital on the next atom along the chain, thus producing a strong minimum in $B(r)$ at $r = R_B$. In this case the negative sign indicates a bonding interaction. The geometry of the orbitals and the $B(r)$ function derived by Pattison and Schneider (1980) from the model of Seth and Ellis (1977) is shown in figure 26. They were also able to identify a π antibonding interaction through second neighbour band overlap as discussed by Pantelides and Harrison (1975).

Other anisotropic features arise from the orthogonalisation of the crystalline wavefunctions which is absent in a simple MO or cluster calculation and the interpretation of data on the basis of molecular rather than Bloch wavefunctions is fraught with danger. In common with crystallographers who present difference density maps the interpretation of $\Delta B(r)$ or $\Delta n(p)$ plots is affected by the choice of atomic basis for subtraction of the atomic or isotropic part.

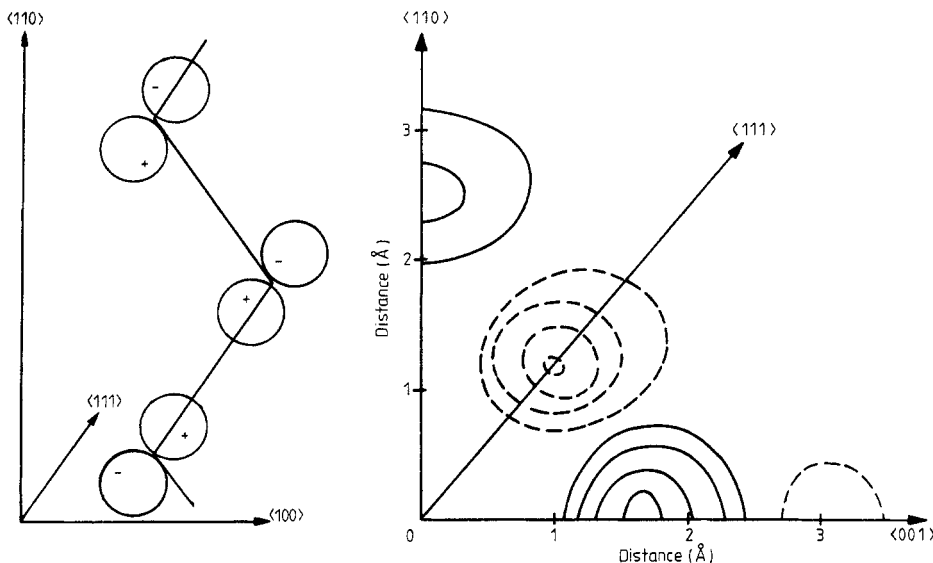


Figure 26. The anisotropy in the $B(r)$ function for diamond derived from the Compton profile calculations of Seth and Ellis (1977). The contours are given in intervals of 0.05 electrons. The chain structure is shown to the left with the $2p$ σ bonding orbitals indicated schematically. The nearest-neighbour and second nearest-neighbour distances are 1.54 Å and 2.52 Å, respectively. The strong negative depression along [111] is at a separation of 1.54 Å as is the peak along [001]. The weaker positive feature along [110] is associated with the second nearest-neighbour separation (from Pattison *et al* 1981b).

Hansen *et al* (1984) have recently comprehensively re-measured silicon and reconstructed the momentum density $n(p)$. Their results are shown in figure 27. The momentum density shows maxima along [100] and [111] and a minimum along [011], all around $p = 1$ au. The first two features are qualitatively reproduced by filling the Brillouin zone with plane waves (figure 27(b)) but they are overpronounced. The Seth and Ellis LCAO model (figure 27(c)) comes closer to a complete description of the data; only the [100] minimum now appears to be overestimated.

So far there has been little experimental work on the III-V and II-VI semiconductors (some is in progress in the present author's group) where the increasing ionicity can be expected to decrease the anisotropy in $n(p)$ in line with the calculations of Nara *et al* (1984).

5.4. Light metals—beryllium

Research on simple, non-transition metals is best exemplified by the recent spate of work on beryllium. This element should afford the best opportunity of all to study solid-state effects in the charge density distribution because as many as half of its electrons, two out of the four, are involved in bonding.

Beryllium has the hexagonal close-packed structure but the interatomic spacing is 4% less between the basal planes than within them, indicating a degree of covalent bonding along the c -axis direction. Charge density maps obtained by Stewart (1977) and Yang and Coppens (1978) based upon the x-ray diffraction data of Brown (1972) indicate enhancement of the population of $2p_z$ orbitals and depletion of the charge density near the nuclei. Recent x-ray and neutron diffraction studies (Manninen and Suortti 1979, Larsen *et al* 1980, respectively) challenge this view; they consistently

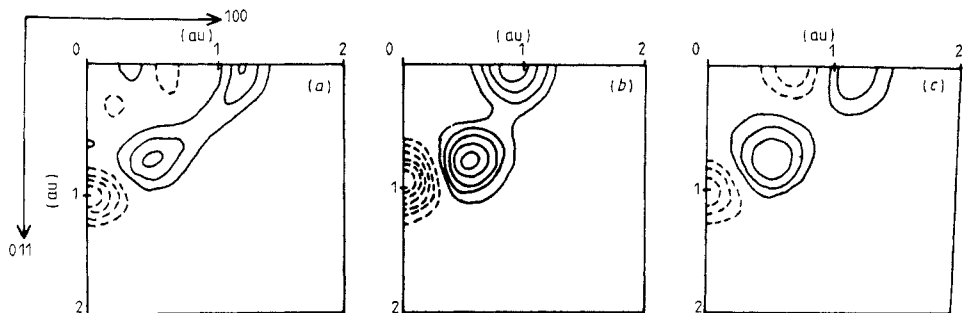


Figure 27. The anisotropic part of the momentum density, $n(p_x, p_y, p_z)$ in silicon in the plane perpendicular to the [011] zone axis. (a) This contour map is reconstructed from six directional Compton profiles derived from ^{198}Au 412 keV measurements via an expansion in the first four cubic harmonics. The contour interval is 0.01 electrons (au^{-3}). The error level decreases away from the origin and is estimated to be generally less than the contour interval beyond $p = 0.5 \text{ au}$. (b) This map shows the momentum density anisotropy predicted by a pseudo-plane-wave model in which the fourth Brillouin zone is filled by electrons in plane-wave states. The contour interval is twice that of the experimental map and despite the fact that the model densities have been convoluted with the experimental resolution the scale of the anisotropy greatly exceeds that observed experimentally. (c) The momentum density anisotropy reconstructed from the Compton profiles calculated by Seth and Ellis (1977) in a Hartree-Fock-Slater approximation. The experimental resolution has been folded into the data and the contour interval is the same as in the experimental map (a). This last map is clearly closer to the experiment than (b) (from Hansen *et al* 1984).

yield lower vibrational parameters which indicates a degree of extinction in Brown's data. Manninen and Suortti also measured the Compton profile of polycrystalline beryllium and found no evidence of deformation of the free-atom core density.

Since that study there have been two further Compton measurements on single crystals; one by Hansen *et al* (1979) using ^{198}Au 412 keV γ radiation and the other by Loupias *et al* (1980) using 10 keV synchrotron radiation and the focusing spectrometer shown earlier in figure 16. The synchrotron measurements enjoy the benefit of much better resolution as discussed in § 4.1 and table 4: allowing for this, the two data sets are in good agreement. They are shown compared with theory in figure 28. Hansen *et al* compared measurements on five orientations with three models. Firstly one in which the one and two Brillouin zones are filled with plane wave states, secondly a pseudopotential model calculated by Rennert *et al* (1978) and thirdly an LCAO model calculated according to the Lowdin orthogonalisation procedure by Aikala (1976b).

As with the tetrahedral semiconductors the structural nature of the anisotropy is emphasised by the fact that the Brillouin zone model qualitatively describes the oscillations of the directional difference profiles. As Currat *et al* (1971a) pointed out in an earlier study it is the second zone, which is almost full, that determines the anisotropy. However, the zone model again overestimates the scale of the anisotropy, this time by a factor of two or more. The pseudopotential calculation of Rennert *et al* shown in figure 28 reduces the scale of the mismatch by 30% but this still leaves a significant quantitative difference unaccounted for. The LCAO model predicts the smallest anisotropies and in that sense shows the best overall agreement with the individual profiles, but the anisotropy that it predicts is qualitatively different from that observed. The best agreement with the directional difference profiles is shown by a density functional pseudopotential calculation by Chou *et al* (1982a) which is also shown in figure 29 below. This theory is also compared with experiment in the earlier joint paper by Chou *et al* (1982b).

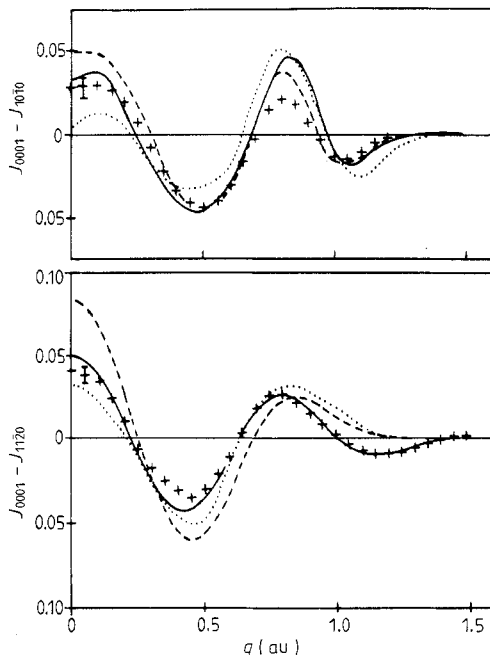


Figure 28. The directional difference Compton profiles of beryllium. In the upper diagram the experimental anisotropy, denoted by crosses, was measured with the focusing spectrometer shown in figure 16 and a synchrotron source monochromated at 10 keV; the momentum resolution is 0.15 au. In the lower diagram the experimental results were obtained in a 412 keV γ -ray experiment at a resolution of 0.40 au (Hansen *et al* 1979). The theoretical anisotropies have been convoluted with the appropriate experimental resolution function in all cases. They are identified as follows: — local density functional pseudopotentials (Chou *et al* 1982b); ···, LCAO (Aikala 1976b); ---, pseudopotential (Rennert *et al* 1978) (from Chou *et al* 1982b).

Meanwhile another calculation (*ab initio* Hartree-Fock LCAO SCF) was published by Dovesi *et al* (1982a, b). It also reduced the mismatch between the scale of experimental and theoretical difference profiles. That calculation predicted form factors which are in good agreement with those measured by Larsen *et al* and has a total energy close to the Hartree-Fock limit.

Some differences between experiment and theory are suppressed if directional differences alone are considered. When the individual profiles are compared on an absolute basis a small difference is found that is common to all orientations, namely the theoretical profiles are too large at $p < p_F$, the Fermi momentum, and too small above it. As Chou *et al* point out this is clear evidence of the neglect of electron correlation which will spill electrons out of the Fermi volume. Even a simple calculation, based upon the homogeneous interacting electron gas model of Daniel and Vosko (1960), shows that the inclusion of electron-electron Coulomb interactions produces an isotropic correction which halves the difference between experiment and theory. This is quite clear in the profiles shown in figure 29. The authors suggest that the residual differences between theory and experiment are due to the tendency of pseudopotential calculations to underestimate the high momentum contribution. Recently Bauer and Schneider (1984a, b, c) have calculated a more accurate correction. They have derived the momentum density correlation correction in the local density formalism according to the method developed by Bauer (1983). Their correlation functional removes almost all the difference between experiment and theory.

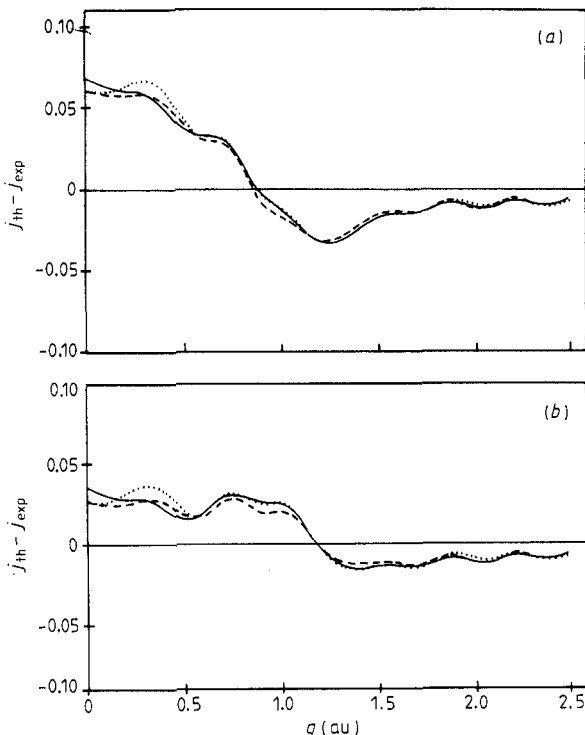


Figure 29. The directional Compton profiles of beryllium compared with a local density functional pseudopotential. The upper diagram compares the experimental γ -ray profiles of Hansen *et al* (1979) with the local density approximation result. The differences are independent of crystal orientation. In the lower diagram an isotropic correction for electron correlation effects has been included. This has been calculated by a method proposed by Rennert *et al* (1978) which is in the spirit of the random phase approximation calculation of Daniel and Vosko (1960). The difference between experiment and theory are roughly halved and barely exceed $\frac{1}{2}\% J(0)$ (from Chou *et al* 1982b). —, 0001; - - -, 10\bar{1}0; · · ·, 11\bar{2}0.

This intensive study of beryllium has shown that Compton data can not only discriminate between band models but can detect correlation effects. The latter is particularly pleasing because in the related positron annihilation method the positron-electron correlations mask such effects (see West 1973). In the case of beryllium the local density correlation functional appears adequate. However, this does not appear to be the case for the heavier metals discussed below.

5.5. Transition metals

Despite the tremendous interest in the properties of all transition metals and their alloys accurate descriptions of their electron density distributions have proved elusive because of the localised nature of the d-electron distribution (the problem is greater for the 3d electrons of the first series than the 4d electrons of the second). This very difficulty increases the importance of measuring the ground-state densities accurately and testing the band models.

The need has long been recognised and x-ray diffraction studies of elements in the first series are widely reported (see Sirota 1969, Weiss and Mazzone 1981). Unfortunately x-ray form factors are dominated by the preponderance of core electrons as

mentioned earlier; moreover, they are beset by difficulties associated with the establishment of the absolute scale and the description of extinction in the crystal. Indeed the ^{198}Au γ diffractometer (Schneider 1974), from which the Compton spectrometers are derived, was itself developed to minimise the extinction problem. Another approach, specific to cubic materials, is to use the paired-reflection technique (the comparison of the Bragg intensities of different hkl reflections occurring at the same $\sin \theta/\lambda$) to eliminate the systematic errors such as extinction in the study of the aspherical part of the density distribution.

There is an historical legacy of x-ray diffraction studies dating from the 1960s which purports to show that the charge density distribution is more anisotropic than the contemporary theoretical prediction, e.g. vanadium (Weiss and DeMarco 1965, Diana and Mazzone 1975) or iron (Phillips and Weiss 1972, Diana and Mazzone 1974). Research by Suortti and Jennings (1977) indicates that these results suffered from extinction and other problems, a view reinforced by recent measurements of Ohba *et al* (1981, 1982) on vanadium and chromium. Nevertheless, the majority of published results are at variance with the momentum space behaviour where the aspherical part is smaller than the model prediction.

The early Compton studies of transition metals, most of which are reviewed in the book edited by Williams (1977), consisted of measurements on polycrystalline or powder samples. They were compared with isotropic models such as the renormalised free atom. The last decade has seen far more measurements on oriented single crystals and an emphasis on directional difference profiles, absolute profiles and reciprocal form factors.

Progress in the interpretation of results is in part due to the improved accuracy and reliability of data which was discussed in § 4.4 and illustrated in figure 20. It owes an equal debt, as is evident from table 7, to the activity of two principal groups in calculating momentum density distributions in addition to the more familiar parameters of band theory. Wakoh and co-workers have adopted the APW approach whereas Callaway and co-workers have used the LCAO model with Gaussian basis for their calculations. Both groups have tackled the majority of the first series metals. Although the two approaches are very different they generally predict similar directional difference profiles. This should be no surprise, as was shown earlier in the case of the tetrahedral semiconductors and beryllium ‘geometrical’ nearly-free electron models are successful in predicting qualitatively correct profile anisotropies. A marked tendency to overestimate the scale of the anisotropy is found in the majority of the metals and when present it is common to all the band theory models. This is a most important observation because it leads to the suggestion that local density approximation, the starting point for these band theory calculations, has failed. The same feature, observed in insulators, probably has a different explanation since it is difficult to see how correlations can promote electrons to higher momenta states in materials with filled bands.

Differences among the band theories become apparent when the Compton profiles are compared individually with theory. The momentum density is obtained from a reciprocal lattice expansion of Bloch functions which is limited to a few hundred terms in the APW calculations compared with a few thousand in the LCAO calculations. High momentum components are missing in the APW model of $n(\mathbf{p})$ and this means that the Compton profile is deficient in electron density at all momenta. Not surprisingly the more extensive LCAO calculation produces the better description of the Compton profile.

Table 7. Recent Compton studies of transition metals.

Material	Nature of the investigation	References
	Review	Weiss (1978) Krishna Gandhi and Singru (1981)
Ti	Experiment: ^{241}Am γ rays, polycrystal Experiment: Ti and TiC (polycrystalline)	Felsteiner and Pattison (1976) Manninen and Paakkari (1976)
V	Theory: KKR method, state-dependent potential, $J(p)$ Theory: APW method (also Cr) Theory: LCAO, Gaussian basis, $J(p)$, $\Delta J(p)$ Experiment: ^{241}Am γ rays, single crystals Experiment: ^{198}Au γ rays, single crystals $J(p)$, $\Delta J(p)$, $B(z)$	Wakoh and Yamashita (1973) Wakoh <i>et al</i> (1976) Laurent <i>et al</i> (1978) Manninen and Paakkari (1983) Rollason <i>et al</i> (1981) Rollason <i>et al</i> (1983a, b)
Nb	Theory: APW, $J(p)$ Experiment: ^{241}Am γ rays, single crystals Experiment: ^{198}Au γ rays, single crystals of metal plus hydrided/deutrided material	Wakoh <i>et al</i> (1975) Pattison <i>et al</i> (1976) Pattison <i>et al</i> (1977a) Alexandropoulos and Reed (1977) Theodoridou and Alexandropoulos (1984)
Fe	Theory: APW, $J(p)$ Theory: LCAO Gaussian basis (also Cr, Ni), $J(p)$ Experiment: ^{137}Cs γ rays, polycrystal Experiment: ^{198}Au γ rays, $B(z)$, single crystals, $J(p)$, $\Delta J(p)$ Experiment: ^{191}Os γ rays, cooled source, circularly polarised radiation	Wakoh and Kubo (1977) Rath <i>et al</i> (1973) DuBard (1978) Rollason <i>et al</i> (1983a, b) Sakai <i>et al</i> (1984)
Cu	Experiment: Au γ rays, single crystals, $J(p)$, $\Delta J(p)$, $B(z)$ Theory: density functional theory Theory: Tight binding LCAO	Pattison <i>et al</i> (1982) Schneider <i>et al</i> (1984) Bauer and Schneider (1984a) Bauer and Schneider (1983) Bauer and Schneider (1984b)
Zn	Theory: LCAO	Aikala (1976a, b)
Ce	Experiment: ^{51}Cr γ rays Theory: RFA Theory: LMTO-APW	Kornstadt <i>et al</i> (1980) Podloucky and Glotzel (1983)

5.5.1. *Niobium and vanadium.* The four d electrons of these BCC metals might be expected to prefer the t_{2g} crystal field orbitals which have lobes pointing along the [111] nearest-neighbour directions. If free-atom 3d functions are assumed for vanadium, as many as 3.2 electrons per atom would have to populate these orbitals in order to reproduce the x-ray data of Weiss and DeMarco (1965) for the paired reflection intensity ratios. Wakoh and Yamashita (1973) were unable to reproduce such a large asphericity in the band density by either varying the exchange parameter α or by introducing a state-dependent potential. The prediction of the LCAO calculation of Laurent *et al* (1978) is similarly distant from the early diffraction result, but close to the more recent measurements of Ohba *et al* (1981).

The [100], [110] and [111] directional Compton profiles of Nb and V and their differences have been measured by a range of experimental groups (see table 7 for a list of references). The directional difference profiles (see figure 20 for a typical set of results from the present author's group) in both niobium and vanadium are readily

understood from the geometry of the Fermi surface. There is an interconnecting network of holes running along the [100] directions in the third Brillouin zone. Thus whenever the plane of the Compton integral slices through the holes $J(p_z)$ is reduced; for example, $J_{100}(p_z)$ is diminished at $p_z = 0, 2\pi/a$, etc, whereas for $J_{110}(p_z)$ the analogous momenta are 0, $\pi/\sqrt{2}a$, etc. The anisotropies are rather large, especially in niobium ($\sim 5\% J(0)$).

In vanadium especially, the scale of the anisotropies is less than the consistent predictions of theory, a result which is at variance with the earlier diffraction results. The contradiction was sufficiently perplexing to initiate an international project under the auspices of the International Union of Crystallography Commission on Charge, Spin and Momentum Density. Although that project is still current it is likely that part of the explanation lies in the inability of the local density approximation to predict the anisotropic part of the electron correlations.

5.5.2. Iron. The anisotropies in iron ($\sim 2\% J(0)$) are on a smaller scale than either niobium or vanadium. Nonetheless they are well established and are once again overestimated by theory. An absolute comparison of the individual profiles shows that the APW calculation with its limited lattice expansion of eigenfunctions misses significant amounts of the high momentum part of $n(\mathbf{p})$. The LCAO model is generally closer to the experiment but appears to overestimate the profile around the Fermi momentum. More alarmingly the $B(z)$ functions predicted by both models differ from experiment at $z = \mathbf{R}_b$, the lattice translation vector. The B function for [111] is shown in figure 30. According to the theorems developed by Schülke (1977) in the independent-particle

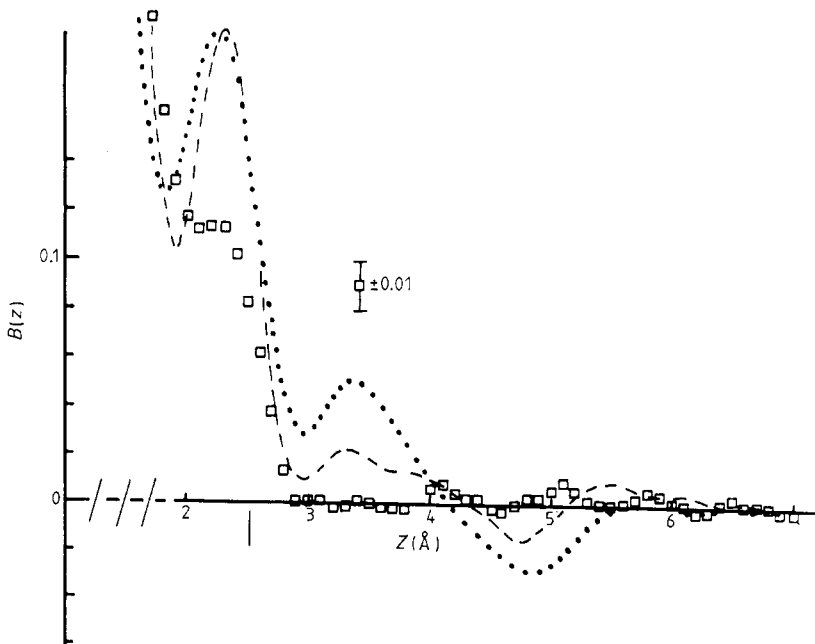


Figure 30. The reciprocal form factor, $B(z)$, for the [111] nearest-neighbour direction in BCC iron. Both APW (---) and LCAO (···) theories (damped by a Gaussian corresponding to the experimental resolution) predict a peak around the lattice translation vector $\mathbf{R}_{111} = a\sqrt{3}/2$. This is only evident in the data (□), which comes from a 412 keV γ -ray experiment, as a ledge. The difference amounts to eight standard deviations at this point (from Rollason *et al* 1983a).

model and repeated in § 2.3, $B(R_i)$ is just a coefficient of the Fermi shape function in the single-particle approximation. It is surprising that such a prediction is wrong for the first term in the series, but a similar problem occurs with copper where the Fermi geometry is particularly well established.

5.5.3. Copper—the failure of the local density approximation. Copper is possibly the simplest, and certainly the most studied, of all the transition metals. Its Fermi surface is sufficiently close to a sphere to encourage elementary calculations of momentum-dependent quantities. Early (Eisenberger and Reed 1974b) and recent (Pattison *et al* 1982, Bauer and Schneider 1984a, b, c) Compton data consistently show directional difference profiles which are approximately half the scale of the theory. A typical directional difference profile is shown in figure 31. Again the discrepancy is relatively insensitive to the quality of the band model as was convincingly demonstrated by a series of model calculations of varying sophistication (Bauer and Schneider 1983). They found that the calculated anisotropy can only be brought down towards the experimental scale by unrealistic modelling which, for example, places the d band at the wrong energy and predicts an electron density more contracted than in the free atom. The B function of copper also disagrees with theory at the repeat distance along the [110] neck direction, the theory being about five standard deviations above the experimental curve.

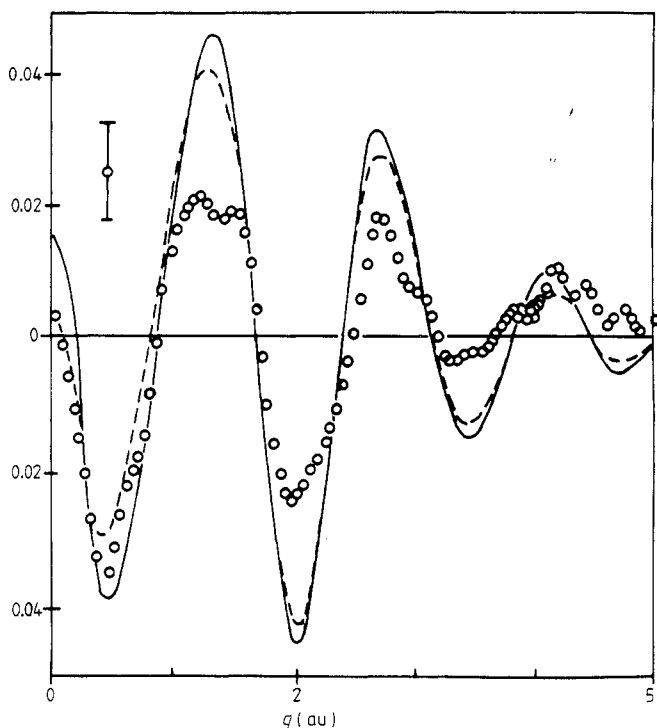


Figure 31. The experimental and theoretical directional difference profile $J_{(110)} - J_{(100)}$ for copper. The full curve is the LCAO-Gaussian basis calculation of Bagayoko *et al* (1980), the broken curve is modified APW band calculation of Bross (1982) and the experimental results (\circ) were obtained in a γ -ray experiment with 412 keV radiation. Despite the fact that the theoretical curves have been convoluted with the experimental resolution the scale of the anisotropy is considerably and consistently over-estimated by the calculations (from Bauer and Schneider 1983).

The Hahn-Meitner group under J R Schneider have concentrated a very considerable effort into understanding the origin of these discrepancies as can be judged from the extensive list of references attributed to them in table 7. Recently they have re-measured several thicknesses of copper crystal to reduce the errors after multiple scattering correction to $\sim \pm 0.2\% J(0)$ at low momenta (Bauer and Schneider 1984a, b, c). This provides an unimpeachable basis for the interpretation of the data.

In the density functional band calculations the exchange correlation is written in terms of the local density $\rho(r)$. Hohenberg and Kohn (1964) and Kohn and Sham (1965) showed that the resulting equation can be solved to yield the correct ground-state energy and charge density, and nothing else. The pseudo-wavefunction obtained by solving the Kohn-Sham equations are not one-electron functions and they cannot be simply Fourier-transformed to yield momentum eigenfunctions. Bauer (1983) has outlined a method whereby a correction term can be calculated. Since the ground-state charge density $\rho(r)$ is correctly predicted no correction is needed to the x-ray form factors, but a correction to the Compton profile is required. This is precisely the term which brought experiment and theory into sensible agreement for beryllium (see figure 29) but it is necessarily an isotropic correction and it cannot make any impact upon the discrepancy found in the difference profiles.

It must be accepted, on the basis of Bauer and Schneider's (1983) work on copper and general experience elsewhere, that the discrepancy is not a function of the accuracy of the particular band model. Therefore the inescapable conclusion is that these experiments show the failure of the local density approximation. The nature of this failure is evident in figure 32, taken from the recent work of Bauer and Schneider (1984a) which relates the difference between the experiment and the local density functional calculation to the Fermi surface geometry in the repeated zone scheme. Bearing in mind that the Compton profile is a series of integrals over planes, the discrepancy corresponds to a need to transfer electrons from the occupied (shaded) regions to the unoccupied regions. This can be achieved by Coulomb correlations which must correspond to non-local effects.

As Bauer and Schneider point out, the fact that the difference is oscillatory means that the energy associated with the extra term may be very small. The kinetic energy contribution, and by the virial theorem the total non-local energy contribution, would be given by the second moment of the difference curve in figure 32. Thus the success of the local approximation appears to be due to the cancellation of sizeable non-local terms.

5.6. Alloys and compounds

Work on transition-metal alloys and compounds has been patchy. Efforts to date have been concentrated on the parent elements where much remains to be learnt before a systematic study of intermetallics, etc, is launched.

The recent work, which is summarised in table 8, has rarely gone beyond the rigid band approximation wherein the minor constituent is considered to donate electrons to the unaltered band of the major constituent. Studies of this kind have the experimental advantage that they may proceed by the analysis of differences, thereby minimising the thorny problems of multiple scattering and other systematic errors. A similar approach has been employed in experiments on polycrystalline alloys where a 'charge transfer' from one element to the other is suspected (see, for example, Manninen *et al* 1981).

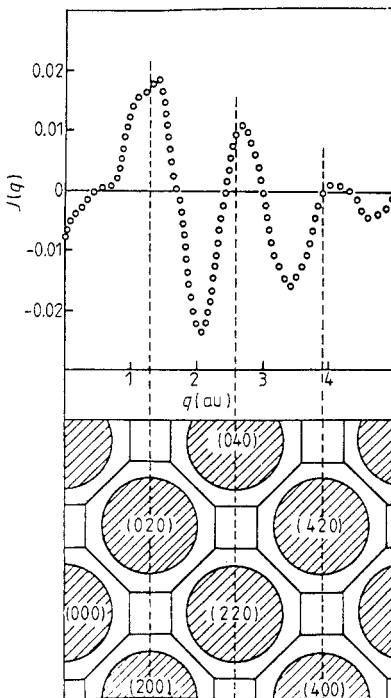


Figure 32. The [11.0] Compton profile of copper, obtained in 412 keV γ -ray experiments, compared with the local density functional LCAO (Gaussian basis) calculation of Bagayoko *et al* (1980) after a local density functional correction to the momentum density has been included. The function plotted is $J_{\text{theory}} - J_{\text{expt}}$ and the theory has been convoluted with the experimental resolution.

The lower diagram shows the Fermi surface of copper in the repeated zone scheme for this orientation of the scattering vector. The oscillations of the upper curve are consistent with the view that the local density approximation does not push sufficient electron momentum outside the Fermi spheres (from Bauer and Schneider 1984a).

Early successes in work of this kind were notched up in studies of hydrogen (or deuterium) in niobium (Pattison *et al* 1976, 1977a, b, Alexandropoulos and Reed 1977). That work showed clearly that the difference profile $J(\text{NbH}_x) - J(\text{Nb})$ was sensitive to the behaviour of the absorbed hydrogen. It was very easy to differentiate among an anionic model in which H^- ions are formed, a protonic model in which the dissolved hydrogen donates electrons to the host bands and an atomic model in which the hydrogen is unchanged. In fact the protonic model was found to be close to the experimental results. Following along similar lines Lässer and Lengeler (1978) were able to reject the anionic model for hydrides of palladium and vanadium. In that case the analysis was taken one stage further: following the approach of Switendick (1972) the behaviour of the added electrons was modelled by donating half to the bands and putting the other half in bonding hybrids which are s-like around the protons and p-like around the metal ions. This produced improved agreement by comparison with the protonic model. Further experiments of this nature, at the level of precision currently attainable, could provide much needed detailed information about the behaviour of hydrogen in these materials.

Some of the other probes of electron density, such as x-ray diffraction or positron annihilation, require a degree of crystalline perfection that may be difficult or impossible

Table 8. Recent Compton studies of alloys.

Material	Nature of the investigation	References
Pd-H, V-H	Experiment: ^{51}Cr γ rays	Lässer and Lengeler (1978)
Lu, Lu-H	Experiment: ^{51}Cr γ rays	Lässer <i>et al</i> (1979)
	Theory: RFA	
Co-P	Experiment: ^{241}Am γ rays	Honda <i>et al</i> (1980)
Ni-P	amorphous samples	
NiB		Honda <i>et al</i> (1981)
FeAl	Experiment: ^{241}Am γ rays	Chaddah and Sahni (1978)
CoAl	polycrystalline samples.	Manninen <i>et al</i> (1981)
NiAl	charge transfer study	
FeAl	Theory: APW	Podloucky and Neckel (1979)
FeTi	Theory and experiment: RFA calculations ^{51}Cr γ rays, polycrystal	Lässer <i>et al</i> (1981)
	Experiment: ^{198}Au γ rays	Bauer <i>et al</i> (1984)
NbO	Theory: average T matrix	Nakao and Wakoh (1980)
Ni_3Ga	Theory: symmetrised APW	Kubo and Wakoh (1983a, b)
	Experiment: ^{198}Au γ rays, single crystals, $\Delta J(p)$	Itoh <i>et al</i> (1984)

to achieve in the alloys. Fortunately Compton scattering is insensitive to the degree of crystalline perfection. In the case of positron annihilation there is a further problem when transition elements and their alloys are studied. The d electrons which are of prime interest do not contribute fully to the annihilation profile because the positron is excluded from the ion cores where the d-electron density is large. The consequence of this is illustrated in figure 33 where both Compton and positron directional difference profiles of Ni_3Ga are reproduced (Itoh *et al* 1984). The anisotropy in the positron experiment is restricted to low momentum; high momentum components are associated with the rapidly varying wavefunction within the core. They are seen by the photon in the Compton experiment but not by the positron in the analogous annihilation experiment. The fact that the Compton result is in better agreement with the APW calculation than the positron result probably indicates an inadequacy in the assumed positron wavefunction.

6. Summary

What conclusions should be drawn from these recent developments in momentum density determination? Has new ground been broken or old ground merely reworked to a fine tilth? Research activity, as measured by publication rate, has after all levelled off: does this foreshadow a decline?

The overriding impression left by the activity of the past decade is of a steady improvement in the quality of the experiments and the refinement of their interpretation. The emphasis has changed from 'quantity' to 'quality'. The crude language of line-shapes and wavefunctions has been superseded by a sophisticated dialogue between experimentalist and theoretician in which density functional theory correlation corrections are discussed. The information content has been raised, for example two-dimensional distributions replace one-dimensional variables.

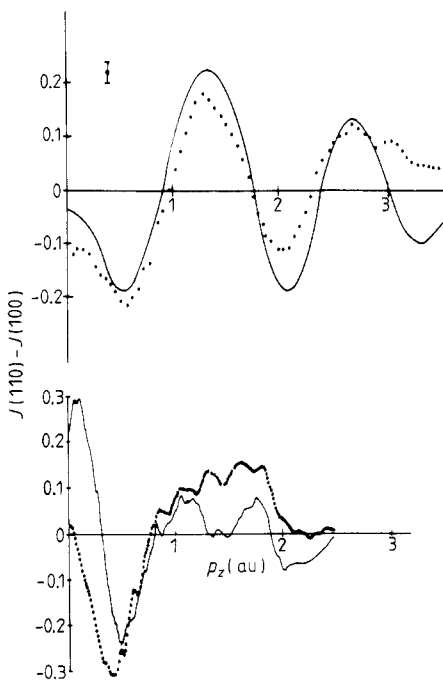


Figure 33. Directional difference profiles for the alloy Ni_3Ga . The upper diagram shows the results of a Compton scattering experiment with ^{198}Au 412 keV radiation compared with the prediction of an APW calculation by Kubo and Wakoh (1983a, b). Both the experimental data and the theory (convoluted with the experimental resolution) show oscillations out to high momentum. They originate from the d-like band electrons which penetrate the ion cores.

The lower diagram shows the analogous positron annihilation results for Ni_3Ga ; the resolution is an order of magnitude higher than in the Compton experiment. In this case the profile anisotropy is limited to low momentum; the positron is excluded from the ion cores and fails to see the high momentum components of the d electrons. The overall agreement between experiment and theory is poorer although the same model has been used to describe band electrons. This suggests that the description of the positron wavefunction may be inadequate (from Itoh *et al* 1985).

There have been identifiable innovations in the experimental work: firstly, the increasing use of high-resolution focusing x-ray spectrometers, a development that results from the availability of position-sensitive detectors and the introduction of short-wavelength synchrotron sources. This is the only route by which high resolution will be achieved in Compton studies with photons; and secondly, the use of circularly polarised radiation to study unpaired spin momentum distributions. A way must surely be found to improve on the current technique of cooled isotopes and provide an adequate flux for wide-ranging studies of magnetic materials to be prosecuted. Thirdly, the technique of measuring Compton scattering at the Bragg condition is more than a novelty and can provide specific information about terms in the electron density matrix.

The major developments have been subtle but nonetheless important. The Compton scattering experiment does its best to disguise and dilute information about outer electron behaviour. To begin with the photon probe samples all electrons with democratic equality. Added to this the experimental information, $J(p_z)$, is a one-dimensional

projection of the real thing, $n(\mathbf{p})$. Despite these disadvantages the information content is significant, the interpretative assumptions are clearly established and the data can be confidently construed. Unfortunately it can hardly be interpreted directly in isolation from the comparative base of theory. All too often in the past the work has been frustrated by the lack of complementary theory. Increased interaction is being encouraged by steady experimental progress, which is manifest in two forms.

In the first place there has been a continuous improvement in the accuracy and reliability of experimental data. The integrity of the processing procedures which convert a measured differential scattering cross section to a Compton profile, a reciprocal form factor, or even a reconstructed density distribution must be very high: it is now. Absolute profiles, such as the one for copper shown in figure 32, can be confidently quoted to a reliability of better than $\frac{1}{2}\% J(0)$. In the second place the interpretation of Compton data has been enriched by the invention of the reciprocal form factor. Thinking about real space comes more naturally than thinking about momentum space, even if the medium of interpretation is an overlap integral. Its particular relevance to molecular bonded species is beginning to be exploited—several research groups are developing a ‘feel’ for the interpretation of $B(r)$ maps as a meeting place for experiment and theory.

In terms of the systems studied, and the results gleaned from them, the work on metals has produced the greatest interaction between experiment and theory and arguably the most interesting results. It is a common, but not universal, observation that Compton profile anisotropies are less than predicted. In the case of metals a link between this observation and the band theory presumptions about electron correlations has been established by the general weight of evidence on the one hand and the specific study of copper on the other. This is a result of undoubtedly general importance, probably the most interesting thing to come out of all the Compton work to date. It is of particular consequence to the technique because it highlights two unique advantages of this experiment. Firstly the ability to measure the Coulomb correlations of the electron system and secondly a sensitivity to the penetrating d-electron distributions in transition elements. These are two areas where Compton scattering can complement high-resolution positron annihilation studies of the Fermi distribution in which the positron turns a ‘blind eye’ to such effects.

What does the future hold? It should include a period of introspection. Now that the level of presumed accuracy has advanced beyond 1% it would be wise to re-validate the process of turning a spectrum into a profile. The move by several laboratories to measure profiles at a series of source energies is an obvious step in the eradication of systematic errors. As to the systems that will be studied, transition metals, their alloys and hydrides will continue to dominate. Relatively few have been measured at the highest precision; there is a wealth of material and an abundance of interest, especially if spin-dependent measurements become a real possibility.

Acknowledgments

I am grateful to those of my colleagues with whom I have discussed the contents and presentation of this review, their comments have been most valuable and their patience profound. I thank all those authors who have kindly permitted their work to be quoted in this review, especially where it has been communicated prior to publication. I apologise for my errors and omissions in the coverage of recent work. I have tried to

produce a representative review rather than an exhaustive catalogue of contemporary research.

I am indebted to the Science and Engineering Research Council for their continuing support for Compton scattering studies in the UK, which has placed me in a position to write this review. Finally I thank the secretarial and photographic staff in the Warwick University Physics Department for their patient help in preparing this material.

References

- Aikala O 1976a *J. Phys. C: Solid St. Phys.* **9** L131-3
— 1976b *Phil. Mag.* **33** 603-11
Aikala O, Paakkari T and Manninen S 1982 *Acta Crystallogr. A* **38** 155-61
Alexandopoulos N G and Reed W A 1977 *Phys. Rev. B* **15** 1970-3
Ameri S, Grosso G and Pastori Parravicini G 1981 *Phys. Rev. B* **23** 4242-5
Bagayoko D, Laurent D G, Singhal S P and Callaway J 1980 *Phys. Lett.* **76A** 187-90
Barlas A D, Rueckner W H E and Wellenstein H F 1977 *Phil. Mag.* **36** 201-7
— 1978 *J. Phys. B: Atom. Molec. Phys.* **11** 3381-400
Bauer G E W 1983 *Phys. Rev. B* **27** 5912-8
Bauer G E W and Schneider J R 1983 *Z. Phys. B* **54** 17-24
— 1984a *Phys. Rev. Lett.* **52** 2061-4
— 1984b *J. Chem. Phys. Solids* **45** 675-84
— 1984c *Solid St. Commun.* **47** 673-6
Bauer G E W, Schneider J R and Welter J-M 1984 *Phys. Lett.* **100A** 207-10
Beardsley G M, Berko S, Mader J J and Shulman M A 1975 *Appl. Phys.* **5** 375-8
Becker P (ed) 1980 *Electron and Magnetisation Densities in Molecules and Crystals* (New York: Plenum)
Berggren K-F 1975 *Department of Physics, Linkoping University Rep.* LiH-IFM-IS 40
Berggren K-F and Martino F 1971 *Phys. Rev. B* **3** 1509-11
Biggs F, Mendelsohn L B and Mann J B 1975 *Atom. Data Nucl. Data Tables* **16** 201-309
Bloch B J and Mendelsohn L B 1974 *Phys. Rev. A* **9** 129-55
Bonham R A and Fink M 1980 *Electron and Magnetisation Densities in Molecules and Crystals* ed P Becker (New York: Plenum) pp 581-632
Bloch F 1934 *Phys. Rev.* **46** 674-87
Bonham R A and Fink M 1974 *High Energy Electron Scattering* (New York: Van Nostrand Reinhold)
Bonham R A and Wellenstein H F 1977 *Compton Scattering* ed B G Williams (New York: McGraw-Hill) chap 8, pp 234-72
Bonse U, Schröder W and Schülke W 1979 *J. Appl. Crystallogr.* **12** 432-5
Brion C E, Hood S T, Suzuki I H, Weigold E and Williams G R J 1980 *J. Electron Spectrosc. Rel. Phenom.* **21** 71-91
Bross H 1982 *J. Phys. F: Metal Phys.* **12** 2249-66
Brown P J 1972 *Phil. Mag.* **26** 1377-94
Chaddah P and Sahni V C 1978 *Phil. Mag.* **37** 305-10
Chou M Y, Lam P K and Cohen M L 1982a *Solid St. Commun.* **42** 861-3
Chou M Y, Lam P K, Cohen M L, Loupias G, Chomilier J and Petiau J 1982b *Phys. Rev. Lett.* **49** 1452-5
Clementi E 1965 *IBM J. Res. Dev.* **9** 2
Compton A H 1923a *Phys. Rev.* **21** 483-502
— 1923b *Phys. Rev.* **22** 409-13
Compton A H and Allison 1935 *X-rays in Theory and Experiment* (New York: Van Nostrand Reinhold)
Cook J D P, Mitroy J and Weigold E 1984 *Phys. Rev. Lett.* **52** 1116-8
Cooper M 1971 *Adv. Phys.* **20** 453-91
— 1977 *Contemp. Phys.* **18** 489-517
— 1979 *Nucl. Instrum. Meth.* **166** 21-7
Cooper M, Leake J A and Weiss R J 1965a *Phil. Mag.* **12** 797-800
— 1965b *Optical Properties and Electronic Structure of Metals and Alloys* ed F A Abeles (Amsterdam: North-Holland) pp 102-5
Cooper M J, Holt R S and DuBard J L 1978 *J. Phys. E: Sci. Instrum.* **11** 1145-8
Cooper M, Pattison P, Williams B G and Pandey K C 1974 *Phil. Mag.* **29** 12-37

- Coulson C A 1941a *Proc. Camb. Phil. Soc.* **37** 55-66
 —— 1941b *Proc. Camb. Phil. Soc.* **37** 74-81
 Coulson C A and Duncanson W E 1941 *Proc. Camb. Phil. Soc.* **37** 67-73
 —— 1942 *Proc. Camb. Phil. Soc.* **38** 100-8
 Coulson C A and March N H 1950 *Proc. Phys. Soc. A* **63** 367-74
 Currat R, DeCicco P D and Kaplow R 1971a *Phys. Rev. B* **3** 243-51
 Currat R, DeCicco P D and Weiss R J 1971b *Phys. Rev. B* **4** 4256-61
 Daniel E and Vosko S H 1960 *Phys. Rev.* **120** 2041-4
 De Bergevin F and Brunel M 1972 *Phys. Lett.* **39A** 141-2
 Diana M and Mazzone G 1974 *Phys. Rev. B* **9** 3898-905
 —— 1975 *Phil. Mag.* **32** 1227-30
 Dirac P A M 1926 *Proc. R. Soc. A* **111** 405-23
 Donovan B and March N H 1956 *Proc. Phys. Soc.* **69** 1249-60
 Dovesi R, Ermondi C, Ferrero E, Pisani C and Roetti C 1984 *Phys. Rev. B* **29** 3591-600
 Dovesi R, Pisani C, Ricca F and Roetti C 1982a *Z. Phys. B* **47** 19-26
 —— 1982b *Phys. Rev. B* **25** 3731-9
 Doyle P A and Turner P S 1968 *Acta Crystallogr. A* **24** 390-7
 DuBard J L 1978 *Phil. Mag.* **37** 273-83
 DuMond J W M 1929 *Phys. Rev.* **33** 643-58
 —— 1930 *Phys. Rev.* **36** 1685-701
 —— 1933 *Rev. Mod. Phys.* **5** 1-33
 DuMond J W M and Kirkpatrick H A 1930 *Rev. Sci. Instrum.* **1** 88
 —— 1937 *Phys. Rev.* **52** 419-36
 Duncanson W E 1941 *Proc. Camb. Phil. Soc.* **37** 397-405
 Duncanson W E and Coulson C A 1941 *Proc. Camb. Phil. Soc.* **37** 406-21
 Einstein A 1905 *Ann. Phys., Lpz.* **17** 132-48
 Eisenberger P and Marra W C 1971 *Phys. Rev. Lett.* **27** 1413-6
 Eisenberger P, Lam L, Platzman P M and Schmidt P 1972 *Phys. Rev. B* **6** 3671-81
 Eisenberger P and Platzman P M 1970 *Phys. Rev. A* **2** 415-23
 Eisenberger P and Reed W A 1972 *Phys. Rev. A* **5** 2085-94
 —— 1974a *Phys. Rev. B* **9** 3237-41
 —— 1974b *Phys. Rev. B* **9** 3242-7
 Epstein I R 1970 *J. Chem. Phys.* **53** 4425-36
 —— 1973 *Acc. Chem. Res.* **6** 145-51
 Epstein I R and Lipscomb W N 1970 *J. Chem. Phys.* **53** 4418-24
 Epstein I R and Tanner A C 1977 *Compton Scattering* ed B G Williams (New York: McGraw-Hill) chap 7, pp 209-33
 Feinberg M J and Rudenberg K 1971 *J. Chem. Phys.* **54** 1495-511
 Felsteiner J and Pattison P 1976 *Phys. Rev. B* **13** 2702-4
 —— 1980 *Nucl. Instrum. Meth.* **173** 323-7
 Felsteiner J, Pattison P and Cooper M 1974 *Phil. Mag.* **30** 537-48
 Fock V 1935 *Z. Phys.* **98** 145-54
 Freund A (ed) 1979 *Proc. Workshop on the Application of intense capture gamma-ray sources, part I (Nucl. Instrum. Meth.)* **166** 1-68
 Fukamachi T and Hosoya S 1972 *Phys. Lett.* **38A** 341-2
 Gasser F 1980 *Doctoral Thesis* University of Strasbourg
 Gasser F and Tavard C 1981a *Chem. Phys. Lett.* **79** 97-9
 —— 1981b *J. Chim. Phys.* **78** 341-5
 —— 1981c *J. Chim. Phys.* **78** 487-91
 Hansen N K 1980 *Reconstruction of the EMD from a set of directional Compton profiles. Hahn-Meitner Institut, Berlin Rep.* HMI B 342
 Hansen N K, Pattison P and Schneider J R 1979 *Z. Phys. B* **35** 215-25
 —— 1984 *Z. Phys. B* in print
 Hedin L and Lundqvist S 1972 *J. Physique C* **3** 731-81
 Heuser-Hofmann and Weyrich W 1984 *Acta Crystallogr.* to be published
 Heuser E and Weyrich W 1981 *X-ray and Electron Scattering for the Determination of Electronic Structures. Communication at the Metz Conference* unpublished
 Hicks B 1937 *Phys. Rev.* **52** 436-42
 Hicks B L 1940 *Phys. Rev.* **57** 665-6

- Hohenberg P and Kohn W 1964 *Phys. Rev.* **136** B864-71
Holt R S and Cooper M 1980 *Phil. Mag.* **41** 117-21
— 1983 *Nucl. Instrum. Meth.* **213** 447-52
Holt R S, Cooper M, DuBard J L, Forsyth J B, Jones T L and Knights K 1979 *J. Phys. E: Sci. Instrum.* **12** 1148-52
Honda T, Itoh F, Fukunaga T and Suzuki K 1980 *Sci. Rep. Ritu. A* **28** 218-31
Honda T, Itoh F and Suzuki K 1981 *Proc. Int. Conf. on Quenched Metals* pp 1303-4
Hughes A L and Enns T 1941 *Phys. Rev.* **60** 345-50
Hughes A L and Mann M M 1938 *Phys. Rev.* **53** 50-63
Itoh F, Cooper M, Holt R S, Laundy D, Cardwell D A and Kawamiya N 1984 *Phil. Mag.* **50** 703-9
Itoh F, Honda T and Suzuki K 1980b *J. Physique* **41** C8 418-21
Jauch J M and Rohrlich F 1976 *The Theory of Photons and Electrons* (Berlin: Springer-Verlag)
Jauncey C E M 1925 *Phys. Rev.* **25** 723-36
Kahana S and Carbotte J P 1965 *Phys. Rev.* **139** A213-22
Kappeler H 1936 *Ann. Phys., Lpz.* **27** 129-68
Kerker G 1981 *Phys. Rev. B* **23** 6312-8
Kilby G E 1963 *Proc. Phys. Soc.* **82** 900-2
Kirkpatrick P, Ross P A and Ritland H O 1936 *Phys. Rev.* **50** 928-35
Klein O and Nishina Y 1929 *Z. Phys.* **52** 853-68
Kodama A, Ishikawa S and Mizuno Y 1981 *J. Phys. Soc. Japan* **50** 920-8
Kohn W and Sham L J 1965 *Phys. Rev.* **140** A1133-40
Kornstädt U, Lässer R and Lengeler B 1980 *Phys. Rev. B* **21** 1898-901
Kramer B, Frusius P, Schröder W and Schülke W 1977 *Phys. Rev. Lett.* **38** 1227-30
Krishna Gandhi K R and Singru R M 1981 *Phil. Mag.* **43** 999-1004
Krusius P 1977 *J. Phys. C: Solid St. Phys.* **10** 1875-86
Krusius P, Pattison P, Kramer B, Schülke W, Bonse U and Treusch 1982 *Phys. Rev. B* **25** 6393-405
Kubo Y and Wakoh S 1983a *Tech. Rep. ISSP Tokyo*
— 1983b *Rep. Univ. Library Inf. Sci.* **2** 11-44
Lahmann-Bennani A, Duguet A and Wellenstein H F 1979 *Chem. Phys. Lett.* **60** 411-3
Larsen F K, Lehmann M S and Merisalo 1980 *Acta Crystallogr. A* **36** 159-63
Lässer R and Lengeler B 1978 *Phys. Rev. B* **18** 637-43
Lässer R, Lengeler B and Arnold G 1981 *Phys. Rev. B* **22** 663-9
Lässer R, Lengeler B, Gschneider K A and Palmer P 1979 *Phys. Rev. B* **20** 1390-7
Laurent D G, Wang C S and Callaway J 1978 *Phys. Rev. B* **17** 455-61
Lipps F W and Tolhoek H A 1954 *Physica* **20** 395-405
Lohmann B and Weigold E 1981 *Phys. Lett.* **86A** 139-41
Lock D G, Crisp V H C and West R N 1973 *J. Phys. F: Metal Phys.* **3** 561-70
Loupia G and Petiau J 1980 *J. Physique* **41** 265-71
Loupia G, Petiau J, Issolah A and Schneider M 1980 *Phys. Stat. Solidi B* **102** 79-95
Mackinnon A and Kramer B 1979 *Solid St. Commun.* **29** 71-4
— 1980 *J. Phys. C: Solid St. Phys.* **13** 37-46
McWeeny R 1949 *Proc. Phys. Soc. A* **62** 519-28
McWeeny R and Coulson C A 1949 *Proc. Phys. Soc. A* **62** 509-18
Manninen S and Paakkari T 1976 *J. Phys. C: Solid St. Phys.* **9** 95-101
— 1978 *Nucl. Instrum. Meth.* **155** 115-21
— 1983 *University of Helsinki Rep.* HU-p-217
Manninen S, Paakkari T and Kajantie K 1974 *Phil. Mag.* **29** 167-78
Manninen S, Sharma B K, Paakkari T, Rundqvist S and Richardson M W 1981 *Phys. Stat. Solidi B* **107** 749-55
Manninen S and Suortti P 1979 *Phil. Mag. B* **40** 199-207
March N H 1954 *Proc. Phys. Soc.* **67** 9-16
Mendelsohn L B and Biggs F 1973 *Inner-shell Ionisation Phenomena and Future Applications US Atomic Energy Conf.* 720404 vol. 3 ed R W Fink p 1142
Mendelsohn L, Biggs F and Mann J B 1973 *Int. J. Quantum. Chem. Symp.* No 7, pp 395-407
Mijnarends P E 1974 *UNFOLD. A Fortran Code for the synthesis of momentum distributions by deconvolution. Rep. RCN*, Petten 217
— 1977 *Compton Scattering* ed B G Williams (New York: McGraw-Hill) chap 10
— 1979 *Positrons in Solids* ed P Hautajarvi (Berlin: Springer-Verlag) pp 25-88
Møller C 1932 *Ann. Phys., Lpz.* **14** 531-85
Mott N F 1930 *Proc. R. Soc. A* **126** 259-67

- Nako Y and Wakoh N 1980 *J. Phys. Soc. Japan* **49** 2423-4
- Nara H, Koboyashi T and Shindo K 1984 *J. Phys. Soc. Japan* in print
- Nara H, Shindo K and Kobayashi T 1979 *J. Phys. Soc. Japan* **46** 77-83
- Ohba S, Saito Y and Wakoh S 1982 *Acta Crystallogr. A* **38** 103-8
- Ohba S, Sato S and Saito Y 1981 *Acta Crystallogr. A* **37** 697-701
- Paatero P, Manninen S and Paakari T 1974 *Phil. Mag.* **30** 1281-94
- Pandey K C and Lam L 1973 *Phys. Lett.* **43A** 319-20
- Pantelides S T and Harrison W A 1974 *Phys. Rev. B* **11** 3006-21
- Pantelides S T, Mickish D J and Kunz A B 1974 *Phys. Rev. B* **10** 5203-12
- Pattison P, Blief H-J and Schneider J R 1981a *J. Phys. E: Sci. Instrum.* **14** 95-9
- Pattison P, Cooper M, Holt R S, Schneider J R and Stump N 1977a *Z. Phys. B* **27** 205-8
- Pattison P, Cooper M and Schneider J R 1976 *Z. Phys. B* **25** 155-8
- Pattison P, Hansen N K and Schneider J R 1981b *Chem. Phys.* **59** 231-42
- 1982 *Z. Phys. B* **46** 285-94
- 1984 *Acta Crystallogr. B* **40** 38-44
- Pattison P and Schneider J R 1978 *Solid St. Commun.* **28** 581-5
- 1979a *J. Phys. B: Atom. Molec. Phys.* **12** 4013-9
- 1979b *Nucl. Instrum. Meth.* **158** 145-52
- 1980 *Acta Crystallogr. A* **36** 390-8
- Pattison P and Weyrich W 1979 *J. Phys. Chem. Solids* **40** 213-22
- 1984 *Proc. IUCr XIII Congr. Abstract* 06.1-2 to be published
- Pattison P, Weyrich W and Williams B G 1977b *Solid St. Commun.* **21** 967-70
- Phillips W C and Chin A K 1973 *Phil. Mag.* **27** 87-93
- Phillips W C and Weiss R J 1968 *Phys. Rev.* **171** 790-800
- 1972 *Phys. Rev. B* **6** 4213-9
- Platzman P and Tzoar N 1970 *Phys. Rev. B* **2** 3556-9
- Platzman P M and Tzoar N 1965 *Phys. Rev.* **139** A410-3
- Podloucky R and Glötzel D 1983 *Phys. Rev. B* **27** 3390-403
- Podloucky R, Lässer R, Wimmer E and Weinberger P 1979 *Phys. Rev. B* **19** 4999-5012
- Podloucky R and Neckel A 1979 *Phys. Stat. Solidi b* **95** 541-8
- Podloucky R and Redinger J 1984 *J. Phys. C: Solid St. Phys.* **16** 6955-69
- Podolski B and Pauling L 1929 *Phys. Rev.* **34** 109-16
- Rath J, Wang C S, Tawil R A and Callaway J 1973 *Phys. Rev. B* **8** 5139-42
- Reed W A 1976 *Acta Crystallogr. A* **32** 676-90
- 1978 *Phys. Rev. B* **18** 1986-90
- Reed W A and Eisenberger P 1972 *Phys. Rev. B* **6** 4596-604
- Reed W A, Eisenberger P, Martino F and Berggren K-F 1974 *Phys. Rev. Lett.* **35** 114-7
- Reed W A, Snyder L C and Guggerheim H J, Weber T A and Wasserman Z R 1978 *J. Chem. Phys.* **69** 288-96
- Rennert P, Dorre Th and Gläser U 1978 *Phys. Stat. Solidi B* **87** 221-6
- Ribberfors R 1975 *Phys. Rev. B* **12** 2067-74, 3136-41
- Ribberfors R and Berggren K-F 1982 *Phys. Rev. A* **26** 3325-33
- Rollason A, Cooper M, Holt R S, Bailey I and Jones T J L 1981 *Phil. Mag. B* **43** 931-6
- Rollason A J, Holt R S and Cooper M J 1983a *J. Phys. F: Metal Phys.* **13** 1807-19
- 1983b *Phil. Mag. B* **47** 51-62
- Ross P A and Kirkpatrick H A 1934 *Phys. Rev.* **45** 223
- Roux M and Epstein R 1973 *Chem. Phys. Lett.* **18** 18-23
- Rueckner W H E, Barlas A D and Wellenstein H F 1978 *Phys. Rev. A* **18** 895-909
- Rullhusen O and Schumacher M 1976 *J. Phys. B: Atom. Molec. Phys.* **9** 2435-46
- Sakai N and Ono K 1976 *Phys. Rev. Lett.* **37** 351-3
- 1977 *J. Phys. Soc. Japan* **42** 770-8
- Sakai N, Terashima O and Sekizawa H 1984 *Nucl. Instrum. Meth.* **22** 419-26
- Schneider J R 1974 *J. Appl. Crystallogr.* **7** 547-54
- Schneider J R, Bauer G E W, Hansen N K and Kretschmer H 1984 *Proc. 1982 Symp. On Local Density Approximation in Quantum Chemistry and Solid State Physics* ed J P Dahl and J Avery (New York: Plenum) pp 679-712
- Schülke W 1977 *Phys. Stat. Solidi B* **82** 229-35
- 1978 *Proc. Int. Conf. on X-ray and XUV Spectroscopy. Japan. J. Appl. Phys.* **17** 332-6
- 1981 *Phys. Lett.* **83A** 451-3
- 1982 *Solid St. Commun.* **43** 863-6

- 1983 *J. Phys. C: Solid St. Phys.* **16** 5629-32
- Schülke W and Kramer B 1979 *Acta Crystallogr. A* **35** 953-7
- Schülke W, Langer T and Lanzki P 1984 *Proc. IUCr XIII Congr.* Abstract 06.3-12 to be published
- Schwarz K and Schulz H 1978 *Acta Crystallogr. A* **34** 994-9, 999-1005
- Seth A and Ellis D E 1977 *J. Phys. C: Solid St. Phys.* **10** 181-94
- Seth A, Paakkari T, Manninen S and Christensen A N 1977 *J. Phys. C: Solid St. Phys.* **10** 3127-39
- Sham L J and Kohn W 1966 *Phys. Rev.* **145** A561-7
- Sirota N N 1969 *Acta Crystallogr. A* **25** 223-43
- Smith V H Jr 1980 *Electron and Magnetisation Densities in Molecules and Crystals* ed P Becker (New York: Plenum) chap 1, pp 3-26
- Smith V H Jr and Whangbo M H 1974 *Chem. Phys.* **5** 234-43, **6** 282
- Snyder L C and Busch H 1972 *Molecular Wavefunctions and Properties* (New York: Wiley)
- Snyder L C and Weber T A 1978 *J. Chem. Phys.* **68** 2974-9
- Steffen R M and Frauenfelder H 1965 *Alpha, Beta and Gamma-ray Spectroscopy* vol 2, ed K Siegbahn (Amsterdam: North-Holland) pp 1453-98
- Stewart R F 1977 *Acta Crystallogr. A* **33** 33-8
- Stroud D and Ehrenreich H 1968 *Phys. Rev.* **171** 399-407
- Stuewer R H 1975 *The Compton Effect—Turning Point in Physics* (New York: Science History Publications)
- Suortti P and Jennings L D 1977 *Acta Crystallogr. A* **33** 1012-27
- Suzuki T 1982 *Advances in X-ray Spectroscopy* ed C Bonnelle and C Mande (Oxford: Pergamon) pp 439-50
- Switendick A C 1972 *Ber. Bunsenges Phys. Chem.* **76** 535-42
- Tawil R A and Callaway J 1973 *Phys. Rev. B* **7** 4242-52
- Theodoridou I and Alexandropoulos N G 1984 *Z. Phys. B* **54** 225-8
- Vidal-Valat G, Vidal J P and Kurki-Suonio K 1978 *Acta Crystallogr. A* **34** 594-602
- Wakoh S, Fukamachi T, Hosoya S and Yamashita J 1975 *J. Phys. Soc. Japan* **38** 1601-6
- Wakoh S and Kubo Y 1977 *ISSP Tokyo Tech. Rep.* A807
- Wakoh S, Kubo Y and Yamashita J 1976 *J. Phys. Soc. Japan* **40** 1043-7
- Wakoh S and Yamashita J 1973 *J. Phys. Soc. Japan* **35** 1394-401
- Waller I and Hartree D R 1929 *Proc. R. Soc. A* **124** 119-42
- Weigold E, Hood S T and Teubner P J O 1973 *Phys. Rev. Lett.* **30** 475-8
- Weiss R J 1965 *X-ray Determination of Electron Density Distributions* (Amsterdam: North-Holland)
- 1978 *Phil. Mag.* **37** 659-62
- Weiss R J, Cooper M and Holt R S 1977 *Phil. Mag.* **36** 193-200
- Weiss R J and DeMarco J J 1965 *Phys. Rev.* **140** A1223-5
- Weiss R J and Mazzone G 1981 *J. Appl. Crystallogr.* **14** 401-16
- Wellenstein H F and Bonham R A 1973 *Phys. Rev. A* **7** 1568-72
- Wepfer G G, Euwema R N, Surrat G T and Wilhite D L 1974 *Phys. Rev. B* **9** 2670-3
- West R N 1973 *Adv. Phys.* **22** 263-382
- 1980 *Physics of Transition Metals. Inst. Phys. Conf. Ser. No 55* ed P Rhodes (Bristol: Institute of Physics) pp 35-44
- Weyrich W 1975 *Ber. Bunsenges Phys. Chem.* **79** 1089-95
- Weyrich W, Pattison P and Williams B G 1979 *Chem. Phys.* **41** 271-84
- Williams B G 1976 *Acta Crystallogr. A* **32** 513-26
- Williams B G (ed) 1977 *Compton Scattering* (New York: McGraw-Hill)
- Williams B G, Parkinson G M, Eckhardt C J, Thomas J M and Sparrow T 1981 *Chem. Phys. Lett.* **78** 434-8
- Williams B G, Sparrow T G and Egerton R F 1984 *Proc. R. Soc. A* **393** 409-22
- Williams B G and Thomas J M 1983 *Int. Rev. Phys. Chem.* **3** 39-82
- Yang Y W and Coppens P 1978 *Acta Crystallogr. A* **34** 61-5